



**Tomas Bata University in Zlín**  
**Faculty of Technology**

# **Crystallization of Polymeric Materials: Study of Nucleation on Active Particles with Large Specific Surface**

**Krystalizace polymerních materiálů: Studium nukleace na  
aktivních částicích s velkým specifickým povrchem**

Author: Ing. Miroslav Janíček  
Study programme: Chemistry and Technology of Materials  
Subject of study: Technology of Macromolecular Substances  
Supervisor: doc. Ing. Roman Čermák, Ph.D.  
Date of defense: April, 2015

© Miroslav Janíček

Keywords: crystallization, nucleation, particles, polymer, structure

Klíčová slova: krystalizace, nukleace, částice, polymer, struktura

## **ABSTRACT**

Crystallization of polymeric materials is a thermodynamic process during which a solid matter with crystalline structure is formed. In comparison with low-molecular substances the crystallization of polymers is complicated by length, periodicity, and structural complexity of macromolecular chains. Kinetics of this process is further driven by thermodynamic conditions – namely by temperature and presence of active surface within the system. This thesis focuses on description of first phase of the crystallization, which is nucleation. An attention is paid to initial and boundary conditions of spontaneous homogeneous and heterogeneous nucleations.

## **ABSTRAKT**

Krystalizace polymerních látek je termodynamický děj, při kterém dochází k vytvoření krystalické struktury tuhé látky z původně amorfní taveniny. Oproti nízkomolekulárním látkám je krystalizace polymerů do značné míry komplikována délkou, pravidelností a strukturní složitostí makromolekulárního řetězce. Kinetika tohoto procesu je dále řízena termodynamickými podmínkami – zejména teplotou a existencí aktivního povrchu v systému. Práce je zaměřena na fyzikální popis počátečního stádia krystalizace, tzv. nukleaci. Zvláštní pozornost je věnována počátečním a okrajovým podmínkám spontánního homogenního a heterogenního nukleačního procesu.



# CONTENTS

<b>LIST OF FIGURES</b> .....	<b>6</b>
<b>LIST OF SYMBOLS AND ABBREVIATIONS</b> .....	<b>7</b>
<b>INTRODUCTION</b> .....	<b>9</b>
<b>1 STATE OF THE ART</b> .....	<b>10</b>
1.1 General Principle of Nucleation and Crystal Growth .....	10
1.2 Crystallization of Polymers.....	11
1.2.1 Effect of Introduced Surface on Crystallization .....	13
1.2.2 Polymorphic Materials .....	14
1.3 Particles with Large Specific Surface .....	15
1.3.1 Transcrystallization on Fibers .....	18
1.3.2 Nucleating Agents.....	18
1.3.3 Crystallization of Semi-Long Branches .....	19
<b>2 AIMS</b> .....	<b>21</b>
<b>3 METHODS</b> .....	<b>22</b>
3.1 Material Preparation.....	22
3.2 Thermal Analysis .....	22
3.3 X-Ray Structural Analysis .....	23
3.4 Optical Microscopy .....	24
3.5 Mechanical Tests.....	25
<b>REFERENCES</b> .....	<b>26</b>
<b>LIST OF PAPERS</b> .....	<b>30</b>
<b>SUMMARIES OF PAPERS</b> .....	<b>31</b>
<b>CONTRIBUTION TO THE SCIENCE AND PRACTICE</b> .....	<b>33</b>
<b>AUTHOR’S PUBLICATIONS</b> .....	<b>34</b>
<b>ARTICLE I</b> .....	<b>35</b>
<b>ARTICLE II</b> .....	<b>45</b>
<b>ARTICLE III</b> .....	<b>59</b>
<b>ARTICLE IV</b> .....	<b>71</b>
<b>CURRICULUM VITAE</b> .....	<b>89</b>

## LIST OF FIGURES

1.1	A) Small molecules approaches the growth surface independently and they can reorganize before reaching the growth front. B) Polymer chain (connected cubes) attaches sequentially with constraints on the attachment possibilities of subsequent chain segments. [1].	10
1.2	$\Delta G$ as function of nucleus size. A: subcritical, B: critical, C: supercritical size, D: stable nucleus.	11
1.3	Nuclei schemes – from left to right: primary, secondary, tertiary nucleus.	11
1.4	Thermal dependency of free energy and enthalpy of A) enantiotropic and B) monotropic system. Adapted from refs. [2,3].	15
1.5	Scheme of A) spherulite-like crystallization on fibre surface and B) transcrystallization after multiple close nucleation [4].	17
1.6	Fibers showing transcrystallinity in kenaf-PP composites. Borrowed from ref. [5].	17
1.7	Colorants with PP-nucleating activity and non-coloring NJStar NU-100 (top right).	19

# LIST OF SYMBOLS AND ABBREVIATIONS

Symbol	Meaning	Unit
$a, b, c$	crystal lattice dimensions	[ $m$ ]
$a, b, a^*, b^*$	size and critical size of nucleus	[ $m$ ]
$B$	full width at half maximum	[ $rad$ ]
$D, d$	diameter, interplanar spacing	[ $m$ ]
$G, \Delta G, \Delta G^*$	Gibbs free energy, change in Gibbs free energy, critical Gibbs free energy	[ $J$ ]
$G_{melt}, G_{\alpha}, G_{\beta}$	Gibbs free energy of melt, $\beta$ and $\alpha$ phase, respectively	[ $J$ ]
$\Delta G_v$	volumetric Gibbs free energy	[ $J/m$ ]
$\Delta G_{\eta}$	activation free energy of segments transport	[ $J/mol$ ]
$H, \Delta H$	enthalpy, change in enthalpy	[ $J$ ]
$H_{melt}, H_{\alpha}, H_{\beta}$	enthalpy of melt, $\beta$ and $\alpha$ phase, respectively	[ $J$ ]
$H_m, \Delta H_m, \Delta H_m^0$	enthalpy of melting, specific heat of melting, specific heat of melting of theoretical fully crystallized material	[ $J/g$ ]
$\Delta h_v$	volumetric heat of melting	[ $J/m$ ]
$k$	Boltzmann constant $k = 1.38065 \cdot 10^{-23} J/K$	
$l, l^*$	length and critical length of nucleus	[ $m$ ]
$l_c, l_a$	thickness of lamella and interlamellar amorphous layer, respectively	[ $m$ ]
$L, LP$	length, long period	[ $m$ ]
$I$	rate of nucleation	[ $1/m s$ ]
$I_c, I_a$	integral intensity of crystalline, and amorphous phase, respectively	
$K$	constant of Scherrer's equation	
$K_{\beta}$	portion of $\beta$ phase	
$N^*$	number of crystallizable units	[ $mol$ ]
$\bar{N}$	mean number	
$n$	integer	
$q$	scattering vector	[ $m^{-1}$ ]
$R$	molar gas constant, $R = 8.3144621 J/K mol$	
$r$	radius	[ $m$ ]
$S, \Delta S, \Delta S_m$	entropy, change in entropy, entropy of melting	[ $J/K$ ]
$S$	surface	[ $m^2$ ]
$T, \Delta T$	temperature, change in temperature	[ $K$ ]
$T_t, T_{m,\alpha}, T_{m,\beta}$	temperature of transformation, temperature of melting of $\alpha$ and $\beta$ phase, respectively	[ $K$ ]

$T_g, T_0$	temperature of glass transition, temperature higher but close to glass transition	[K]
$T_c$	temperature of crystallization	[K]
$T_m, T_m^0$	temperature of melting, equilibrium melting temperature	[K]
$V$	volume	[ $m^3$ ]
$v$	height, altitude	[m]
$x_c, X_c$	crystallinity derived from heat of fusion, and WAXS, respectively	[%]
$X_\alpha, X_\beta$	$\alpha$ - and $\beta$ -crystallinity derived from WAXS, respectively	[%]
$\alpha, \beta, \gamma$	parameters of crystal lattice	[ $^\circ$ ]
$\alpha, \beta, \gamma$	denotation of isomorphous variations	
$\lambda$	wavelength	[m]
$\sigma, \Delta\sigma, \sigma_e$	surface free energy, change in surface free energy, basal plane free energy	[J/m]
$\sigma_{ab}, \sigma_{al}, \sigma_{bl}$	surface free energy of $ab$ , $al$ , and $bl$ plane, respectively	[J/m]
$\sigma_{ns}, \sigma_{sm}$	surface free energy on interface of nucleus and substrate, and substrate and melt, respectively	[J/m]
$\theta$	angle	[ $^\circ$ ]
$\omega$	relative weight concentration	[%]

<b>Abbreviation</b>	<b>Meaning</b>
1D, 2D, 3D	one-dimensional, two-dimensional, three-dimensional
HDPE	high-density polyethylene
LDPE	low-density polyethylene
LLDPE	linear low-density polyethylene
LP	long period
MAO	methylaluminoxane
PE	polyethylene
PP	polypropylene
PTFE	polytetrafluoroethylene
SAXS	small angle X-ray scattering
WAXS, WAXD	wide-angle X-ray scattering, wide-angle X-ray diffraction



## INTRODUCTION

Polymeric materials appear in a great variety covering a broad spectrum of material qualities. These qualities are influenced primarily by the molecular structure of the polymer and its configuration – both direct the structure of the material in solid-state. Depending on the flexibility, mobility, and stereotacticity, the material then can be disordered and amorphous, or partly crystalline.

In comparison with the amorphous materials, which structure is in the solid-state similar to the structure of a melt, the crystalline bulk is highly ordered in long range. The process of reorganization of disordered melt into a crystalline solid is logically called crystallization. Two steps are commonly distinguished in this process: nucleation and crystal growth. This thesis is to describe the very first moments of crystal formation – nucleation, with focus on both – crystallization prerequisites and consequences in formation of specific isomorph.

Understanding the nucleation and whole crystallization process is crucial for prediction and adjustment of end-use properties and also the processing parameters. This can be done by either giving the material special conditions in terms of time and temperature, or by seeding the material with active surface, which may increase nucleation rate, or completely change the supramolecular structure of the bulk.

Both the adjustment of processing conditions and addition of various additives can dramatically change the final macroscopic properties.

# 1 STATE OF THE ART

In daily life, we can find three states of matter, which are gaseous, liquid, and solid. Concerning the solid state, two variations of this condensed matter are usually discussed in literature: disordered amorphous state of immobilized molecules, and ordered crystalline structure. Considering polymers, there are several criteria which must be fulfilled to enable formation of crystalline structure. Beside the thermodynamic conditions, specific composition of the macromolecular chain plays an important role, not only in the ability to arrange itself into crystal lattice but also in the speed of such process [6].

Crystallization process is schematized in Fig. 1.1 which depicts the two main parameters of polymer chain which delimit its crystallizability: tacticity and flexibility [6]. Since the crystallizable segments are bonded together they cannot orient as freely as the crystallizing units of low-molecular substances. The severe constraints then lead to partly crystalline material with usually lamellar structure surrounded with amorphous fraction created by bends, entangled segments, tie molecules or segment with disturbed tacticity [1, 6, 7].

The amorphous phase often comprise movable segments, which can translate, rotate and rearrange to a limited extend [6, 8]. This is, of course, possible only at elevated temperatures, which lower limit is temperature of glass transition ( $T_g$ ). Above  $T_g$  the crystallites can partly increase their thickness and improve their internal structure. Both lead to increase of overall crystallinity. To support this processes, products are sometimes heated to temperatures close to the melting temperature ( $T_m$ ). This procedure is called annealing and is frequently used in metallurgy and glass industry.

## 1.1 General Principle of Nucleation and Crystal Growth

From the thermodynamic point of view, a primary condition of the system to start the crystallization process is decrease of the Gibbs free energy ( $\Delta G$ ) [6, 9].

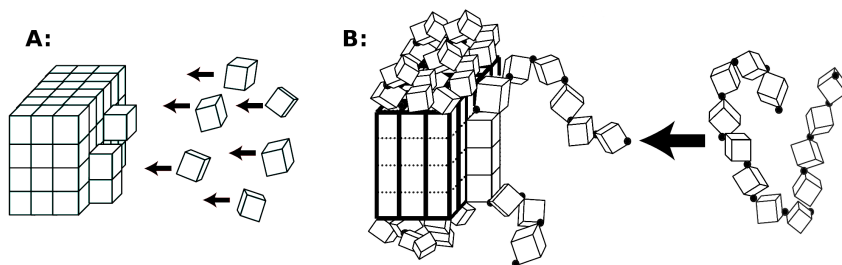


Fig. 1.1: A) Small molecules approaches the growth surface independently and they can reorganize before reaching the growth front. B) Polymer chain (connected cubes) attaches sequentially with constraints on the attachment possibilities of subsequent chain segments. [1].

Since the  $G = H - TS$ , the condition of crystallization is:

$$\Delta G = G_{crystal} - G_{melt} = \Delta H - T\Delta S < 0 \quad (1.1)$$

Arrangement of particles into crystal lattice is usually accompanied with heat emission thus the first addend is negative, which is good for the criterion given by Eq. 1.1. The difference in entropy ( $\Delta S$ ) is, unfortunately, negative ( $S_{melt} > S_{crystal}$ ), which again increases  $\Delta G$ . Thus, the driving force of crystallization is decrease in enthalpy ( $\Delta H$ ) which must overcome the product of  $T\Delta S$  [6, 8, 9].

It should be clear from this simplified description, the material may crystallize in temperatures just below  $T_m$  or after only minute supercooling. In fact, most of polymeric materials crystallize only at temperatures far below  $T_m$  [6].

## 1.2 Crystallization of Polymers

The crystallization is always started with creation of nucleus – a discrete particle, which surface impede the whole process by addition of surface free energy  $\sigma$  to the total free energy of the system [6, 8]. The complication is serious primarily in the first moments of the nucleus formation and growth (see Fig. 1.2 adopted after [9]) as the specific surface is large [6].

Concerning the polymeric material and crystallization as depicted in Fig. 1.1 [9], we can denote the segment length  $l$  and the dimension of the base (i.e. plane perpendicular to the chain axis) as  $a$  and  $b$  (cf. Fig. 1.3).  $\Delta G$  is then equal to the sum of the change in free energy of the crystallized volume ( $\Delta G_v$ ) and contributions of all created surfaces:

$$\Delta G = abl\Delta G_v + 2ab\sigma_{ab} + 2al\sigma_{al} + 2bl\sigma_{bl} \quad (1.2)$$

With the presumption that  $b = a$  and  $l \ll a$ ;  $\sigma_{bl} = \sigma_{al}$  and  $\sigma_{ab} \approx \sigma_{al}$ , the last two addends in Eq. 1.2 can be omitted and the fold surface energy  $\sigma_{ab}$  can be renamed to  $\sigma_e$ . Furthermore, if the flat crystal is large enough (i.e. the effect of surface can be neglected), at the equilibrium melting temperature ( $T_m^0$ ) the

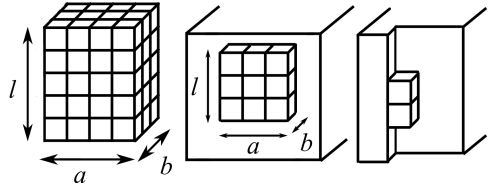
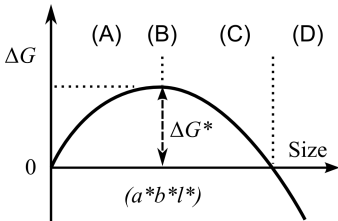


Fig. 1.2:  $\Delta G$  as function of nucleus size. A: subcritical, B: critical, C: primary, secondary, tertiary nucleus, D: stable nucleus.

Fig. 1.3: Nuclei schemes – from left to right:

$-\Delta G_v = 0$ , thus  $\Delta S_m = \Delta H_m / T_m^0$  from Eq. 1.1, then  $\Delta G_v = -\Delta h_v (T_m^0 - T) / T_m^0$ , where  $h_v \propto H_m$  is volumetric heat of fusion. Crystallization free energy of plate crystal (Eq. 1.2) can be modified to:

$$\Delta G = -a^2 l \Delta h_v (T_m^0 - T) / T_m^0 + 2a^2 \sigma_e \quad (1.3)$$

Eq. 1.3 then shows the need of supercooling  $(T_m^0 - T)$ , which must be achieved until the stable nuclei with fold length of  $l$  arise. Since the  $\Delta G = 0$  for the melting temperature ( $T = T_m$ ), Eq. 1.3 can be rewritten into:

$$T_m = T_m^0 - \frac{2\sigma_e T_m^0}{\Delta h_v} \frac{1}{l} \equiv T_m^0 \left( 1 - \frac{2\sigma_e}{\Delta h_v l} \right) \quad (1.4)$$

This expression is often denoted as *Gibbs-Thompson equation* and in calorimetry it is frequently used to calculate lamellar thickness.

The classical conception of nucleation was originally formulated by Gibbs, who presumed that the nucleation barrier  $\Delta G^*$  may be exceeded by local fluctuation [10].  $\Delta G^*$  can be calculated from Eq. 1.2 by partial derivation with respect to  $a$ ,  $b$ , and  $l$ . Obtained system of three equations then gives:

$$a^* = -4\sigma_{bl} / \Delta G_v \quad b^* = -4\sigma_{al} / \Delta G_v \quad l^* = -4\sigma_{ab} / \Delta G_v \quad (1.5)$$

which can substitute the  $a$ ,  $b$ ,  $l$  dimensions in Eq. 1.3:

$$\Delta G^* = 32\sigma_{ab}\sigma_{al}\sigma_{bl} (T_m^0 / \Delta h_v)^2 \frac{1}{(T_m^0 - T)^2} \quad (1.6)$$

This equation explains the above mentioned fact that polymeric materials need supercooling to start to crystallize. For temperatures  $T \simeq T_m^0$  it is evident, the fraction (and whole  $\Delta G^*$ ) become infinite, but with decrease in the temperature, the nucleation barrier drops significantly. The other evident phenomenon is the contributions of the surfaces.

Another process which influences creation of primary nucleus is diffusion of crystallizing segments over an interface between the melt and nucleus. The process is driven by activation free energy of segments transport  $\Delta G_\eta$ :

$$\frac{\Delta G_\eta}{kT} = \frac{C}{T - T_0} \quad (1.7)$$

where  $C$  is constant,  $T_0$  is temperature close to  $T_g$  at which the transport of segments stops and  $k$  is Boltzmann constant. Rate of nucleation  $I$  ( $\text{m}^{-3}\text{s}^{-1}$ ), i.e. number of nuclei arisen in volume and time unit, was originally derived by

Turnbull and Fisher. It is usually presented in this form [6, 7, 9]:

$$I = \frac{N^*kT}{h} \exp\left(-\frac{\Delta G^* + \Delta G_\eta}{kT}\right) \quad (1.8)$$

$N^*$  stands for number of crystallizable units and  $h$  is Planck constant. The rate of primary nucleation is thus according to Eq. 1.8 zero at  $T_0$  (i.e.  $T_g$ ) or  $T_m^0$ , since the  $\Delta G_\eta$  or  $\Delta G^*$  is infinite at the respective temperature (cf. Eqs. 1.6 and 1.7). The nucleation rate passes through maximum within the interval  $(T_0, T_m^0)$ . Meissner and Zilvar also mentioned that measurable values of  $I$  are achieved at supercooling of about 70 K. However, in real systems such large supercoolings are not commonly observed [6, 8].

It is worth to mention, that the current discussion concern *homogeneous* nucleation, however, *heterogeneous* nucleation is prevailing within the real systems. Homogeneous nucleation<sup>1</sup> occurs in the absence of a second phase. Even though the second phase is present, but its surface does not influence the nucleation, the process is still considered as homogeneous. On the other hand, heterogeneous nucleation is caused by presence of the second phase. The process is then localized on the interface of the melt (parent phase) and the second phase [8].

### 1.2.1 Effect of Introduced Surface on Crystallization

For the heterogeneous nucleation is thus needed active surface, which not only immobilizes the macromolecular chain, but also decreases energy of formed nuclei – the energy of the interface should be smaller than  $\sigma_{al}$  or  $\sigma_{bl}$ , which may be a crystal growth front. According to the number of touching sides of the crystal embryo, one can then divide the heterogeneous nucleation into *secondary*<sup>2</sup>, which is characteristic by attachment of straightened chains on flat surface, and *tertiary* for which a step-shaped surface is needed. In the former case one of the  $\sigma_{al}$  or  $\sigma_{bl}$  is decreased by the energy of the interface formed between nucleus and the substrate  $\sigma_{ns}$ , in the latter case, both are substituted. Depiction is in Fig. 1.3.

The driving force of the substrate nucleation activity is driven by removing part of the energy of the interface between substrate and polymer melt  $\sigma_{sm}$ , which should overcome the energy formed on the interface of nucleus and substrate  $\sigma_{ns}$ , thus decreasing the whole energy  $\Delta\sigma$  originally introduced by

---

<sup>1</sup>Homogeneous nucleation can be further divided into *spontaneous* nucleation which happens under no other influence besides supercooling or supersaturation [8], and *orientation-induced* nucleation which is caused by alignment of liquid molecules [11, 12].

<sup>2</sup>Primary nucleation is without any action of any surface, thus homogeneous nucleation.

the nucleus formation ( $\sigma_{al}$  or  $\sigma_{bl}$ ), which is represented with  $\sigma$  in Eq. 1.9 [7].

$$\Delta\sigma = \sigma + \sigma_{ns} - \sigma_{sm} \quad (1.9)$$

Concerning Eq. 1.6, the decrease in the group of multiplicands results in reduction of critical supercooling. This is not only measurable by common thermal techniques, but also beneficial to goods production, where the crystallization (i.e. shape fixation) at higher temperatures may shorten processing times [13]. Beneficial to optical clarity of nucleated material may also be high number of nuclei which leads to formation of smaller spherulites than in the case of unseeded material. Reduction of the scattering elements size may then reduce haze [14].

Another effect, which may be seen during melt crystallization, is preference of thermodynamically less stable and thus less common crystallographic modifications of polymorphic materials [15–19]. By the decrease of necessary supercooling, the less stable phase may start to crystallize at temperatures well above the temperatures connected with supercooling of the common crystallographic modification. If the former phase grows with sufficient rate, it may consume all crystallizable segments, so the latter phase may be suppressed [19].

### 1.2.2 Polymorphic Materials

In general, the solid phase of a material may exist in multiple crystalline structures, which may manifest different properties, although they are created by the very same molecules, i.e. the same chemical composition. This phenomenon is frequent particularly in case of low-molecular substances in which it was originally recognized and described [20]. Nevertheless, polymorphism can be found also in polymeric materials – for example polyamides [21–24] and particularly polypropylene (PP), which polymorphism possesses attention of both industry and research [25–27]. For this reason the PP is favored in the doctoral study. Isotactic PP has four crystalline modifications:  $\alpha$ ,  $\beta$ ,  $\gamma$ , and so-called smectic, which is created with rather small and irregular crystallites [26, 28–30]. The very common  $\alpha$ -form of PP was described by Natta *et al.* in 1956, who find the crystal lattice dimensions are monoclinic with  $a = 6.65 \text{ \AA}$ ,  $b = 20.96 \text{ \AA}$ ,  $c = 6.5 \text{ \AA}$ , and  $\beta = 99.80^\circ$ . This principal and the most stable form can be obtained by both melt and solution crystallization [26, 31]. Later,  $\beta$ - and  $\gamma$ -forms were described by Keith and Padden [32] and Turner-Jones *et al.* [28, 29], who discussed two possible  $\beta$ -form lattices: trigonal  $a = b = 6.38 \text{ \AA}$ ,  $c = 6.33 \text{ \AA}$ , and hexagonal with  $a = b = 6.36 \text{ \AA}$ , and  $c = 6.49 \text{ \AA}$ . The hexagonal was then presupposed to be more suitable for observed X-ray patterns, however, in 1994 independently Meille *et al.* and Lotz *et al.* solved the structure as a trigonal cell with parameters  $a = b = 11.01 \text{ \AA}$ , and  $c = 6.5 \text{ \AA}$  [26]. The last

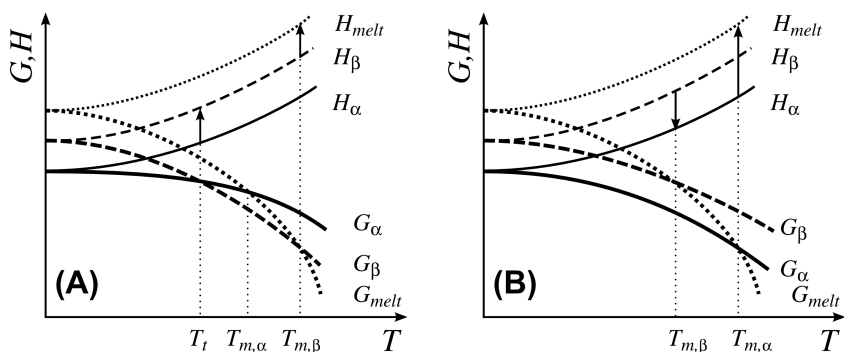


Fig. 1.4: Thermal dependency of free energy and enthalpy of A) enantiotropic and B) monotropic system. Adapted from refs. [2, 3].

isomorph –  $\gamma$ -form, is usually not observed separately, but in co-crystallization with  $\alpha$ -form. Structure of  $\gamma$ -form was published by Meille and Brückner in 1989, who noted, that calculated triclinic cell should be considered as a part of face-centered orthorhombic unit cell with parameters:  $a = 8.54 \text{ \AA}$ ,  $b = 9.93 \text{ \AA}$ , and  $c = 42.41 \text{ \AA}$  [26].

In this place, it is worth to note that the  $\beta$ -form is created under special conditions which are hard to achieve in common processing, thus PP must be seeded with particles – nucleating agent, which nucleate the  $\beta$ -form growth. This points a fact, the material is rather monotropic than enantiotropic, for which would be both isomorphs common in certain temperature range (cf. Fig. 1.4-A). In contrast, subsequent heating of unseeded PP, in which it was achieved  $\beta$ - crystallization, leads to formation of  $\alpha$ -form at temperature of transformation ( $T_t$ ), which equals to the melting temperature of the  $\beta$  crystals ( $T_{m,\beta}$ ) in Fig. 1.4-B. On the other side, the cooling does not lead to  $\alpha \rightarrow \beta$  transformation. The free energy of the system in case of  $\alpha$  form is always lower than the energy of system with  $\beta$  form [2, 3].

### 1.3 Particles with Large Specific Surface

One common purpose of adding fillers to polymers is cost reduction. On the other hand, number of additives are mixed into the polymeric matrix in order to increase its stiffness or stability in time. Some are also added to increase aesthetic value – namely pigments, which were soon recognized as agents influencing nucleation [33–38]. Concerning particles, three principal types are generally recognized:

**Spheres** are one of the most common particle shape if the filler is prepared by simple milling or precipitation either in liquid or gaseous media, e.g. calcite, fumed silica. This shape is also denoted as one-dimensional (1D) particle with the principal dimension given by its diameter.

**Fibers** are two-dimensional (2D) fillers for which formation a special processing is usually required (carbon fibers) or they may originate from plants (cotton linters). The relevant two dimensions are fiber diameter ( $D$ ) and length ( $L$ ). A slenderness ratio ( $L/D$ ) is then usually employed as characteristic number.

**Lamellae** or flaky shapes are typical for layered materials such as silicates, clays and some organic materials – for example wood flour. These fillers are then characterized with three dimensions: length, width, and thickness.

These three basic shapes can be taken as extremes and the real particles may be only approximation of these particular shapes. In addition, a more precise classification should comprise also cubic, nodular, angular, needle-like, etc.

Critical for any interaction of any material is the surface and primarily its size and quality. Regarding the surface size, i.e. the contact area between polymer and particles, a term *specific surface* should be introduced. Any real object has volume ( $V$ ) and surface ( $S$ ) which are always in close relationship, that can be shortened into a simple theorem: The bigger the volume is, the less significant the surface effects are, and *vice versa*. Mathematically it can be easily described on sphere or cylinder, which ratios of surface and volume are in Eqs. 1.10 and 1.11:

$$\text{Sphere: } \frac{S}{V} = \frac{6\pi d^2}{\pi d^3} \quad (1.10)$$

$$\text{Cylinder: } \frac{S}{V} = \frac{2\pi r(r+v)}{\pi r^2 v} \quad (1.11)$$

In case of sphere, it is clear, the volume grows with cube of the particle size, while the surface only with a square of the size. In contrast, when the particle size is reduced, the surface is reduced only with square, but the volume is reduced with cube of the size. The specific surface, i.e. surface related to the volume, then grows as much as small the size (diameter) is. The situation in case of cylindrical particles is analogous with one difference – there are two dimensions, and the reduction of just one of them may increase the specific surface.

Large surface is then helpful in interaction with the polymer and many typical nucleating agents are present in micro- and nanoscale sizes, yet some cases exists in which the better results are achieved not with nanosized and well dispersed particles, but with rather agglomerates of submicro- and microsize [39].



Whether nanoscaled or microscaled the particles should be wettable by the polymer matrix. This condition facilitates the filler dispersion in the material and ensures better interaction with the polymer. For instance, cellulose or wood particles in general have been mixed into polymers for decades [40–43]. Since cellulose is original to plants, it is highly hygroscopic. Despite this, the material itself shows some nucleation activity particularly to PP, which is typical hydrophobic polyolefin. It was also reported, that this effect can be improved by mercerization in aqueous solution of sodium hydroxide [37]. On the other hand, achieving good distribution and dispersion of the filler is in this case uneasy, concerning relatively low thermal stability of the cellulose and brittleness of its fibers.

Some techniques were developed to hydrophobize cellulose fibers [41, 44, 45]. The main focus of these publications is the process of hydrophobization itself or the mechanical properties and utility value of such composites. Not many authors studied directly the structure or nucleation tendency of hydrophobized cellulose. In recent times, vegetable fibers are intensively studied as potential reinforcement [40]. In case of good interaction with the polymer, particularly in case of nucleation of their surface, a specific supramolecular morphology can be observed. It is obvious, the spherulitic morphology is created in case of seeded material with relatively small particles, which are then located in the center of spherulite. Concerning fibers, each length unit behaves as such small nucleating center, so the growth front is not spherical, but rather cylindrical with growth direction normal to the fiber surface [4, 5, 37, 46]. This situation is illustrated in Figs. 1.5 and 1.6. Such phenomenon is then called *transcrystallization* and it is common to natural, organic, and mineral surfaces [46].

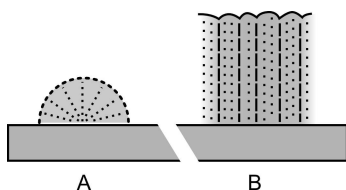


Fig. 1.5: Scheme of A) spherulite-like crystallization on fibre surface and B) transcrystallization after multiple close nucleation [4].

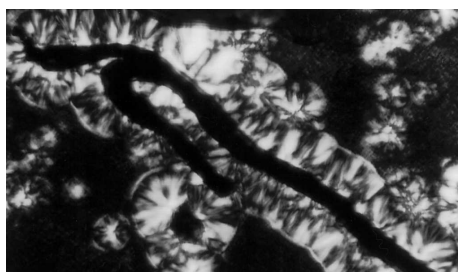


Fig. 1.6: Fibers showing transcrystallinity in kenaf-PP composites. Borrowed from ref. [5].

### 1.3.1 Transcrystallization on Fibers

Although Sanadi and Caulfield [5] stated that the transcrystallinity developed on surfaces complicates the mechanisms of stress transfer from the matrix to the fiber, Klein *et al.* [47] demonstrated that the transcrystalline layer has higher Young's modulus than bulk material. Another authors also admits controversy of this layer on the polymer/fiber interfacial strength [4, 48]. In any case, the transcrystallization changes the composite morphology and PP was reported to be able to transcrystallize on various fibers including polytetrafluoroethylene (PTFE), carbon and vegetable fibers [4, 5, 47, 48]. A question then arises, whether the hydrophobized cellulose fiber surface will retain its quality towards the polyolefinic matrix. Improvement in nucleating activity then may lead to formation of thicker transcrystalline layer, on the other hand, suppression of this effect can give an advantage to nucleation of impurities in the bulk and subsequent consumption of material in spherulitic crystallization with fibers located on their edges.

Concerning cellulose and other particles such as mineral fillers, carbon or glass fibers, one is used to think about the surface presence no matter what is the state of the matrix. In case of mineral fillers (e.g. clay) it is true, but some materials tends to melt or dissolve in the polymer, which causes at certain temperature a homogeneous system with no surface present. For instance a commercial product NJStar NU-100, which is non-specific  $\beta$ -nucleating agent with chemical name *N,N'*-dicyclohexyl-2,6-naphthalene dicarboxamide, tends to dissolve in the PP melt and as the melt cools down, precipitate in a nano-rods or even a nano-network [19].

### 1.3.2 Nucleating Agents

NJStar NU-100 belongs among *non-specific* nucleating agents, which initiates crystallization of practically all possible isomorphs of PP. This contrast with *specific* nucleating agents, which are a group of substances with ability to nucleate crystallization of single isomorph [15]. In case of PP the non-specific nucleating agents are in fact usually understood as  $\beta$ -nucleating agents since the  $\beta$  isomorph crystallize with higher rate than the also-nucleated  $\alpha$  isomorph. This leads to formation of polymorphic material with both forms present, yet the  $\beta$  crystallites are predominant [19].

Nucleating ability of some substances was found by coincidence, and the very first nucleating agents were not originally used to nucleate the material. A good example are colorants such as  $\gamma$  modification of *trans* quinacridone, copper phthalocyanine, or isoindolinone (see Fig. 1.7) – all very active  $\beta$  nucleators [36, 38, 49].

The *N,N'*-dicyclohexyl-2,6-naphthalene dicarboxamide is one of the first non-coloring  $\beta$ -nucleating agents of PP. This substance was broadly studied by

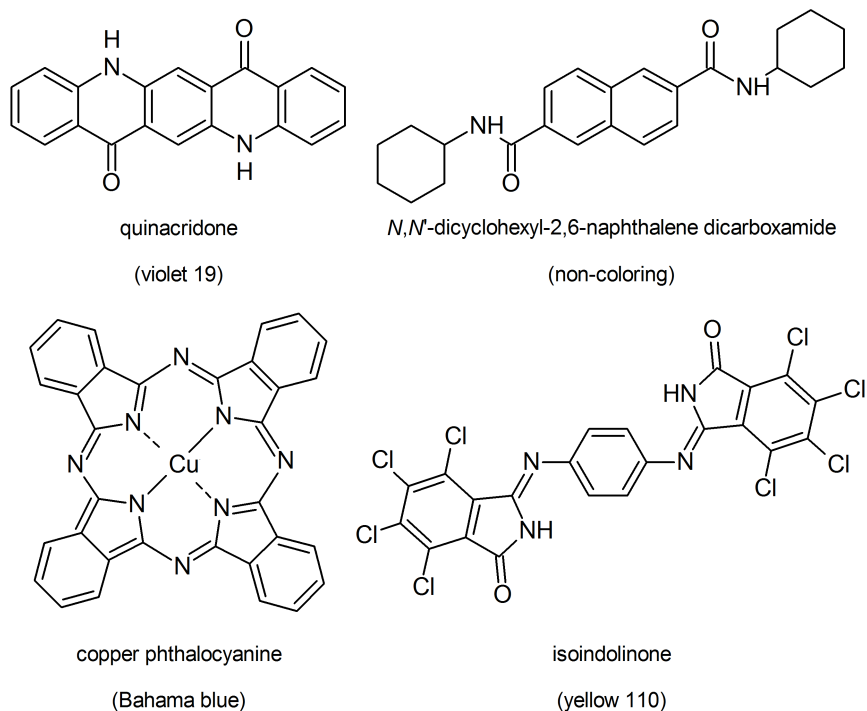


Fig. 1.7: Colorants with PP-nucleating activity and non-coloring NJStar NU-100 (top right).

many authors, who showed the orientation of the polymer lamella growth plane with respect to the nanocrystal of the nucleator [50], and the fact that both  $\alpha$  and  $\beta$  crystallites are nucleated at the same time, yet the  $\beta$  form is predominant due to its higher growth rate [19]. Thermal stability, ageing by photo-oxidation, mechanical properties and the structure of nucleated PP was broadly investigated by teams at Tomas Bata University in Zlín, which results were successfully published during the last decade [18, 31, 51–56].

### 1.3.3 Crystallization of Semi-Long Branches

Polyethylene (PE), which belongs to the polyolefine group together with mentioned PP, crystallizes also in the folded lamellae structure. This crystallization is logically influenced by the macromolecular chain branching – predominantly linear chains of high-density polyethylene (HDPE) are easily packed into crystallites in contrast with highly branched chains of low-density polyethylene (LDPE) [57]. Many catalytic systems and processing technologies have been developed since the first commercial production of PE. Each of them for to create specific branch structure – amount, length, or distribution along the main macromolecular chain [58, 59].

Non like the LDPE, which is synthesized by free radical polymerization, linear low-density polyethylene (LLDPE) is usually produced with metallocene catalysts which results in linear chain with only short branches created by incorporated comonomer. But-1-ene, hex-1-ene, or oct-1-ene is then commonly used in the copolymerization to disrupt the linearity of the chain and reduction of its ability to crystallize. On the other hand, metallocene catalysts can provide regular comonomer distribution, since the metallocene supramolecular structure enable tailoring of the macromolecule configuration. Although these catalysts were broadly studied and applied primarily in polymerization of stereoregular PP, they were also successfully used for copolymerization of LLDPE [60–65].

For instance, Kaminsky *et al.* [63] showed that cocatalyst system based on zirconocene and methylaluminumoxane (MAO) is very active system for the copolymerization of ethylene and oct-1-ene. This zirconocene/MAO was used to prepare several ethylene- $\alpha$ -olefin copolymers where the oct-1-ene, dodec-1-ene, octadec-1-ene, and hexacos-1-ene were used as comonomers. Obtained LLDPEs had regular side-chains distribution along the main chain, and their properties were subject to many studies [66–68].

Generally agreed models also suppose that the side chains are incorporated in the amorphous phase, and only a small portion of the side chain atoms are located inside crystalline regions, where they create packing errors [69]. On the contrary, Piel *et al.* suggested that in some cases these short chains, namely those based on rather long comonomers, can crystallize and possibly create separated aggregates [67]. Lamella of the main chain – its fold surface, then can act as an nucleator which may facilitate the nucleation and crystallization process by arranging short chains into spatial vicinity.

## 2 AIMS

Polyolefins are versatile materials with favorable price-performance ratio. Therefore, understanding their crystallization process and ways how to tailor it can bring new applications and potential replacement of more expensive polymers and/or materials with difficult processing. In case of current materials a controlled crystallization may also create a specific structure with potentially enhanced mechanical properties, which can make e.g. filling with mineral or glass fibers unnecessary.

Thus, the aims of this thesis are experimental study of the crystallization process primarily on polyethylene and polypropylene samples. The study can be divided into following points:

- Investigation of structure of linear low-density polyethylene with regular distribution of long comonomer in order to verify possible crystallization of side chains created by incorporated comonomer.
- Chemical hydrophobization of cellulose microparticles to increase its compatibility with polyolefinic matrix and check of its ability to nucleate crystal growth.
- $\beta$ -nucleation of isotactic polypropylene with different nucleating agents and investigation of thermal behavior under controlled crystallization process by means of conventional differential scanning calorimetry and flash differential scanning calorimetry.

## 3 METHODS

This chapter is a brief introduction of material preparation and analytic methods, which will be used in the doctoral study.

### 3.1 Material Preparation

Nucleated material may be either obtained in commercial grade from supplier, or nucleated in house, which is rather complicated operation involving seeding the material with usually tiny amount of the nucleating agent. The process consist of at least two steps – the first is preparing of masterbatch with nucleating agent at concentrations of about several percents. Second step is dissolving this initial concentration by mixing the masterbatch into large amount of pure material with masterbatch : pure material ratio close to 1 : 100. When smaller concentrations are required, then this material is diluted further with pure material. This consecutive processing is needed to obtain very homogeneous distribution of the nucleating agent, however, repetitive melting may induce degradation.

Test specimen preparation is needed namely for standardized testing such as mechanical tests are. The test specimen shape with tolerances and conditioning is usually included in the relevant ISO or ASTM standard.

### 3.2 Thermal Analysis

Thermal analysis is together with X-ray structural analysis widely used in case of polymeric materials. Non like the X-ray analysis, the thermal analysis is destructive method, which heats, cools, or burns small amount of sample material. Intended study will use primarily differential scanning calorimetry (DSC), which typically heats and/or cools sample with programmed rate of several  $K/min$  up to a hundred  $K/min$ . In addition, newly introduced chip-calorimeter technology, commonly denoted as flash DSC (FDSC), can simulate processes at the very same heating/cooling rates as observed in common processing – i.e. from several  $K/s$  up to tens of thousands  $K/s$ .

Either from the DSC or FDSC technology the amount of crystalline phase,  $x_c$ , can be calculated with Eq. 3.1, where the relative polymer amount  $\omega = 1$  in case of pure polymer and  $\omega < 1$  in case of composites.

$$x_c = \frac{\Delta H_m}{\omega \cdot \Delta H_m^0} \cdot 100 [\%] \quad (3.1)$$

The  $\Delta H_m$  is specific heat of melting, which derived from an area under the calorimetric curve, while the  $\Delta H_m^0$  is specific heat of melting of theoretic completely crystalline material, which is usually taken from relevant publications.

In addition, from Eq. 1.3 (page 12) one can easily calculate mean lamellar thickness,  $l$ , which is proportional to the peak of melting.

Beside the quantitative information, DSC can provide information also on the quality of the material, in other words, the crystallographic forms present in the material and possible nucleation activity of present additives.

### 3.3 X-Ray Structural Analysis

X-ray structural analysis is nondestructive tool for investigation of periodical structures within the material, which may be the periodicity of atoms within the crystals characterized by the inter planar spacing,  $d$ , or periodicity of lamellar stacking so-called *long period*,  $LP$ . The relevant relationships are defined with Eqs. 3.2 and 3.3. In these Eqs.  $n$  stands for the reflection order,  $\lambda$  is the wavelength of used radiation,  $\theta$  is angle between the incident beam and diffracting planes, and  $q$  is scattering vector defined as  $q = 4\pi \sin \theta / \lambda$ .

$$n\lambda = 2d \cdot \sin \theta \quad (3.2)$$

$$LP = 2\pi n / q \quad (3.3)$$

X-ray analysis is usually performed in two principal setups: one is measurement of diffracted radiation intensity in wide angle (wide-angle X-ray scattering, WAXS), which then gives  $d$ , the other is measurement in small angle (small-angle X-ray scattering, SAXS), which is measured in angles  $2\theta < 5^\circ$ . SAXS is sensitive to change in electron density in long distances, which is in fact the  $LP$ .

Beside the obvious length,  $d$  and  $LP$ , both methods can provide another information. For example the crystallinity,  $X_c$ , can be derived from the intensities,  $I_c$  and  $I_a$ , measured by WAXS (Eq. 3.4) is common for many materials, although it is rather empirical. The relevant peaks of crystalline phase reflections are mentioned in literature, for example Turner-Jones *et al.* [28] in case of PP takes reflections of planes (100), (040) and (130) of the  $\alpha$  form, and (300) of the  $\beta$  form [28, 29].

$$X_c = \frac{\sum I_c}{\sum I_c + \sum I_a} \cdot 100 [\%] \quad (3.4)$$

Turner-Jones *et al.* [29] also published fraction, here presented as Eq. 3.5, which may be used for division of the total crystallinity,  $X_c$ , to the amount of

$\beta$ -form (Eq. 3.6) and indirectly to the amount of  $\alpha$ -form (Eq. 3.7).

$$K_{\beta} = \frac{I_{(300)}^{\beta}}{I_{(300)}^{\beta} + I_{(100)}^{\alpha} + I_{(040)}^{\alpha} + I_{(130)}^{\alpha}} \quad (3.5)$$

$$X_{\beta} = K_{\beta} \cdot X_c \quad (3.6)$$

$$X_{\alpha} = X_c - X_{\beta} \quad (3.7)$$

In case of isotropic material and statistically homogeneous distribution of lamellae and amorphous phase,  $LP$  provided by SAXS method can give mean thickness of the lamellar structures,  $l_a$ , according to Eq. 3.8, which then subtracted from  $LP$  gives thickness of the inter-lamellar amorphous regions,  $l_a$ , Eq. 3.9.

$$l_c = \frac{X_c}{100[\%]} \cdot LP \quad (3.8)$$

$$l_a = LP - l_c \quad (3.9)$$

Furthermore, sufficiently small structures cause broadening of the measured reflections, thus the WAXS-related peaks may be used for calculation of size of the relevant structure with Scherrer Eq. 3.10 in which  $K$  is a constant selected according to refracting particle shape and  $B$  is full width at half maximum of the relevant reflection peak. In case of polymer bulk, the  $L_{(hkl)}$  value is usually not giving information about the total size, but rather length of part of perfect structure with no distortion, since the  $L_{(hkl)}$  may be also expressed as mean number,  $\bar{N}$ , of parallel  $(hkl)$  planes multiplied by their normal distance,  $d_{(hkl)}$ , as presented in Eq. 3.10 [70].

$$L_{(hkl)} = \frac{K \cdot \lambda}{B \cdot \cos \theta} \approx \bar{N} \cdot d_{(hkl)} \quad (3.10)$$

### 3.4 Optical Microscopy

Optical microscopy is a direct method for observing structure of materials in which different using of visible light reveals different qualities of the material. Two basic setups are transmission and reflection mode. The former uses thin slices of material through which the light passes. This method can reveal namely fillers and quality of their dispersion and distribution, or material defect such as holes, shrinkage etc. The latter setup is used to observe surface of the material, which is usually done in case of investigation of surface integrity, roughness, or degradation. Frequently and not only in case of polymers, the transmission mode is modified into polarized-light microscopy by inserting two



polarizing filters below and above the sample. This modification then helps to gain contrast and additional information on the structure namely in case of birefringent materials.

### **3.5 Mechanical Tests**

Mechanical testing is commonly done according to ISO standards. In case of plastic material, the proper standard intended to use are ISO 527 (Plastics – Determination of Tensile Properties), and ISO 179 (Plastics – Determination of Charpy impact properties).

## REFERENCES

- [1] J. Xu, Y. Ma, W. Hu, M. Rehahn, and G. Reiter. Cloning Polymer Single Crystals Through Self-Seeding. *Nature Materials*, 8(4):348–53, 2009.
- [2] J. Karger-Kocsis. *Polypropylene: Structure, Blends and Composites – Volume 1: Structure and Morphology*. Chapman&Hall, London, 1 edition, 1995.
- [3] K. Kawakami. Modification of Physicochemical Characteristics of Active Pharmaceutical Ingredients and Application of Supersaturatable Dosage Forms for Improving Bioavailability of Poorly Absorbed Drugs. *Advanced Drug Delivery Reviews*, 64(6):480–95, 2012.
- [4] B.G. Lee, S. Lee, and B.K. Via. Influence of Surface Morphology of the Kraft Pulp Fibers on the Growth of the Transcrystalline Layer of Polypropylene. *Journal of Applied Polymer Science*, pages 1958–1966, 2010.
- [5] A.R. Sanadi and D.F. Caulfield. Transcrystalline Interphases in Natural Fiber-PP Composites: Effect of Coupling Agent. *Composite Interfaces*, 7(1):31–43, 2000.
- [6] B. Wunderlich. *Macromolecular Physics. Volume 2: Crystal Nucleation, Growth, Annealing*. Academic Press, Inc., New York, 1976.
- [7] M. Hikosaka, K. Watanabe, K. Okada, and S. Yamazaki. Topological Mechanism of Polymer Nucleation and Growth—The Role of Chain Sliding Diffusion and Entanglement. *Interphases and Mesophases in Polymer Crystallization III*, pages 137–186, 2005.
- [8] F.L. Binsbergen. Heterogeneous Nucleation of Crystallization. *Progress in Solid State Chemistry*, 8:189–238, 1973.
- [9] B. Meissner and V. Zilvar. *Fyzika polymerů – Struktura a vlastnosti polymerních materiálů*. SNTL, Praha, 1987.
- [10] J.W. Gibbs. On the Equilibrium of Heterogeneous Substances. In *Transactions of the Connecticut Academy of Arts and Sciences*, volume 3, pages 108–248 and 343–520. New Haven, 1874.
- [11] H. Janeschitz-Kriegl, E. Ratajski, and M. Stadlbauer. Flow as an Effective Promotor of Nucleation in Polymer Melts: A Quantitative Evaluation. *Rheologica Acta*, 42(4):355–364, 2003.
- [12] H. Janeschitz-Kriegl and E. Ratajski. Some Fundamental Aspects of the Kinetics of Flow-Induced crystallization of polymers. *Colloid and Polymer Science*, 288(16-17):1525–1537, 2010.
- [13] J.K. Fink. *A Concise Introduction to Additives for Thermoplastic Polymers*. Wiley, Salem, 2010.
- [14] A. Menyhard, M. Gahleitner, J. Varga, K. Bernreitner, P. Jaaskelainen, H. Oysaed, and B. Pukanszky. The Influence of Nucleus Density on Optical Properties in Nucleated Isotactic Polypropylene. *European Polymer Journal*, 45(11):3138–3148, 2009.
- [15] J. Varga, I. Mudra, and G.W. Ehrenstein. Highly Active Thermally Stable  $\beta$ -Nucleating Agents for Isotactic Polypropylene. *Journal of applied polymer science*, 74(10):2357–2368, 1999.
- [16] M. Gahleitner and J. Wolfschwenger. Polymer Crystal Nucleating Agents. In K.H.J. Buschow, R Cahn, MC Flemings, B Ilschner, EJ Kramer, S Mahajan, and P Veysiere, editors, *Encyclopedia of Materials: Science and Technology*, pages 7239–7244. Elsevier, Oxford, 2001.
- [17] J. Varga.  $\beta$ -Modification of Isotactic Polypropylene: Preparation, Structure, Processing, Properties, and Application. *Journal of Macromolecular Science, Part B*, 41(4):1121–1171, 2002.

- [18] M. Obadal, R. Cermak, and K. Stoklasa. Tailoring of Three-Phase Crystalline Systems in Isotactic Poly(propylene). *Macromolecular Rapid Communications*, 26(15):1253–1257, 2005.
- [19] J. Varga and A. Menyhard. Effect of Solubility and Nucleating Duality of N,N'-Dicyclohexyl-2,6-naphthalenedicarboxamide on the Supermolecular Structure of Isotactic Polypropylene. *Macromolecules*, 40(7):2422–2431, 2007.
- [20] D. Braga, F. Grepioni, L. Maini, and M. Polito. Crystal Polymorphism and Multiple Crystal Forms. In M.W. Hosseini, editor, *Molecular Networks*, volume 132 of *Structure and Bonding*, pages 87–95. Springer, 2009.
- [21] S. Muñoz Guerra and A. Prieto. Lamellar Structure and Morphology of Odd Nylon Crystals. In M. Dosière, editor, *Crystallization of Polymers*, volume 405 of *NATO ASI Series*, pages 277–282. Springer, 1993.
- [22] B.L. Deopura and A.K. Mukherjee. Nylon 6 and Nylon 66 Fibres. In V.B. Gupta and V.K. Kothari, editors, *Manufactured Fibre Technology*, pages 318–359. Springer Netherlands, 1997.
- [23] P. Duhovic M., Maitrot and S. Fakirov. Polyamide 66 Polymorphic Single Polymer Composites. *The Open Macromolecules Journal*, 3:37–40, 2009.
- [24] P. Pan and Y. Inoue. Polymorphism and Isomorphism in Biodegradable Polyesters. *Progress in Polymer Science*, 34(7):605–640, 2009.
- [25] B. Lotz and J.C. Wittmann. Isotactic Polypropylene: Growth Transitions and Crystal Polymorphism. In J.F. Jansson and U.W. Gedde, editors, *Solidification Processes in Polymers*, volume 87 of *Progress in Colloid & Polymer Science*, pages 2–7. Steinkopff, 1992.
- [26] B. Lotz, J.C. Wittmann, and A.J. Lovinger. Structure and Morphology of Poly(propylenes): A Molecular Analysis. *Polymer*, 37(22):4979–4992, 1996.
- [27] S. Brückner and S.V. Meille. Polymorphism in Crystalline Polypropylene. In J. Karger-Kocsis, editor, *Polypropylene*, volume 2 of *Polymer Science and Technology Series*, pages 606–614. Springer Netherlands, 1999.
- [28] A. Turner-Jones, J.M. Aizlewood, and D.R. Beckett. Crystalline Forms of Isotactic Polypropylene. *Die Makromolekulare Chemie*, 75(1):134–158, 1964.
- [29] A. Turner-Jones and A.J. Cobbold. The  $\beta$  Crystalline Form of Isotactic Polypropylene. *Journal of Polymer Science Part B: Polymer Letters*, 6(8):539–546, 1968.
- [30] R. Androsch, M.L. Di Lorenzo, C. Schick, and B. Wunderlich. Mesophases in Polyethylene, Polypropylene, and Poly(1-butene). *Polymer*, 51(21):4639–4662, 2010.
- [31] J. Vychopnova, V. Habrova, M. Obadal, R. Cermak, and R. Cabla. Crystallization of Polypropylene with a Minute Amount of  $\beta$ -Nucleator. *Journal of Thermal Analysis and Calorimetry*, 86(3):687–691, 2006.
- [32] H.D. Keith, F.J. Padden, N.M. Walter, and H.W. Wyckoff. Evidence for a Second Crystal Form of Polypropylene. *Journal of Applied Physics*, 30(10):1485–1488, 1959.
- [33] F.L. Binsbergen. Heterogeneous Nucleation in the Crystallization of Polyolefins: Part 1. Chemical and Physical Nature of Nucleating Agents. *Polymer*, 11(5):253–267, 1970.
- [34] T. Sterzynski, P. Calo, M. Lambla, and M. Thomas. Quinacridone Nucleation of Isotactic Polypropylene. *Polymer Engineering and Science*, 37(12):1917–1927, 1997.
- [35] Z. Bartczak, A.S. Argon, Cohen. R.E., and M. Weinberg. Toughness Mechanism in Semi-Crystalline Polymer Blends: II. High-Density Polyethylene Toughened with Calcium Carbonate Filler Particles. *Polymer*, 40(9):2347–2365, 1999.
- [36] S. Suzuki and J. Mizuguchi. Pigment-Induced Crystallization in Colored Plastics Based on Partially Crystalline Polymers. *Dyes and Pigments*, 61(1):69–77, 2004.

- [37] H. Quan, Z.M. Li, M.B. Yang, and R. Huang. On Transcrystallinity in Semi-Crystalline Polymer Composites. *Composites Science and Technology*, 65(7-8):999–1021, 2005.
- [38] D. Lee Wo and R.I. Tanner. The Impact of Blue Organic and Inorganic Pigments on the Crystallization and Rheological Properties of Isotactic Polypropylene. *Rheologica Acta*, 49(1):75–88, 2009.
- [39] X. Huang, Q. Ke, C. Kim, H. Zhong, P. Wei, G. Wang, F. Liu, and P. Jiang. Nonisothermal Crystallization Behavior and Nucleation of LDPE/Al Nano- and Microcomposites. *Polymer Engineering & Science*, 47(7):1052–1061, 2007.
- [40] J. George, M.S. Sreekala, and S. Thomas. A Review on Interface Modification and Characterization of Natural Fiber Reinforced Plastic Composites. *Polymer Engineering & Science*, 41(9):1471–1485, 2001.
- [41] M.N. Belgacem and A. Gandini. The Surface Modification of Cellulose Fibres for Use as Reinforcing Elements in Composite Materials. *Composite Interfaces*, 12(1):41–75, 2005.
- [42] Z. Dominkovics, L. Danyadi, and B. Pukanszky. Surface Modification of Wood Flour and Its Effect on the Properties of PP/Wood Composites. *Composites Part A: Applied Science and Manufacturing*, 38(8):1893–1901, 2007.
- [43] A.G. Cunha and A. Gandini. Turning Polysaccharides into Hydrophobic Materials: A Critical Review. Part 1. Cellulose. *Cellulose*, 17(5):875–889, 2010.
- [44] T. Heinze and T. Liebert. Unconventional Methods in Cellulose Functionalization. *Progress in Polymer Science*, 26(9):1689–1762, 2001.
- [45] P. Uschanov, L.S. Johansson, S.L. Maunu, and J. Laine. Heterogeneous Modification of Various Celluloses with Fatty Acids. *Cellulose*, 18(2):393–404, 2010.
- [46] S. Zhang, M.L. Minus, L. Zhu, C.P. Wong, and S. Kumar. Polymer Transcrystallinity Induced by Carbon Nanotubes. *Polymer*, 49(5):1356–1364, 2008.
- [47] N. Klei, G. Marom, A. Pegoretti, and C. Migliaresi. Determining the Role of Interfacial Transcrystallinity in Composite Materials by Dynamic Mechanical Thermal Analysis. *Composites*, 26(10):707–712, 1995.
- [48] C. Wang and C.R. Liu. Transcrystallization of Polypropylene Composites: Nucleating Ability of Fibres. *Polymer*, 40(2):289–298, 1999.
- [49] J. Broda. Nucleating Activity of the Quinacridone and Phthalocyanine Pigments in Polypropylene Crystallization. *Journal of Applied Polymer Science*, 90(14):3957–3964, 2003.
- [50] M. Yamaguchi, T. Fukui, K. Okamoto, S. Sasaki, Y. Uchiyama, and C. Ueoka. Anomalous Molecular Orientation of Isotactic Polypropylene Sheet Containing N,N'-dicyclohexyl-2,6-naphthalenedicarboxamide. *Polymer*, 50(6):1497–1504, 2009.
- [51] R. Cermak, M. Obadal, P. Ponizil, M. Polaskova, K. Stoklasa, and A. Lengalova. Injection-Moulded  $\alpha$ - and  $\beta$ -Polypropylenes: I. Structure vs. Processing Parameters. *European Polymer Journal*, 41(8):1838–1845, 2005.
- [52] M. Obadal, R. Cermak, M. Raab, V. Verney, S. Commereuc, and F. Fraisse. Structure Evolution of  $\alpha$ - and  $\beta$ -Polypropylenes upon UV Irradiation: A Multiscale Comparison. *Polymer Degradation and Stability*, 88(3):532–539, 2005.
- [53] R. Cermak, M. Obadal, P. Ponizil, M. Polaskova, K. Stoklasa, and J. Heckova. Injection-Moulded  $\alpha$ - and  $\beta$ -Polypropylenes: II. Tensile Properties vs. Processing Parameters. *European Polymer Journal*, 42(9):2185–2191, 2006.
- [54] J. Vychopnova, R. Cermak, M. Obadal, M. Raab, V. Verney, and S. Commereuc. The Role of Specific Nucleation in Polypropylene Photodegradation. *Polymer Degradation and Stability*, 92(10):1763–1768, 2007.

- [55] L. Chvatalova, J. Navratilova, R. Cermak, M. Raab, and M. Obadal. Joint Effects of Molecular Structure and Processing History on Specific Nucleation of Isotactic Polypropylene. *Macromolecules*, 42(19):7413–7417, 2009.
- [56] J. Vychopnova, R. Cermak, M. Obadal, V. Verney, and S. Commereuc. Effect of  $\beta$ -Nucleation on Crystallization of Photodegraded polypropylene. *Journal of Thermal Analysis and Calorimetry*, 95(1):215–220, 2009.
- [57] J. Mleziva and J. Šňupárek. *Polymery: Výroba, struktura, vlastnosti a použití*. Sobotáles, Praha, 2000.
- [58] B. Abu-Sharkh and I.A. Hussein. MD Simulation of the Influence of Branch Content on Collapse and Conformation of LLDPE Chains Crystallizing from Highly Dilute Solutions. *Polymer*, 43(23):6333–6340, 2002.
- [59] M. Zhang, D.T. Lynch, and S.E. Wanke. Effect of Molecular Structure Distribution on Melting and Crystallization Behavior of 1-Butene/Ethylene Copolymers. *Polymer*, 42(7):3067–3075, 2001.
- [60] W. Kaminsky. Zirconocene Catalysts for Olefin Polymerization. *Catalysis Today*, 20(2):257–271, 1994.
- [61] W. Kaminsky. New Polymers by Metallocene Catalysis. *Macromolecular Chemistry and Physics*, 197(12):3907–3945, 1996.
- [62] W. Kaminsky, A. Hopf, and C. Piel. Cs-Symmetric Hafnocene Complexes for Synthesis of Syndiotactic Polypropene. *Journal of Organometallic Chemistry*, 684(1-2):200–205, 2003.
- [63] W. Kaminsky. Tailoring Polyolefins by Metallocene Catalysis: Kinetic and Mechanistic Aspects. *Journal of Molecular Catalysis A: Chemical*, 213(1):15–19, 2004.
- [64] A. Razavi and U. Thewalt. Site Selective Ligand Modification and Tactic Variation in Polypropylene Chains Produced with Metallocene Catalysts. *Coordination Chemistry Reviews*, 250(1-2):155–169, 2006.
- [65] K. Klimke, M. Parkinson, C. Piel, W. Kaminsky, H.W. Spiess, and M. Wilhelm. Optimisation and Application of Polyolefin Branch Quantification by Melt-State  $^{13}\text{C}$  NMR Spectroscopy. *Macromolecular Chemistry and Physics*, 207(4):382–395, 2006.
- [66] C. Piel, P. Starck, J.V. Seppälä, and W. Kaminsky. Thermal and Mechanical Analysis of Metallocene-Catalyzed Ethene- $\alpha$ -Olefin Copolymers: The Influence of the Length and Number of the Crystallizing Side Chains. *Journal of Polymer Science Part A: Polymer Chemistry*, 44(5):1600–1612, 2006.
- [67] C. Piel, F.J. Stadler, J. Kaschta, S. Rulhoff, H. Münstedt, and W. Kaminsky. Structure-Property Relationships of Linear and Long-Chain Branched Metallocene High-Density Polyethylenes Characterized by Shear Rheology and SEC-MALLS. *Macromolecular Chemistry and Physics*, 207(1):26–38, 2006.
- [68] F.J. Stadler, C. Piel, K. Klimke, J. Kaschta, M. Parkinson, M. Wilhelm, W. Kaminsky, and H. Münstedt. Influence of Type and Content of Various Comonomers on Long-Chain Branching of Ethene/ $\alpha$ -Olefin Copolymers. *Macromolecules*, 39(4):1474–1482, 2006.
- [69] F.J. Stadler. Lattice sizes, Crystallinities, and Spacing Between Amorphous Chains – Characterization of Ethene-/ $\alpha$ -Olefin Copolymers with Various Comonomers and Comonomer Contents Measured by Wide Angle X-Ray Scattering. *e-Polymers*, page 040, 2009.
- [70] L.E. Alexander. *X-ray Diffraction Methods in Polymer Science*. Wiley, New York, 1969.

## LIST OF PAPERS

- ARTICLE I:** Janicek M., R. Cermak, M. Obadal, C. Piel, and P. Ponizil. Ethylene Copolymers with Crystallizable Side Chains. *Macromolecules*, 44(17):6759–6766, 2011. DOI: 10.1021/ma201017m  
Share: 30 %
- ARTICLE II:** Janicek M., O. Krejci, and R. Cermak. Thermal Stability of Surface-Esterified Cellulose and its Composite with Polyolefinic Matrix. *Cellulose*, 20(6):2745–2755, 2013. DOI: 10.1007/s10570-013-0070-9  
Share: 70 %
- ARTICLE III:** Janicek M., M. Polaskova, R. Holubar, and R. Cermak. Surface-Esterified Cellulose Fiber in a Polypropylene Matrix: Impact of Esterification on Crystallization Kinetics and Dispersion. *Cellulose*, 21(6):4039–4048, 2014. DOI: 10.1007/s10570-014-0404-2  
Share: 60 %
- ARTICLE IV:** Janicek M., R. Holubar, M. Polaskova, and R. Cermak. Crystallization of Nucleated Isotactic Polypropylene Studied by Means of Conventional and Flash Differential Scanning Calorimetry. *submitted article*  
Share: 60 %

## SUMMARIES OF PAPERS

### Paper I

Metallocene-catalyzed copolymers of ethylene and  $\alpha$ -olefins were investigated by X-ray scattering and differential scanning calorimetry. Evaluated  $\alpha$ -olefin comonomers consisted of 8, 12, 18, or 26 carbons. As it was indicated in the small-angle X-ray scattering, ethylene–hexacosene copolymer with comonomer content of 3 mol % may contain second crystallites. Because no other reflections were observed in the wide-angle X-ray scattering patterns, the side-chain crystallites should have the same crystal lattice dimensions as the prevailing main-chain crystallites. Since this potential side chains crystallization can only be found in the ethylene–hexacosene copolymer with 3 mol % of comonomer, a critical concentration of long-chain comonomer should be reached for this secondary crystallite formation. It was also found that the thickness of the interlamellar amorphous layer stays virtually constant regardless of the changes in comonomer content and side-chain length.

### Paper II

Thermal stability of hydrophobized cellulose powders was investigated from the perspective of potential use as filler in non-polar polyolefinic matrix. The hydrophobization was done by heterogeneous esterification with three carboxylic acids which differ in chain length (3, 10 and 18 carbons). Data measured by means of thermogravimetry were recalculated according to model-free iso-conversional method to construct time–temperature plots. It was demonstrated that the esterification significantly decreases thermal stability of the material, which reduces feasible processing window. Under non-oxidative atmosphere, the single-step decomposition of materials is prevailing, while the process is more complex in air. In both cases the oleic acid esters showed the lowest stability and the original cellulose was the most stable. Finally, all powders were compounded with polyethylene or polypropylene. Obtained composites were then subjected to color measurement and thermogravimetry. Even though the materials were partly degraded, which was indicated by the yellowish hue of the composites, virtually no impact of the filler pyrolysis on the polymer matrix decomposition was observed, particularly in case of decanoyl esters.

### Paper III

Cellulose powders hydrophobized by surface-esterification with carboxylic acids which differ in chain length (3, 10 and 18 carbons) were dispersed in polypropylene matrix. Quality of the dispersion and the nucleation activity of the filler were investigated by means of differential scanning calorimetry and optical microscopy. The results showed that the esterification decreases the crystallization

rate in case of cellulose esterified with propionic or decanoic acid. On the other hand, the oleic acid ester demonstrated slightly higher crystallization rates than the unmodified cellulose, which was ascribed primarily to the newly arisen non-esterified surface after disintegration of the filler. Optical microscopy with hot stage showed high nucleation ability of the natural cellulose fiber and its suppression in case of esterified surfaces. A complete inability to nucleate polypropylene crystallization was observed in case of decanoyl ester, while the other two retained some activity; yet lower than the natural fiber. Finally, analysis of the filler dispersion and distribution revealed that the decanoyl and octadecanoyl esters disintegrate during melt mixing, while both dispersion and distribution of the fibers modified with propionic acid is poor.

## **Paper IV**

Thermal behavior and structure of the neat and nucleated iPP is studied in this paper. The nucleation agents were common colorants which possess either  $\alpha$ -nucleating (phthalocyanine and indolone), or non-specific (quinacridone) nucleating activity. Besides the colorants, a non-coloring commercially available NJ Star NU-100 is used in the study. Nucleation ability and efficiency of the individual substances in concentration of 0.1 wt. % and under extreme cooling rates provided by flash differential scanning calorimetry (DSC) are assessed within this paper. The records obtained from flash DSC showed no evidence of the  $\beta$  phase presence, even though the melting of  $\beta$  phase is observed by the conventional DSC for the corresponding material. Concerning the high cooling rates, the absence of the  $\beta$  phase was probably caused by higher crystallization rate of the  $\alpha$  phase at the given temperatures of isothermal crystallization, or given cooling rates during the non-isothermal study. For the studied material, the measurements showed that neat polypropylene cease to crystallize at cooling rates of about 250 K/s, while the nucleated materials are still crystallizing up to the cooling rates of about 600 K/s at which the amount of amorphous material grows. There was no crystallization observed when cooled with rates above 1200 K/s.



# CONTRIBUTION TO THE SCIENCE AND PRACTICE

## Paper I

From the scientific point of view, the Paper I contributed to the knowledge on the crystallization ability and morphology of the short and semi-long branches of LLDPE. This knowledge may be used in future for instance to compatibilize different materials to possess better surface interaction, thus enhanced mechanical properties.

## Paper II

Paper II is chronological predecessor of the Paper III in which the same surface-esterified cellulose was used. This paper showed the decrease in thermal stability with increase in length of the carboxylic acid chain length. Recalculation of the obtained data into the time-temperature-degradation plots then serves as an easy way to predict feasibility of melt mixing of the thermally less stable esters.

## Paper III

Transcrystallization of iPP on cellulose fibers could be used both - to nucleate material, thus speed up the processing cycle, and to change morphology of the matrix. Unfortunately, the esterification decreases the ability of the cellulose fiber to nucleate and more over, it causes the fibers to break. On the other hand, this may be somehow used in practice when the fibrous character is not necessary, because the esterified cellulose was better dispersed and evenly distributed.

## Paper IV

The study presented within this article revealed the critical cooling rates for the used nucleating agents, above which the material does not crystallize. Besides, the high speeds of cooling proved that the materials nucleated with non-specific nucleating agents are predominantly created by  $\alpha$  phase. This imply, even the  $\beta$ -nucleated material may possess  $\alpha$  phase in the skin layers, which freezes the most rapidly, especially during injection molding.

## AUTHOR'S PUBLICATIONS

### *Articles in Journals Listed in Thompson Reuters' Journal Citation Reports*

1. **Janicek M.**, R. Cermak, M. Obadal, C. Piel, and P. Ponizil. Ethylene Copolymers with Crystallizable Side Chains. *Macromolecules*, 44(17):6759–6766, 2011. DOI: 10.1021/ma201017m
2. **Janicek M.**, O. Krejci, R. Cermak. Thermal stability of surface-esterified cellulose and its composite with polyolefinic matrix. *Cellulose*, 20(6):2745–2755, 2013. DOI: 10.1007/s10570-013-0070-9
3. **Janicek M.**, M. Polaskova, R. Holubar, and R. Cermak. Surface-Esterified Cellulose Fiber in Polypropylene Matrix: Impact of Esterification on Crystallization Kinetics and Dispersion. *Cellulose*, 21(6):4039–4048, 2014. DOI: 10.1007/s10570-014-0404-2
4. **Janicek M.**, R. Holubar, M. Polaskova, and R. Cermak. Crystallization of Nucleated Isotactic Polypropylene Studied by Means of Conventional and Flash Differential Scanning Calorimetry. *submitted article*

### *Conference Contribution Listed in SCOPUS*

1. **Janicek M.**, R. Cermak, and P. Ponizil. Morphology of polyethylene with regular side chains distribution. Corfu Island, Greece, July 14–16, 2011. In: *Recent Researches in Geography, Geology, Energy, Environment and Biomedicine – Proceedings of the 4<sup>th</sup> WSEAS International Conference on EMESEG'11, 2<sup>nd</sup> International Conference on WORLD-GEO'11, 5<sup>th</sup> International Conference on EDEB'11*, pp. 312–317. ISBN 978-1-61804-022-0.

### *Articles in Czech Journal*

1. **Janíček M.**, R. Čermák, M. Obadal, and P. Ponižil. Krystalizace bočních řetězců u etylenových kopolymerů. *Plasty a Kaučuk*, 48(7–8):199–205, 2011.
2. **Janíček M.**, O. Krejčí, R. Holubář, and R. Čermák. Zvýšení hydrofobity celulóзовého povrchu esterifikací: Teplotní stabilita plniva a kompozitu. *Plasty a Kaučuk*, 50(11–12):339–345, 2013.

### *Patents and Utility Models*

1. **Janicek M.**, O. Grulich, A. Mracek, and P. Bures. Device for surface treatment by plasma generated under normal pressure. Czech Republic, Utility Model Reg.No. 26261. 2013-11-08.

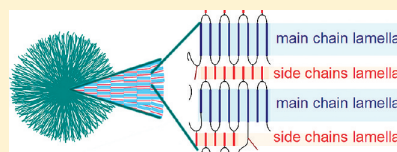
## **ARTICLE I**



## Ethylene Copolymers with Crystallizable Side Chains

Miroslav Janicek,<sup>\*,†</sup> Roman Cermak,<sup>†,‡</sup> Martin Obadal,<sup>§</sup> Christian Piel,<sup>§</sup> and Petr Ponizil<sup>†,‡,⊥</sup><sup>†</sup>Faculty of Technology, Department of Polymer Engineering, Tomas Bata University in Zlin, nam. T. G. Masaryka 275, 762 72 Zlin, Czech Republic<sup>‡</sup>University Institute, Centre of Polymer Systems, Tomas Bata University in Zlin, Nad Ovcirnou 3658, 760 01 Zlin, Czech Republic<sup>§</sup>Borealis Polyolefine GmbH, St. Peter Strasse 25, 4021 Linz, Austria<sup>⊥</sup>Faculty of Technology, Department of Physics and Material Engineering, Tomas Bata University in Zlin, nam. T. G. Masaryka 275, 762 72 Zlin, Czech Republic

**ABSTRACT:** Metallocene-catalyzed copolymers of ethylene and  $\alpha$ -olefins were investigated by X-ray scattering and differential scanning calorimetry. Evaluated  $\alpha$ -olefin comonomers consisted of 8, 12, 18, or 26 carbons. As indicated from the small-angle X-ray scattering, ethylene–hexacosene copolymer with comonomer content of 3 mol % may contain second crystallites. Because no other reflections were observed in the wide-angle X-ray scattering patterns, the side-chain crystallites should have the same crystal lattice dimensions as the prevailing main-chain crystallites. Since this potential side chains crystallization can only be found in the ethylene–hexacosene copolymer with 3 mol % of comonomer, a critical concentration of long-chain comonomer should be reached for this secondary crystallite formation. It was also found that the thickness of the interlamellar amorphous layer stays virtually constant regardless of the changes in comonomer content and side-chain length.



## ■ INTRODUCTION

Linear low-density polyethylene (LLDPE) is a copolymer of ethylene with small percentage of but-1-ene, hex-1-ene, or oct-1-ene, which represents a significant portion of 60 million tons worldwide annual production of polyethylenes (PE).<sup>1</sup> LLDPE could be produced using Ziegler–Natta catalysts, resulting in random comonomer distribution in the main chain.<sup>2–4</sup> On the other hand, metallocene catalysts can provide regular comonomer distribution, since the metallocene supramolecular structure enable tailoring of the macromolecule configuration.<sup>5–8</sup> Although these catalysts were broadly studied and applied primarily in polymerization of stereoregular polypropylene,<sup>8–12</sup> they were also successfully used for copolymerization of LLDPE.<sup>6</sup>

Kaminsky et al.<sup>3</sup> showed that cocatalyst system based on zirconocene and methylaluminoxane (MAO) is very active system for the copolymerization of ethylene and oct-1-ene. This zirconocene/MAO was used to prepare several ethylene– $\alpha$ -olefin copolymers where the oct-1-ene, dodec-1-ene, octadec-1-ene, and hexacos-1-ene were used as comonomers. Obtained LLDPEs had regular side-chains distribution along the main chain, and their properties were subject to study elsewhere.<sup>5,13–16</sup>

It is commonly known that the macroscopic properties of polyolefins strongly depend on the chain structure, and therefore, the quality of PE in both molten and solid state could be tuned by presence of side chains of various lengths and quantities. This dependence is caused by steric hindrances of the side chains what affects primarily the polymer crystallinity.<sup>5,7</sup> Generally agreed models also suppose that the side chains are incorporated in the amorphous phase, and only a small portion of the side-chain atoms

are located inside crystalline regions, where they create packing errors.<sup>13</sup> On the contrary, Piel et al.<sup>16</sup> suggested that in some cases these short chains, namely those based on rather long comonomers, can crystallize and possibly create separated aggregates. The present article directs attention to assess the presence of second crystalline phase using X-ray scattering (both the wide-angle and small-angle setup) and differential scanning calorimetry (DSC).

## ■ EXPERIMENTAL SECTION

**Materials.** Copolymers of ethylene with oct-1-ene, dodec-1-ene, octadec-1-ene, and hexacos-1-ene as a comonomer were synthesized by a technique outlined elsewhere.<sup>15–17</sup> They are here denoted according to the comonomer length (the number following the letter “C”) and the initial comonomer concentration (mol %) in a polymerization mixture (the number preceding the letter “C”), which fairly corresponds to the 1.5 and 3.0 mol % comonomer concentration in the macromolecule when comonomer conversion is considered. An overview of the copolymers and their previously published characteristics<sup>15–17</sup> is given in Table 1, where the reference ethylene homopolymer is denoted as L-PE.

**Differential Scanning Calorimetry.** The investigation of thermal behavior was done using a Perkin-Elmer Pyris 1 DSC power-compensated instrument calibrated with indium ( $T_m = 156.6$  °C). About 6–8 mg of each sample was closed in an aluminum pan and measured with an empty pan as a reference. All measurements were initiated by rapid heating (50 K min<sup>-1</sup>) from room temperature (20 °C) to 160 °C. At this temperature

Received: May 4, 2011

Revised: July 29, 2011

Published: August 17, 2011

Table 1. Ethylene Copolymers Characteristics and Branching Information Calculated from NMR and DSC Data by Piel et al.<sup>16,17</sup>

	$M_w$ [kg mol <sup>-1</sup> ]	MWD	comonomer conv <sup>a</sup> [%]	DSC			NMR	
				$T_m$ [°C]	$T_c$ [°C]	$x_c$ [%]	MSL <sup>b</sup> (bonds)	MSL <sup>c</sup> [Å]
L-PE	368	2.13	N/A	139.0	115.6	65.6	N/A	N/A
15C8	321	2.19	10.1	115.2	100.6	41.3	120	151.2
15C12	316	2.05	8.8	116.5	100.2	40.5	128	161.3
15C18	328	2.08	8.8	116.5	102.9	41.3	134	168.8
15C26	352	2.22	7.1	118.7	99.7	42.9	140	176.4
30C8	269	2.02	8.8	103.3	85.4	31.3	55	69.3
30C12	280	1.94	7.3	103.3	86.1	31.1	47	59.2
30C18	276	1.98	9.8	104.1	86.9	30.0	50	63.0
30C26	334	2.00	7.7	103.3	85.9	40.2	49	61.7

<sup>a</sup> Portion of the initial comonomer content incorporated into the macromolecule. <sup>b</sup> Methylene sequence length – the number of C–C bonds. <sup>c</sup> Methylene sequence length recalculated in Å; (MSL [Å]) = (MSL [bonds]/2) × 2.52).

the samples were kept isothermally for 5 min. Afterward, they were cooled with rate  $-10 \text{ K min}^{-1}$  down to  $20 \text{ °C}$ , and after 5 min of settling the material was heated with the same rate ( $10 \text{ K min}^{-1}$ ) back to  $160 \text{ °C}$ . All the measurements were performed under nitrogen as a purge constantly passing ( $20 \text{ mL min}^{-1}$ ) the DSC cells.

The values of each enthalpy change ( $\Delta H_m$ ) were gained using the instrument software, and they were recalculated using eq 1 to estimate crystallinity ( $x_c$ ) of each material.

$$x_c = \frac{\Delta H_m}{\Delta H_m^0} \times 100 \quad [\%] \quad (1)$$

The heat of fusion of fully crystallized PE ( $\Delta H_m^0 = 290 \text{ J g}^{-1}$ ) was taken from the value listed in previous publications.<sup>16,17</sup>

Lamellar thickness ( $L_c$ ) can be estimated from the position of a melting peak maximum by employing the Gibbs–Thomson equation (2) and the Flory equation (3).

$$T_m = T_m^c \left( 1 - \frac{2\sigma_c}{\Delta H_u L_c} \right) \quad (2)$$

$$\frac{1}{T_m^c} = \frac{1}{T_m^0} - \frac{R}{\Delta H_u} \ln X_c \quad (3)$$

$T_m$  is a melting temperature (maximum of melting peak),  $T_m^c$  stands for a copolymer melting temperature,  $X_c$  is a molar fraction of ethylene comonomer (for homopolymer  $X_c = 1$ ),  $T_m^0 = 418.6 \text{ K}$  represents an equilibrium melting temperature of PE,  $\Delta H_u = 2.96 \times 10^8 \text{ J m}^{-3}$  is a volumetric heat of fusion,  $\sigma_c = 0.09 \text{ J m}^{-2}$  represents a basal surface free energy, and  $R = 8.314 \text{ Pa m}^3 \text{ K}^{-1} \text{ mol}^{-1}$  is a molar gas constant. The relation between  $X_c$  and  $T_m$  (eq 4) originates from curve fitting published elsewhere.<sup>16</sup>

$$\ln X_c = 0.331 - \frac{135.5}{T_m} \quad (4)$$

**Sample Preparation for X-ray Scattering and Electron Microscopy.** All the samples were subjected to recrystallization under controlled thermal conditions with a Perkin-Elmer DSC instrument. The specimens were in a shape of discs of 4 mm in diameter and thickness of  $\sim 1 \text{ mm}$ . They were placed in open DSC pans into both sample cells of the DSC apparatus simultaneously. Then heating from room temperature ( $20 \text{ °C}$ ) up to  $160 \text{ °C}$  was done with rate of  $50 \text{ K min}^{-1}$ . In the molten state, the materials were held for 5 min before cooling was performed with rate of  $-1 \text{ K min}^{-1}$ . Specimens were cooled down to ambient temperature ( $20 \text{ °C}$ ). Subsequently, these specimens were used for X-ray diffraction studies directly, while for the scanning

electron microscopy (SEM) the surface was additionally treated at room temperature by chemical etching in 1 wt % solution of  $\text{KMnO}_4$  in 86%  $\text{H}_2\text{SO}_4$  for 15 min. After washing in running water (10 min), specimens were washed in acetone and sputter-coated with Pd/Au alloy.

**Scanning Electron Microscopy.** A FEI Quanta FEG scanning electron microscope was used for the observation of the etched specimen surfaces; the Everhart-Thornley detector and 5 kV accelerated voltage were employed.

**X-ray Scattering.** Small-angle X-ray scattering (SAXS) was performed using a Molecular Metrology SAXS System with a pinhole camera attached to a microfocussed X-ray beam generator (Osmic MicroMax-002) operating at 45 kV and 0.66 mA (30 W). The camera was equipped with a multiwire, gas-filled area detector with an active area diameter of 20 cm (Gabriel design). Two experimental setups were used to cover the scattering vector  $q$  in range of  $0.005\text{--}1.1 \text{ \AA}^{-1}$ . The scattering intensities were put on an absolute scale using a glassy carbon standard. Additionally, the spectrum of the 30C26 copolymer was fit with a convolution curve of two peaks, which were calculated by means of iterative method using Pearson VII function.

To measure wide-angle X-ray scattering (WAXS) of the DSC-recrystallized samples a Bruker D8 Discover was used. The diffractometer was equipped with an X-ray tube with a copper target operating at 30 kV and 30 mA and a GADDS 2-D detector. To direct the beam on the surface, point-collimation (0.5 mm) was used. The measurement was done in reflection geometry, and  $2\theta$  angle was in the range from  $11^\circ$  to  $32.5^\circ$ . Data were collected for 300 s. Mathematical functions were used for fitting of individual intensity vs  $2\theta$  curves using TOPAS software (Bruker) to describe the amorphous and crystalline curves. The crystallinity index ( $X_c$ ) was subsequently calculated from eq 5, where  $I_c$  and  $I_a$  are intensities of crystalline and amorphous phase, respectively, expressed by the area under WAXS curve.

$$X_c = \frac{I_c}{I_c + I_a} \times 100 \quad [\%] \quad (5)$$

## RESULTS AND DISCUSSION

**Differential Scanning Calorimetry.** Table 2 summarizes crystallinity values obtained from eq 1. The characteristic temperatures ( $T_c$  and  $T_m$ ) are the peak maxima shown in Figures 1 and 2. It is clear that the temperatures of transitions of the L-PE are the highest as compared to the rest of the samples (copolymers). This indicates better evolution of ordered structures in L-PE which is also confirmed by its highest  $x_c$ .

The dependences of the crystallinity index on the length of comonomer are plotted in Figure 3. Calculating from the heat of crystallization, only slight variation of the crystallinity can be seen

Table 2. Recorded and Evaluated DSC Data

	crystallization			melting			$L_c$ [Å]
	$T_c$ [°C]	$\Delta H_c$ [J g <sup>-1</sup> ]	$x_c$ [%]	$T_m$ [°C]	$\Delta H_m$ [J g <sup>-1</sup> ]	$x_c$ [%]	
L-PE	116.0	157.9	54.4	135.0	170.6	58.8	241.3
15C8	99.6	71.4	24.6	113.2	86.4	29.8	78.7
15C12	100.3	76.8	26.5	113.2	90.2	31.1	78.7
15C18	102.1	83.0	28.6	114.2	91.3	31.5	81.2
15C26	100.4	75.3	26.0	115.0	76.4	26.3	83.3
30C8	85.3	72.5	25.0	99.7	58.4	20.1	55.5
30C12	86.1	56.5	19.5	100.5	65.1	22.4	56.5
30C18	85.7	58.3	20.1	102.6	54.7	18.9	59.3
30C26 major peak	85.9	54.6	18.8	101.0	58.0	20.0	57.2
30C26 minor peak				49.0	6.0		26.3

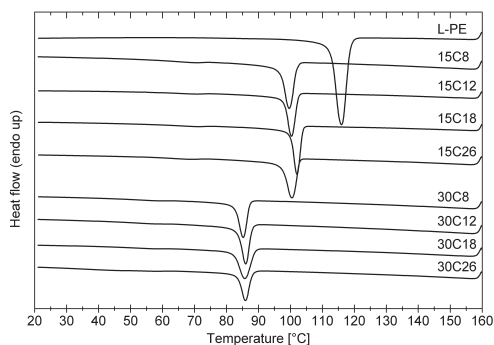


Figure 1. Comparison of cooling records. Curves are shifted vertically to better distinguish.

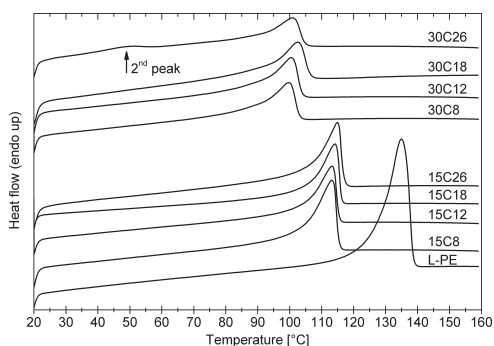


Figure 2. Comparison of heating records. Curves are shifted vertically to better distinguish; the second peak in 30C26 record is marked.

in 15C8, 15C12, 15C18, and 15C26. In the set of samples with higher content of side chains the 30C8 shows the highest crystallinity. The other samples, i.e., 30C12, 30C18, and 30C26, display nearly identical values. The values calculated from the heat of fusion show similar dependence for the copolymers with lower content of side chains. However, for

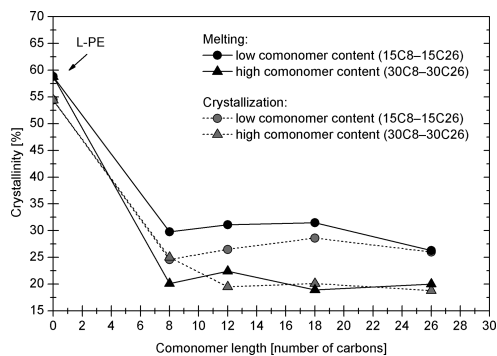


Figure 3. Crystallinity dependence on comonomer length. Values calculated using the heat of fusion and heat of crystallization.

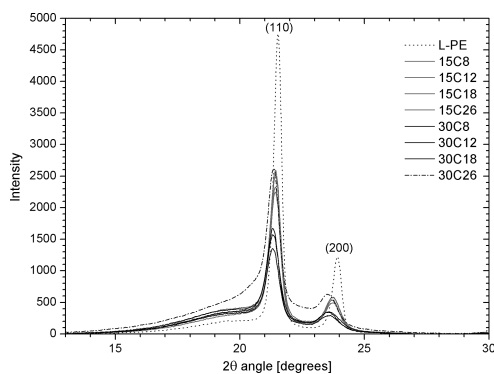
the copolymers with more side chains the crystallinity nonmonotonically varies. As expected, the crystallinity indexes and melting/crystallization temperatures for the copolymers with higher content of side chains are always below those with lower side chains content.

In the DSC record (Figures 1 and 2) no second peak could be observed for any sample except for 30C26. This peak at  $T_m = 49$  °C represents heat of  $\sim 6$  J g<sup>-1</sup>. It is worth noting that the pure hexacosene wax shows two melting peaks—at 37.3 and 52.6 °C—and the investigated copolymer was purified by repeated recrystallization to eliminate any erroneous signals.<sup>16</sup> As a consequence, the revealed peak should be ascribed to the polymer transition.

**Wide-Angle X-ray Scattering.** Table 3 shows the peak positions of the (110) and (200) reflections of all samples. As can be seen, the position of these maxima in case of L-PE is above all the values obtained for the copolymers. This implies that the distance between reflection planes is smaller (according to Bragg's law) when compared to other samples. As mentioned before, we cannot assume that all the side chains will be excluded from the crystalline regions and also Stadler et al.<sup>18</sup> admit the presence of side chains inside the crystallites, which widens the crystal lattice. On the other hand, they suppose that the short side chains will be most likely present in the lattice in comparison with longer side chains, which should remain outside the crystalline

**Table 3.** Peak Positions in X-ray Patterns and Recalculated Material Characteristics

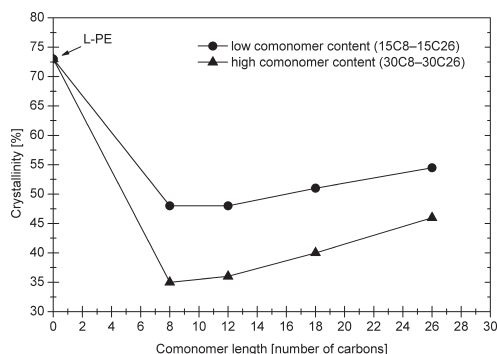
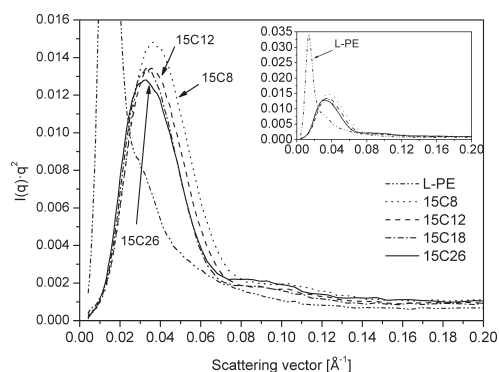
	peak position $2\theta$ [deg]		$X_c$ [%]	$q_{\max}$ [ $\text{\AA}^{-1}$ ]	LP [ $\text{\AA}$ ]	$l_c$ [ $\text{\AA}$ ]	$l_a$ [ $\text{\AA}$ ]
	(110)	(200)					
L-PE	21.537	23.906	73	0.013 57	463	338	125
15C8	21.432	23.715	48	0.036 90	170	82	88
15C12	21.432	23.715	48	0.035 51	177	85	92
15C18	21.432	23.732	51	0.032 88	191	97	94
15C26	21.415	23.732	55	0.032 88	191	104	87
30C8	21.327	23.593	35	0.046 48	135	47	88
30C12	21.310	23.575	36	0.044 72	141	51	90
30C18	21.310	23.523	40	0.039 85	158	63	95
30C26	21.362	23.506	46	0.032 88	191	88	103

**Figure 4.** Summary of WAXS 1D spectra.

regions. These chains are then concentrated on the boundary of crystallites.

A considerable peak of L-PE points to the highest crystallinity index ( $X_c$ ) if compared to all the other samples (Figure 4). Comparing copolymers with different comonomer amount – 15C8 with 30C8, etc., it can be seen that both the  $2\theta$  angle and the crystallinity index are smaller for the samples with higher side chains content than the corresponding values for the samples with low number of side chains, which is in accordance with DSC data. The crystallinity index increases with the increasing comonomer chain length for both sets of samples (Figure 5). However, the WAXS-determined crystallinities are different from those calculated from the DSC as could arise from recrystallization effect during DSC measurement. In further text, the values mostly from X-ray scattering will be discussed.

**Small-Angle X-ray Scattering.** Figures 6 and 7 show Lorentz-corrected intensity vs scattering vector spectra. Expectably, the intensity maximum of L-PE points to the lowest scattering vector  $q$  of all measured samples, what refers to the biggest long period (LP), i.e., well-developed crystalline structure. The shoulder in the  $q$  range of 0.02–0.03  $\text{\AA}^{-1}$  is a manifestation of a second peak hidden in the main peak. Deconvolution of this spectrum gives peaks with maxima at 0.0140 and 0.0287  $\text{\AA}^{-1}$ , which can be recalculated to LP of 449 and 224  $\text{\AA}$ , according to the Bragg's law (eq 6), where  $n$  is an integer which represents the order of

**Figure 5.** Crystallinity dependence on comonomer length. Values calculated from WAXS spectra.**Figure 6.** Lorentz-corrected SAXS patterns of homopolymer and samples with low comonomer content.

reflection. It is obvious the second peak is a second-order reflection.

$$LP = \frac{2\pi n}{q} \quad (6)$$

Combining the WAXS and SAXS data (Table 3), we are able to estimate thicknesses of lamella ( $l_c$ ) and amorphous layer ( $l_a$ ). The relations are given by eqs 7 and 8.<sup>19</sup>

$$l_c = \frac{X_c}{100} \times LP \quad (7)$$

$$LP = l_c + l_a \quad (8)$$

**Model.** Figure 8 gives a summary of values of methylene sequence length (MSL) from nuclear magnetic resonance (NMR) data given by Piel et al.<sup>16</sup> compared to  $L_G$ ,  $l_c$ , and  $l_a$  established in this paper. From the comparison of  $L_c$  and  $l_c$  with MSL, it is evident that the MSL values are higher than  $L_c$  or  $l_c$  for the low comonomer materials and that the MSLs are similar to  $L_c$



or  $l_c$  for the materials with higher comonomer content. This can be, particularly in the first case, explained by the entanglements restricting whole regular methylene sequences to be incorporated into lamellae within melt crystallization; also, the maximum lamellar thickness thermodynamically achievable at given crystallization conditions should be considered. It is worth noting that the length of the crystallizing sequences (from MSL, see Table 1) for the copolymer with 1.5 mol % of comonomer is nearly 1 time higher as compared to the relevant  $l_c$  in Table 3. As for the copolymers with higher comonomer content the values are similar. Even for the copolymer with lower comonomer content the length of crystallizing sequence does not allow to create two consecutive stems during lamellae formation. In both cases the lamellae should not be thus created via regular chain folding.

The phenomena described in the previous paragraph should certainly have an influence on the variation of amorphous layers. In the presented graph (Figure 8) the thickness of amorphous layer remains virtually constant within all copolymer samples. The same phenomenon was observed also by Nitta and Tanaka,<sup>20</sup> who have investigated primarily the dynamic mechanical properties of both metallocene-catalyzed linear PEs varying in weight-average molar mass ( $M_w$ ) and copolymers of ethylene

with 0.8–3.5 mol % of  $\alpha$ -olefin as a comonomer. Beside the broad study of mechanical behavior, they investigated the crystalline structure by X-ray measurement. In the paper they stated that the thickness of amorphous layer is independent of the side chains amount. Stadler et al.<sup>18</sup> investigated the crystal lattice dimensions within the broad sample set prepared via both metallocene and Ziegler–Natta copolymerization where the comonomers were  $\alpha$ -olefins of different lengths (4–26 carbons) and with different concentration of the comonomer. Concerning the  $l_a$  dependences, Stadler et al. found that the amorphous layer is widening with increase in  $M_w$ . Even though there was presented a fitting curve which describes the relation between  $l_a$  and the molar fraction of the comonomer, the influence of side chain length on the  $l_a$  was not investigated. Focusing on the  $l_a$  values in the present paper, it is obvious that the amorphous layer thickness is also independent of the side chains length. It can be presumed that the  $l_a$  value could be driven primarily by the  $M_w$ .

The  $l_c$  calculated from the SAXS/WAXS data for 30C26 sample is significantly higher than the others in the set of copolymers with 3.0 mol % of comonomer (Figure 8). The explanation of this phenomenon could be that the calculated thickness of the main chain lamellae is increased by the thickness of the lamellae created by the side chains. The maximum lamellar thickness of side chains lamella is the length of straighten chain—approximately 30 Å. Regarding the DSC data, the secondary peak in thermogram of 30C26 points lamellar thickness of 26.3 Å, which is in accordance with previously stated. If this length is subtracted from the calculated length of 88 Å, the overestimation is eliminated and the value fits with the others in the set. Moreover, the peak in the SAXS spectrum of 30C26 was found asymmetrical (Figure 7); thus, the deconvolution into two peaks was done by means of an iterative method (Figure 9). The positions of the individual peaks then pointed to LP of 194 and 122 Å, which means  $l_c$  is equal to 89 and 56 Å. This implies that in some cases the side chains can crystallize in the way that their thickness is added to the thickness of main-chain lamellae.

A model comprising two structures of crystalline regions could be proposed. In the material, there should be regions where the crystallites are created solely by main chain lamellae and the side chains are in an amorphous stay and regions where the side chains create crystallites on the surface of main chain lamellae. As no other diffraction peaks are seen in the WAXS record, we

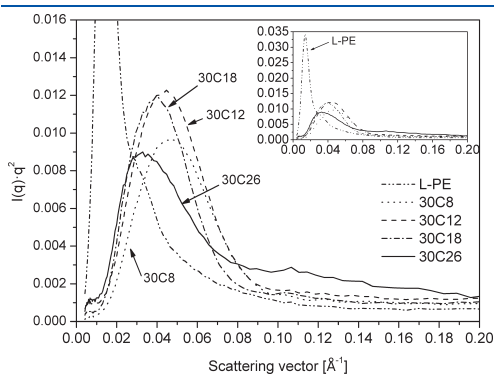


**Figure 7.** Lorentz-corrected SAXS patterns of homopolymer and samples with high comonomer content.

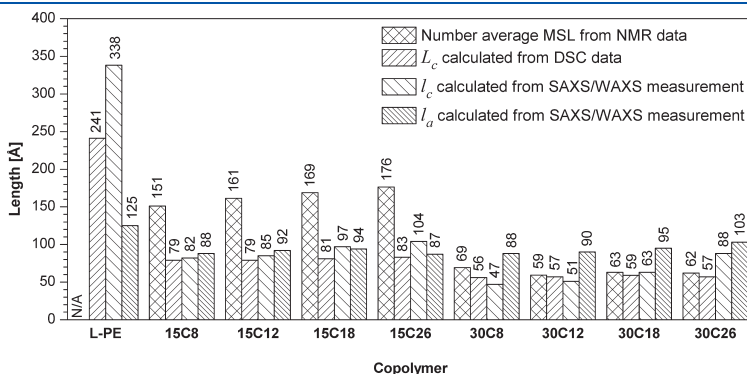


**Figure 8.** Comparison of number-average MSL calculated from NMR spectra<sup>16</sup> with  $L_c$  calculated from DSC data and  $l_c$  and  $l_a$  calculated from SAXS/WAXS measurement.

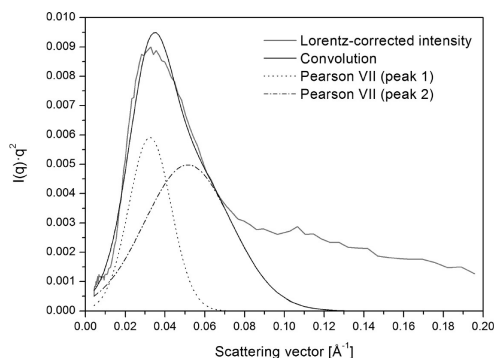


**Figure 9.** Deconvolution of the 30C26 SAXS spectrum with two peaks described by the Pearson VII function.

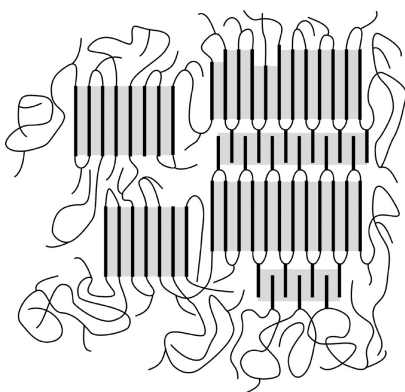


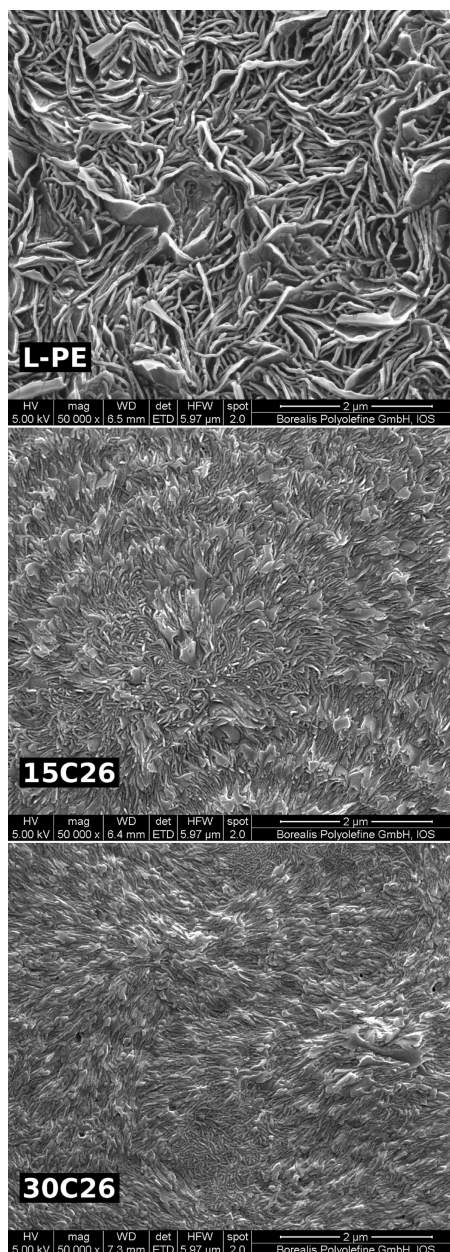
**Figure 10.** Idealized model of the folded chain with excluded branches on the lamella surface, which are in amorphous state (left) and crystallized (right).

suppose the side chains are crystallizing in the same crystal lattice dimensions as the main chain. An idealized model is given in Figure 10.

Since the second crystallites were proved only within the 30C26 sample, two main criteria for their formation can be stated: they are the comonomer length and concentration. The sufficient length is necessary to form initial nuclei while the concentration is needed both to have enough of chains to crystallize and to have enough of crystallites to get a signal of detectable intensity. Both seem to be fulfilled only in case of the hexacosene copolymer with high comonomer content.

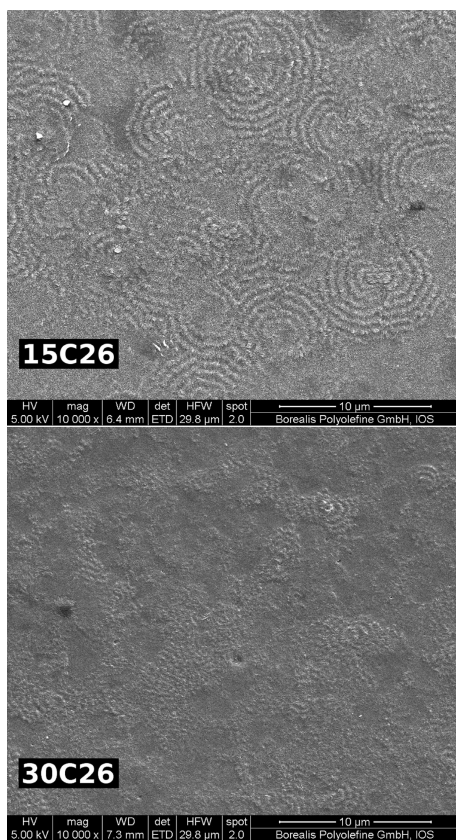
It is obvious that the values of MSL and  $L_c$  are similar for the materials with 3 mol % of a given comonomer. This implies that the side chains can be in higher concentration localized close to the vicinity of the primary lamellae. Consequently, a strict spatial localization of the side chains can be supportive to their interaction and nucleation and overall crystallization.

Figure 11 shows SEM pictures of the homopolymer and hexacosene copolymer of both values of comonomer content. It should be pointed out that all previous discussions can only be



**Figure 11.** SEM pictures of the homopolymer and hexacosene copolymers, both low and high comonomer content.

considered if the materials crystallize into the lamellar morphology. To verify this point, scanning electron microscopy was employed showing clearly the formation of lamellar textures. The



**Figure 12.** SEM pictures of the hexacosene copolymers, both low and high comonomer content, with lower magnification.

lamellar thickness is obviously reduced with the increasing comonomer content. However, in comparison with the SAXS data, the lamellae are thicker as might be related to the effects arising from the etching or metal sputtering. The SEM analysis is therefore used here in terms of qualitative assessment only. Unlike L-PE, the copolymers tend to form spherulites consisting of twisted lamellae; however, this effect is reduced again with further increasing comonomer amount. While in the material with lower comonomer content the lamellae are predominantly twisted, the 30C26 material consists of two distinctly different lamellar textures (cf. Figure 12). This might be related with the second maximum in the SAXS spectrum. Nevertheless, the existence of side chains lamellae in 30C26 cannot be unambiguously confirmed by SEM.

## CONCLUSION

In the presented paper, we have studied the morphology of metallocene-catalyzed copolymers of ethylene and different  $\alpha$ -olefins as a comonomer. These  $\alpha$ -olefins were namely oct-1-ene, dodec-1-ene, octadec-1-ene, and hexacos-1-ene which provided copolymers with different side-chain lengths. Two sets of materials

were studied: one with comonomer content  $\sim 1.5$  mol % and the other with  $\sim 3.0$  mol %. The aim was to prove whether the side chains are able to crystallize separately to the main-chain crystallites. DSC measurements gave evidence of secondary crystalline structures in the case of the hexacosene copolymer with high comonomer content, while the WAXS pattern pointed out that these structures have the same crystal lattice size as the prevailing crystallites. Data derived from the X-ray diffraction indicated the second crystalline structures in a size expected for the side chains lamellae. As the evidence of secondary crystallization was given only for the hexacosene copolymer with high comonomer content, two main criteria driving the potential side-chain crystals formation can be discussed; the side chain length and the side chains concentration should be high enough to let crystallization initiate and proceed. A sufficient amount of the side chains and its specific localization close to the primary lamellae are needed both to have enough crystallizable material and to create enough of crystallites to detect them. Regarding the interlamellar amorphous layer thickness estimated by the combination of SAXS and WAXS data, we have found it relatively constant regardless the side-chains length and the comonomer concentration.

## AUTHOR INFORMATION

### Corresponding Author

\*E-mail: mjanicek@ft.utb.cz.

## ACKNOWLEDGMENT

We thank Dr. Senthil K. Kaliappan of Borealis Polyolefine GmbH for WAXS measurements and to Dr. Gottfried Kandioller of Borealis Polyolefine GmbH for SEM pictures. The work was supported by the Operational Programme Research and Development for Innovations cofunded by the European Regional Development Fund (ERDF) and national budget of Czech Republic within the framework of the Centre of Polymer Systems project (reg. no.: CZ.1.05/2.1.00/03.0111). Miroslav Janicek gratefully acknowledges the financial support of this work by the internal grant of TBU in Zlin, No. IGA/11/FT/11/D, funded from the resources of specific university research.

## REFERENCES

- (1) Rojas, G.; Berda, E. B.; Wagener, K. B. *Polymer* **2008**, *49*, 2985–2995.
- (2) Hernandez, R. J. *Plastics in Packaging*. In *Handbook of Plastics, Elastomers & Composites*; Harper, C. A., Ed.; McGraw-Hill Professional: New York, 2002.
- (3) Abu-Sharkh, B.; Hussein, I. H. *Polymer* **2002**, *43*, 6333–6340.
- (4) Zhang, M.; Lynch, D. T.; Wanke, S. E. *Polymer* **2001**, *42*, 3067–3075.
- (5) Kaminsky, W.; Piel, C. *J. Mol. Catal. A: Chem.* **2004**, *213*, 15–19.
- (6) Kaminsky, W. *Macromol. Chem. Phys.* **1996**, *197*, 3907–3945.
- (7) Klimke, K.; Parkinson, M.; Piel, C.; Kaminsky, W.; Spiess, H. W.; Wilhelm, M. *Macromol. Chem. Phys.* **2006**, *207*, 382–395.
- (8) Kaminsky, W. *Catal. Today* **1994**, *20*, 257–271.
- (9) Shamsoum, E. S.; Rauscher, D. *New Approaches for Ziegler-Natta Catalysts for Polypropylene*. In *Metallocene-Catalyzed Polymers – Materials, Properties, Processing and Markets*. Benedikt, G. M., Goodall, B. L., Eds.; *Plastics Design Library*: Norwich, 1998.
- (10) Kaminsky, W.; Hopf, A.; Piel, C. *J. Organomet. Chem.* **2003**, *684*, 200–205.
- (11) Gómez-Elvira, J. M.; Tiemblo, P.; Elvira, M.; Matisova-Rychly, L.; Rychly, J. *Polym. Degrad. Stab.* **2004**, *85*, 873–882.
- (12) Razavi, A.; Thewalt, U. *Coord. Chem. Rev.* **2006**, *250*, 155–169.

- (13) Stadler, F. J.; Takahashi, T.; Yonetake, K. *e-Polym.* **2009**, 40.
- (14) Stadler, F. J.; Piel, C.; Klimke, K.; Kaschta, J.; Parkinson, M.; Wilhelm, M.; Kaminsky, W.; Münstedt, H. *Macromolecules* **2006**, 39, 1474–1482.
- (15) Piel, C.; Stadler, F. J.; Kaschta, J.; Rulhoff, S.; Münstedt, H.; Kaminsky, W. *Macromol. Chem. Phys.* **2006**, 207, 26–38.
- (16) Piel, C.; Starck, P.; Seppälä, J. V.; Kaminsky, W. *J. Polym. Sci., Polym. Chem.* **2006**, 44, 1600–1612.
- (17) Piel, C. Polymerization of Ethene and Ethene-co-alpha-Olefin: Investigations on Short- and Long-Chain Branching and Structure-Property Relationships. Dissertation, Department of Chemistry, University of Hamburg, 2005.
- (18) Stadler, F. J.; Takahashi, T.; Yonetake, K. *e-Polym.* **2009**, 41.
- (19) Roe, R. J. *Methods of X-Ray and Neutron Scattering in Polymer Science*. In *Topics in Polymer Science*; Mark, J. E., Ed.; Oxford University Press: New York, 2000.
- (20) Nitta, K.; Tanaka, A. *Polymer* **2001**, 42, 1219–1226.

## **ARTICLE II**



# Thermal stability of surface-esterified cellulose and its composite with polyolefinic matrix

Miroslav Janicek · Ondrej Krejci ·  
Roman Cermak

Received: 5 July 2013 / Accepted: 24 September 2013 / Published online: 29 September 2013  
© Springer Science+Business Media Dordrecht 2013

**Abstract** Thermal stability of hydrophobized cellulose powders was investigated from the perspective of potential use as filler in non-polar polyolefinic matrix. The hydrophobization was done by heterogeneous esterification with three carboxylic acids which differ in chain length (3, 10 and 18 carbons). Data measured by means of thermogravimetry (TG) were recalculated according to model-free isoconversional method to construct time–temperature plots. It was demonstrated that the esterification significantly decreases thermal stability of the material, which reduces feasible processing window. Under non-oxidative atmosphere, the single-step decomposition of materials is prevailing, while the process is more complex in air. In both cases the oleic acid esters showed the lowest stability and the original cellulose was the most stable. Finally, all powders were compounded with polyethylene or polypropylene. Obtained composites were then subjected to color measurement and TG. Even though the materials were partly degraded, which was indicated

by the yellowish hue of the composites, virtually no impact of the filler pyrolysis on the polymer matrix decomposition was observed, particularly in case of decanoyl esters.

**Keywords** Cellulose · Esterification · Hydrophobization · Stability · Degradation · Composite

## Introduction

Cellulose is a polydisperse linear homopolymer produced primarily by living plants and thus it is counted among renewable bio-materials, which are promising for future utilization (George et al. 2001). However, scientific and industrial interest in cellulose and its derivatives is not new and the cellulose-based materials have been intensively studied for decades (John and Thomas 2008; Jawaid and Abdul Khalil 2011). Many methods were developed to change namely its structure, crystallinity, solubility, and interaction with synthetic materials. Some of them are based on complete dissolution of original cellulose (Heinze and Liebert 2001; Klemm et al. 2005; Polaskova et al. 2013), while others are based on preserving its supramolecular structure (Jandura et al. 2000a; Heinze and Liebert 2001; Abdelmouleh et al. 2007; Uschanov et al. 2010; Tome et al. 2011). In the latter case, the chemical reaction usually takes place only on the surface of cellulose particles during so-called

---

M. Janicek (✉) · O. Krejci · R. Cermak  
Department of Polymer Engineering, Faculty of  
Technology, Tomas Bata University in Zlin, Nam. T. G.  
Masaryka 275, 762 72 Zlin, Czech Republic  
e-mail: mjanicek@ft.utb.cz  
URL: <http://www.ft.utb.cz>

M. Janicek · O. Krejci · R. Cermak  
Centre of Polymer Systems, University Institute, Tomas  
Bata University in Zlin, Nad Ovcirnou 3685, 760 01 Zlin,  
Czech Republic

heterogeneous modification. Since the original surface is already hydrophilic, expectably, hydrophobization is the most studied reaction, because it is the hydrophobicity which is often necessary to achieve good dispersion of the filler in synthetic polymer matrix and good adhesion between the filler and the matrix (Spoljaric et al. 2009; Uschanov et al. 2010).

Despite the number of procedures of achieving hydrophobic surface, not many studies of these modified materials behavior during and after mixing into polymer matrix were published. In addition, many papers dealing with cellulose pyrolysis present solely activation energy, which is contained in the well-known Arrhenius equation, or they present combination of the energy and pre-exponential factor (Huang and Li 1998; Li 1999; Li et al. 1999). Unfortunately, these numbers gives only rough information for the stability comparison under certain conditions, which is usually insufficient for the practical use, since the feasibility of filler dispersion in molten polymer matrix is determined by time for which the cellulose can be held at given temperature.

In this work, the stability of original and surface-esterified cellulose is investigated by thermogravimetry (TG). Obtained data are then transformed by means of model-free isoconversional method into time–temperature plots to assess the impact of chemical modification on both the stability of the filler and the reduction of processing time–temperature area. Beside this, the polyethylene (PE) and polypropylene (PP) composites are prepared and subjected to TG and colorimetry.

## Experimental

### Materials

Two types of fibrous cellulose were used in this study: fibrous cellulose prepared from cotton linters was purchased from Sigma-Aldrich (SA) and natural cellulose fiber Arbocel<sup>®</sup> FD 600-30 was kindly provided by J. Rettenmaier & Söhne GmbH + Co. KG, Germany. The former material is high purity cellulose fibrous powder with mean fiber length 50–350  $\mu\text{m}$  and diameter in range of 12–15  $\mu\text{m}$  and it is intended for partition chromatography (information taken from data sheet). The latter material is sulphite bleached non-coniferous cellulose with

**Table 1** Chemical composition of Arbocel<sup>®</sup> FD 600-30 (data found in material data sheet)

Alpha cellulose	73.1 %
Hemicellulose	9.1 %
Lignin	7.2 %
Extracts	0.7 %
Ash	3.2 %
Water	6.7 %

typical composition as presented in Table 1. Although the Arbocel is commonly denoted as cellulose fibers, the shape is rather flaky with average length of 45  $\mu\text{m}$  and average thickness 25  $\mu\text{m}$ .

Pyridine (99 %) as a liquid medium for chemical reactions and oleic acid (OA) (>97 %) which was used for surface modification, were purchased from Lach-Ner, Czech Republic, other carboxylic acids for esterification were decanoic acid (DA) (98 %) and propionic acid (PA) (99 %), both purchased from Sigma-Aldrich. *p*-Toluenesulfonyl chloride (TsCl) (>99 %) as an esterification mediator and potassium bromide (KBr) for infrared spectroscopy (>99 %) were provided by Acros Organics. All the chemicals were used as obtained with no purification.

For the cellulose/polymer composites preparation, two matrices were used: isotactic polypropylene HD601CF produced by Borealis AG, Austria, and high-density polyethylene Liten VB 33 produced by Unipetrol RPA, Czech Republic. The former material is characterized by melt flow rate (MFR) of 8 g/10 min (ISO 1133, 230 °C/2.16 kg), the latter has MFR of 0.33 g/10 min (ISO 1133, 190 °C/2.16 kg); both values are taken from relevant data sheets.

### Cellulose surface modification

Process of the surface modification was adopted after Uschanov et al. (2010) Esterification reaction was carried out in round-bottom flask equipped with reflux condenser and paddle stirrer. The flask was charged with 250 mL of pyridine and 10 g of cellulose which was dried in vacuum oven at 0.1 bar and 100 °C overnight. About 53 g of TsCl were added to the suspension together with carboxylic acid. The amount of the acid was 21 g in case of PA, 48 g in case of DA and 79 g for the OA. In all the cases the amount was calculated to achieve cellulose hydroxyl groups:TsCl:carboxylic groups molar ratio of 1:1.5:1.5. Since the cellulose does



not dissolve during the heterogeneous reaction, many hydroxyl groups, primarily those in the bulk, are inaccessible for the esterification. Thus the molar amount of acid is more than 1.5 relatively to the hydroxyl groups.

The mixture was then heated in water bath at 50 °C with vigorous stirring for 4 h. Subsequently, the suspension was filtered out, yellowish filter cake was washed with plenty of ethanol and transferred to Soxhlet apparatus in which it was purified by extraction (cycle time about 10 min) with ordinary ethanol for 8 h. The pure powder was dried in air and subsequently in vacuum oven at 0.1 bar and 80 °C overnight. Denotation of the materials is “SA” and “A” for Sigma-Aldrich and Arboel powder, respectively, followed by number representing the acid length: 0 for original cellulose, 3, 10 and 18 for PA, DA and OA esterified materials, respectively.

#### Composite preparation

Unmodified cellulose and products of esterification were used as filler in PP and PE matrices. Filler concentration was 10 wt% and the dispersion was performed with laboratory kneader Brabender PL 2000 heated to 180 °C. Loading the kneader chamber and polymer melting took approx. 5 min after which the speed of rotors was increased from initial 15 to 45 rpm. Molten composite was removed from the chamber after additional 5 min of kneading and compression molded at 185 °C to obtain 15 × 15 × 1 mm sheet. Molding was initiated by 2 min of pre-heating, molding itself then took 1 min with closing pressure of 150 MPa which was kept also during cooling in cold press for 10 min. Composite name is then derived from the cellulose denotation with prefix “PE” or “PP” according to used matrix.

#### Characterization

Thermo Nicolet Avatar 360 FTIR spectrometer was used to measure Fourier-transformed infrared (FT-IR) spectra. To check the chemical modification, cellulose powder was mixed into KBr and subsequently compressed into solid plate and measured in transmission mode.

Thermogravimetric analyzer Q500 TA Instruments was used to compare thermal stability of both fillers and final composites. A sample of approx. 8 mg was

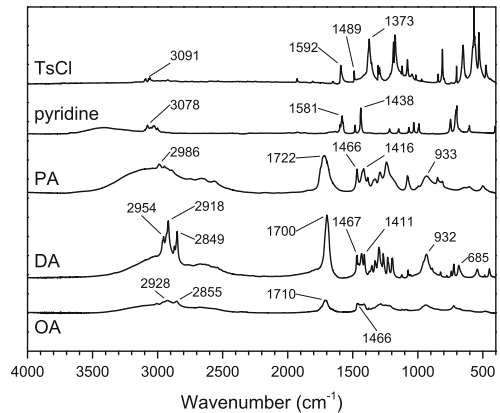


**Fig. 1** FT-IR spectra of reactants

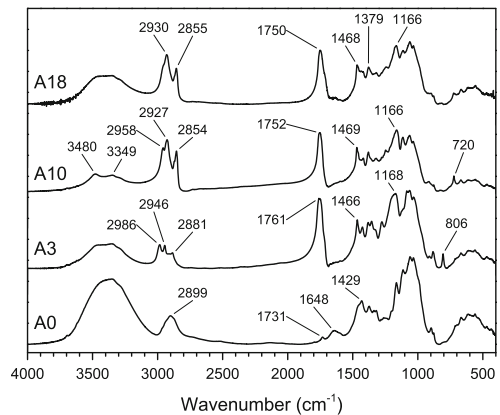


**Fig. 2** FT-IR spectra of original and esterified Arboel powder—note the ester-related peak at  $\sim 1,750\text{ cm}^{-1}$

placed in a pan and subsequently heated with heating rate of 20 K/min from 25 to 600 °C. Nitrogen or air was constantly passing (20 mL/min) through the measuring cell. In order to predict the modified filler stability a model-free isoconversial method was used to assess kinetics of pyrolysis from thermogravimetric data obtained with heating rates of 5 and 10 K/min in addition to previous 20 K/min. The calculation was done according to procedure broadly elaborated by Vyazovkin and coworkers (Vyazovkin 1997; Vyazovkin and Wight 1999; Vyazovkin et al. 2011).

Even though some authors use for thermal analysis  $n$ -th reaction order model or Avrami–Erofeev model (Devallencourt et al. 1996; Jandura et al. 2000b), in

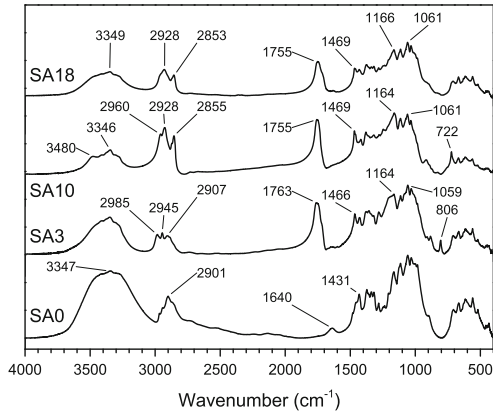


**Fig. 3** FT-IR spectra of original and esterified Sigma-Aldrich cellulose fibers—note the ester-related peak at  $\sim 1,755\text{ cm}^{-1}$

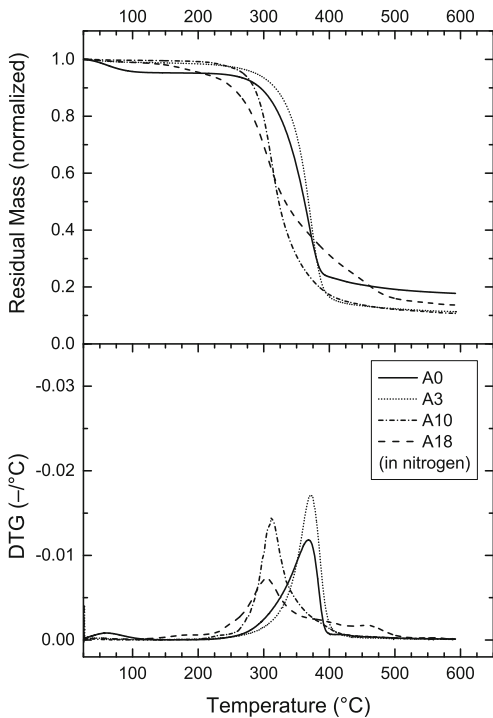


**Fig. 4** Records of mass loss and their derivations of Arbocel-based materials in nitrogen

this paper, the need of model definition is omitted by use of the isoconversional method, which is based on the parametrization of extend of conversion,  $\alpha$ , in

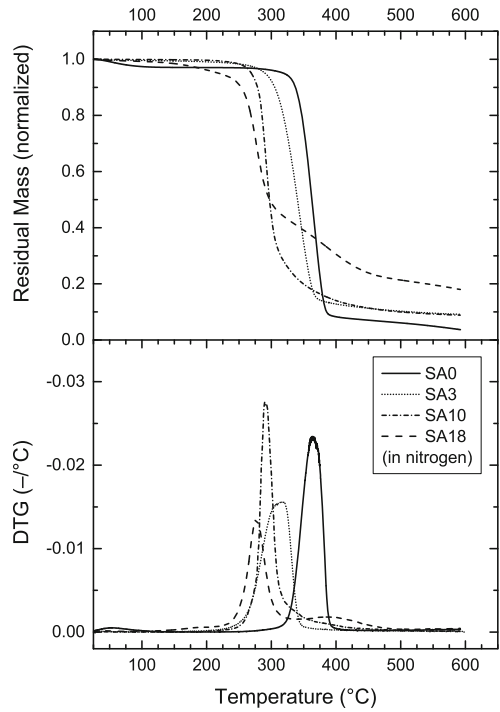


**Fig. 5** Records of mass loss and their derivations of Sigma-Aldrich-based materials in nitrogen

differential form related to reaction rate  $k(T)$ , reaction model  $f(\alpha)$ , and pressure dependency  $h(P)$ :

$$\frac{d\alpha}{dt} = k(T)f(\alpha)h(P) \tag{1}$$

By omission of  $h(P)$ , since no reactants in gaseous stay are expected, substitution of  $k(T)$  by the Arrhenius expression (Eq. 2), and taking into account the non-isothermal process characterized by heating rate,  $\beta$ , defined with Eq. (3):

$$k(T) = A \exp\left(-\frac{E}{RT}\right) \tag{2}$$

$$\beta = \frac{dT}{dt} = \text{const.} \tag{3}$$

Eq. 1 can be then rewritten in logarithmic form:

$$\ln \left[ \beta_i \left( \frac{d\alpha}{dT} \right)_{\alpha,i} \right] = \ln[f(\alpha)A_{\alpha}] - \frac{E_{\alpha}}{RT_{\alpha,i}} \tag{4}$$

where  $i$  identifies the individual heating rate, and  $E_{\alpha}$  is the isoconversional value of activation energy, while

the  $T_{x,i}$  stands for the temperature at which the specific conversion was achieved.

Advantage of this method is no need to assess the model, which is hidden together with the pre-exponential factor in the shift of linear regression of Eq. (4). The slope of the left side of the equation against reciprocal time then determines  $E_x$ . Kinetic predictions can also be made by means of this model-free method by solving Eq. (5), which was originally proposed by Vyazovkin (1996) in the following form valid for processes taking place under isothermal conditions ( $T_0 = \text{const.}$ ) (Vyazovkin et al. 2011).

$$t_x = \frac{\frac{1}{\beta} \int_0^{T_x} \exp(-E_x/RT) dT}{\exp(-E_x/RT_0)} \quad (5)$$

Color measurement of prepared composites was performed with HunterLab spectrophotometer Ultra-Scan PRO in reflectance mode with the exclusion of specular reflectance. Diameter of the port plate was 0.390 in. Software provided with the instrument was used to transform obtained spectral data into CIELAB

color coordinates ( $L^*$ ,  $a^*$  and  $b^*$ ) based on a D65 light source. Hue of each composite was obtained by averaging values measured in three locations. The total deviation in color  $\Delta E_{ab}$  was calculated using the following Euclidean distance equation:

$$\Delta E_{ab} = \sqrt{\Delta L^2 + \Delta a^2 + \Delta b^2} \quad (6)$$

where  $\Delta L$ ,  $\Delta a$  and  $\Delta b$  represents the differences between the pure polymer and composite values of  $L^*$ ,  $a^*$ , and  $b^*$ , respectively. Yellowness Index (YI) according to ASTM Method E313 was calculated by the instrument software.

## Results and discussion

Figure 1 shows FT-IR spectra of used chemicals in which one can see the characteristic intensive peaks vibrating at 1,722, 1,700 and 1,710  $\text{cm}^{-1}$ , which are related to carboxylic groups of PA, DA, and OA, respectively. Since these peaks can be found also in

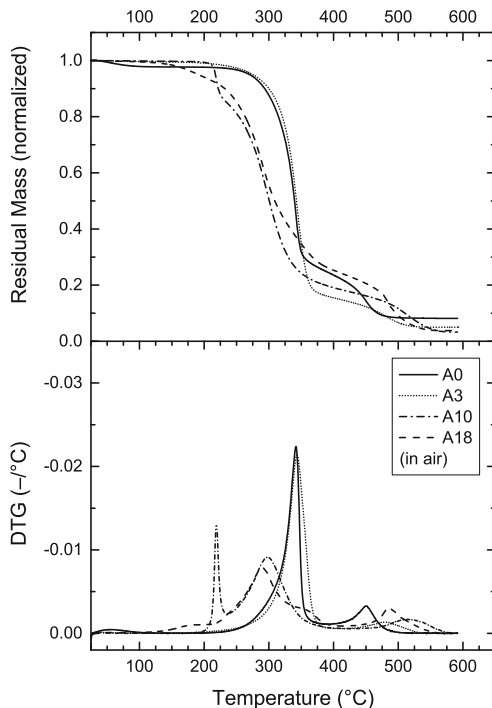


**Fig. 6** Records of mass loss and their derivations of Arbocel-based materials in air

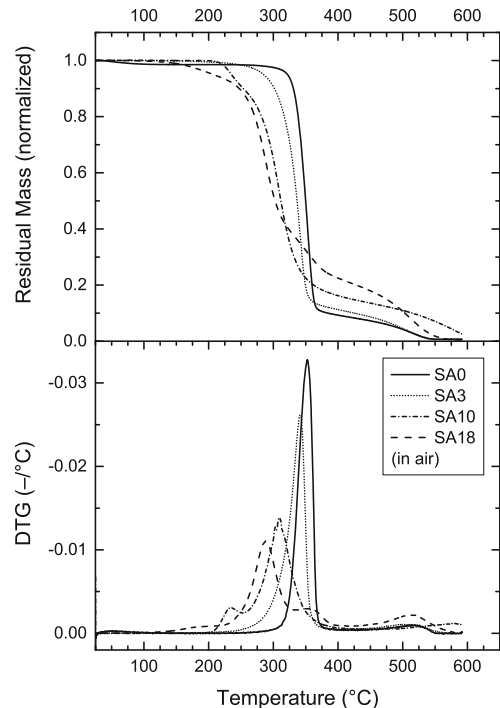


**Fig. 7** Records of mass loss and their derivations of Sigma-Aldrich-based materials in air

**Table 2** Summary of TG data evaluation

	A0	A3	A10	A18	SA0	SA3	SA10	SA18
	Nitrogen							
Onset (°C)	324	340	288	148 270	342	310	279	144 259
Inflection <sup>a</sup> (°C)	368	372	311	304	363	341	290	277
Humidity (%)	4.7	1.2	0.4	1.0	2.9	0.6	0.05	0.7
Residue (%)	18.6	11.4	10.6	13.4	3.6	9.1	8.9	18.1
	Air							
Onset (°C)	319	319	214	151 258	335	315	219	153 264
Inflection (°C)	342	344	219 (298)	291	352	341	309	289
Humidity (%)	2.2	0.3	0.1	0.5	1.3	0.06	– <sup>b</sup>	0.2
Residue (%)	8.3	5.0	3.3	3.8	0.8	0.5	2.5	0.5

<sup>a</sup> Inflection position represents the main peak of DTG curves, i.e. the temperature of the fastest mass loss

<sup>b</sup> Not detectable

**Table 3** Calculated mean isoconversional activation energies

	A0	A3	A10	A18	SA0	SA3	SA10	SA18
$E_x$ (kJ/mol)	111 ± 1	111 ± 1	104 ± 4	–	126 ± 5	131 ± 2	102 ± 5	–

spectra of modified celluloses (Figs. 2, 3), the esterification reaction was successful in case of pure (SA) cellulose as well as in case of natural Arbocecel powder which holds many accompanying substances (cf. Table 1). As can be seen in the spectra, the carbonyl vibration varies in between 1,750 and 1,763  $\text{cm}^{-1}$  which may be due to both—the different acid use and also different degree of substitution. The higher degree of substitution, the more is this peak shifted towards higher frequencies (Jandura et al. 2000a). Regarding this fact, we can suppose the SA-based materials will be more substituted than the Arbocecel-based, since the reaction is not disturbed by accompanying substances. The shift of the carbonyl vibration in case of SA-based materials (Fig. 3) may be then ascribed to this supposition.

Characteristic vibrations of individual reagents are not found in Figs. 2 and 3, thus the 8-h washing procedure may be sufficient.

Figures 4, 5, 6 and 7 show record of TG performed at heating rate of 20 K/min. The first two (Figs. 4, 5) are pyrolysis in non-oxidative nitrogen atmosphere. With omission of initial drying and very slow mass loss at temperatures above 400 °C, only one step can be found in all records except the A18 and SA18 which showed three steps indicating complex decomposition. In the latter case, the first onset is at about 150 °C and the mass loss is rather slow in comparison with the

second occurring at 250 °C and third step starting at about 300 °C. The last decomposition is again slower than the second one. This complex process is usually reported as a two-step pyrolysis in other papers (Lee and Park 1999; Park et al. 1999; Jandura et al. 2000b) and it was ascribed to the tendency of unsaturated side chains to make cross-links. The second less intensive peak in DTG curve at temperature about 400 °C is then related to the decomposition of the cross-linked material (Jandura et al. 2000b). The last observed decomposition is very slow and occurs at about 500 °C in case of A18 and SA18, and at lower temperature (400 °C) for the rest celluloses. Analogously, Figs. 6 and 7 show the same materials heated with the same rate but in oxidative atmosphere (air) revealing much more complex decomposition represented by several steps. Results from TG are collected in Table 2.

From the given data it is evident, that the increase in carboxylic acid length is followed with decrease of thermal stability in both inert and oxidative atmospheres. It is also evident, that the modification causes decrease in water intake since practically no drying is seen in case of modified cellulose, particularly those based on SA. The smallest water content was in case of cellulose esterified with DA, which had also fatty haptic properties.

Equation (4) was employed to obtain isoconversional activation energies. The mean values are listed

in Table 3 and dependences on conversion extent are plotted in Fig. 8. In the plot, one can clearly see growth of SA18 and A18 values, which indicates

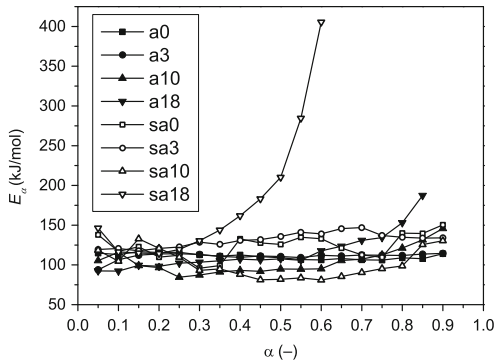


**Fig. 8** Dependence of isoconverional activation energy on the extent of conversion

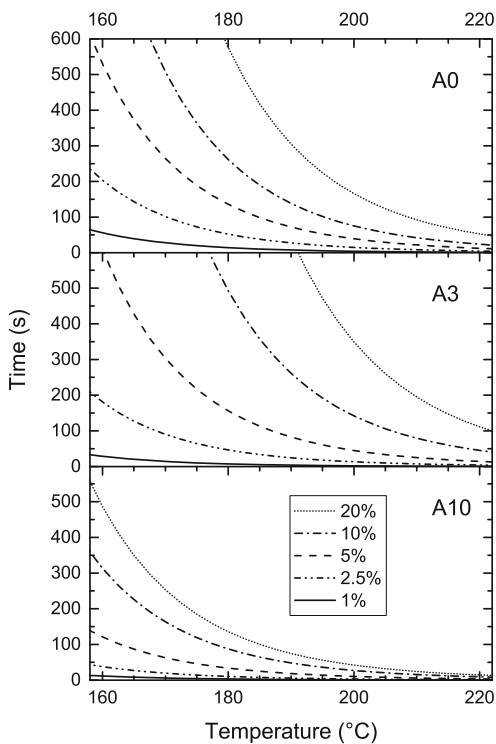


**Fig. 9** Time-temperature contour plot of 1, 2.5, 5, 10 and 20 % conversion showing thermal stability of Arbocel-based esters

complex process. Due to the variation of the  $E_a$ , these two pyrolytic processes must be described with more complex model and the isoconverional method is inappropriate to evaluate stability of this material (Vyazovkin and Sbirrazzuoli 2006). The Eq. (5) was thus numerically solved only for the rest of the analyzed celluloses. The value of  $\alpha$  was set to 1, 2.5, 5, 10, and 20 % for which the time of achieving this extent,  $t_x$ , at the particular temperature of isothermal heating is plotted in Figs. 9 and 10. These plots are supportive to the estimation of stability already shown in the TG record (Figs. 4, 5). In addition to that, they can be used to estimate safe time of processing at particular temperature—i.e. the maximal time of processing until unacceptable degradation is reached. The DA esterified cellulose is the less stable, considering only original, PA and DA modified materials. The decrease could be caused by higher tendency to scission off decanoyl radical in case of A10 and SA10

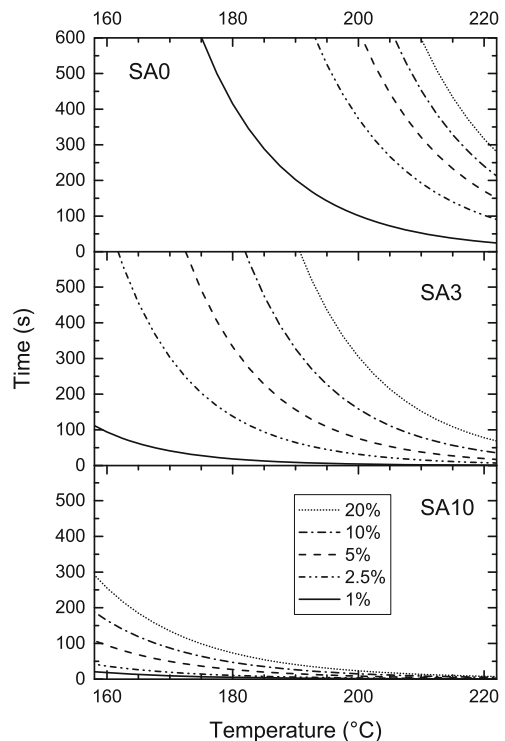


**Fig. 10** Time-temperature contour plot of 1, 2.5, 5, 10 and 20 % conversion showing thermal stability of Sigma-Aldrich-based esters

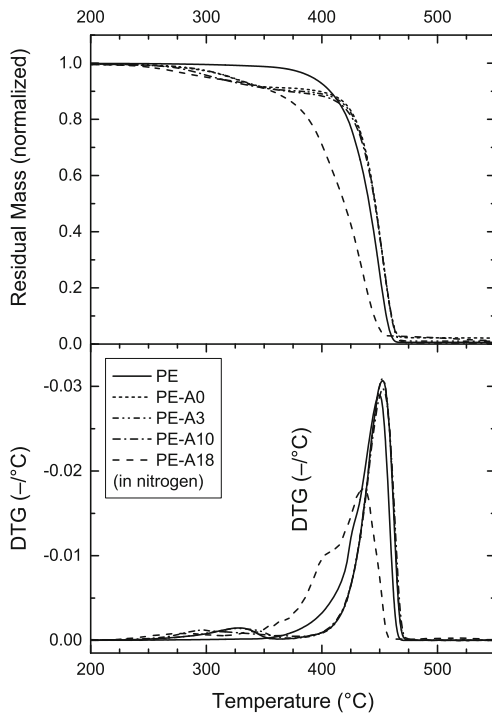


**Fig. 11** Records of mass loss and their derivation of PE-Arbocel-based composites

than scission off the propionyl group. Discrepancy is found in stability of A3 and SA3. While the SA3 is between SA0 and SA10, A3 is virtually more stable even than the unmodified cellulose (cf. onset and inflection temperatures in Table 2). Explanation could be in the different processing—both materials were extracted for 8 h with ethanol, but A3 was previously stirred in reaction mixture (pyridine, TsCl, PA) for 4 h at higher temperature during the modification. It is then possible to assume, that some of the accompanying low-molecular substances in the Arbocel were washed out, which can increase the cellulose crystallinity and finally its stability. The increase of crystallinity induced by heating (drying at 100 °C) can be neglected, because this transformation occurs at the temperature  $\sim 200$  °C (Bhuiyan et al. 2000). Discussed enhancement of crystalline regions may also explain the relative vicinity of A0 and A10 stability (for example at 180 °C only 4 times higher) in comparison with SA0 and SA10. One can suppose that the stability of A0 would be higher if the cellulose

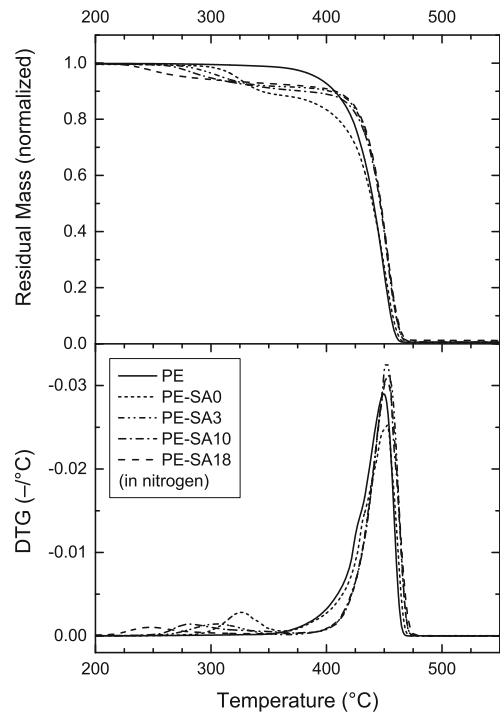


**Fig. 12** Records of mass loss and their derivation of PE-Sigma-Aldrich based composites

was also stirred several hours in the reaction bath, or held at elevated temperature.

#### Polymer/cellulose composite

Evaluation of impact of the esterified celluloses decomposition on the thermal behavior and stability of polymeric matrix is difficult. This is due to relative uncertainty of the processing time and temperature as well as the amount of oxygen, which is trapped in the material during melt mixing. It is worth to mention, the above presented time–temperature degradation plots (Figs. 9, 10) are calculated from data obtained in the non-oxidative atmosphere of nitrogen. In the real conditions, the material is always in some extent exposed to air. This happens particularly during feeding or initial stage of compounding, which is, fortunately, at lower temperatures so the decomposition may not be too quick. Including polymers used in this study, commercial grade materials are commonly stabilized against oxidative degradation, which can be

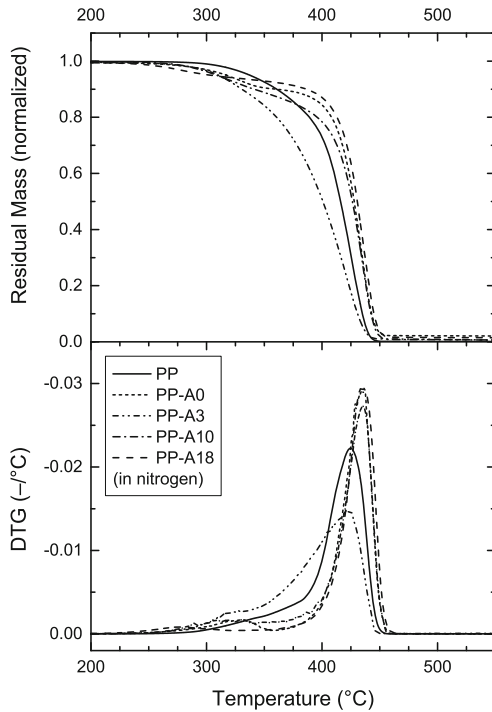


**Fig. 13** Records of mass loss and their derivation of PP-Arbocel-based composites

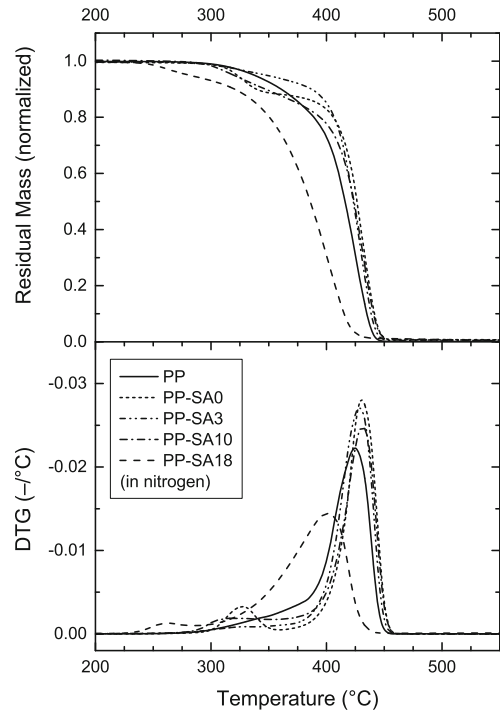


**Fig. 14** Records of mass loss and their derivation of PP-Sigma-Aldrich based composites

also helpful in prevention of the filler decomposition. However, the main effect is the prevention of fatal degradation of the matrix, since the evolved radicals and other product of cellulose decomposition can easily attack surrounding polymer.

Figures 11, 12, 13 and 14 show TG curves of the prepared composites. In all of them, the initial drop of about 0.1 can be found. This represents the cellulose decomposition, since their onset is spread around 300 °C (cf. Table 2) and the mass loss is equal to the filler content. As the temperature rises, the TG curve shape is very similar to the trend of neat polymer, which indicates that the products of cellulose decomposition did not affect the matrix. Differences are, however, observed in case of PE-A18 and PP-SA18, which were expected, since the composites exhibited higher yellowness typical for partly degraded polymers and the OA-modified celluloses were the most unstable. On the other hand, the PE-SA18 starts degradation at lower

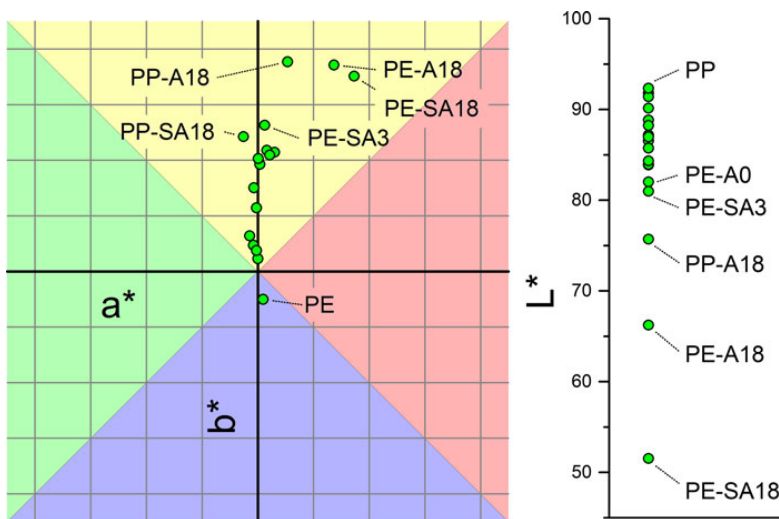
temperatures, but after its vaporization, the trend of TG curve follows the neat polymer. The PE-SA3 and PE-SA10 exhibited similar behavior, but the curve of PE-SA0 drops faster than the record of the neat matrix. Similar discrepancy is found in case of PP-A3 (Fig. 13).

Comparing these data with YI (see Table 4) or color deviation of the composites (Fig. 15), no correlation is evident. Prediction of the impact of esterified cellulose on the thermal stability or yellowing of the matrices would be thus unreliable and strongly dependent on the cellulose origin and matrix type as well as its additives and cellulose accompanying substances.

The final yellowish hue is, however, limiting for many applications. This should be prevented by compounding with additional thermal stabilizers. Alternatively, yellowish hue may also be compensated by addition of blue dye, which on the one hand enhance the color perception—the yellow saturation is

**Table 4** Color coordinates in CIELAB space with valuated deviations from pure matrix and calculated yellowness indices

Material	$L^*$	$a^*$	$b^*$	$\Delta E_{ab}$	YI [D65/2]	Material	$L^*$	$a^*$	$b^*$	$\Delta E_{ab}$	YI [D65/2]
PE	91.81	0.97	-5.03		-9.29	PP	92.33	0.02	2.31		4.41
PE-A0	82.02	3.02	21.42	28.3	42.70	PP-A0	86.56	0.39	19.26	17.9	35.14
PE-A3	83.88	1.61	21.77	28.0	41.14	PP-A3	87.19	0.09	20.30	18.7	36.26
PE-A10	83.94	2.14	20.92	27.1	40.35	PP-A10	88.85	-0.69	15.04	13.2	26.65
PE-A18	66.23	13.69	37.11	50.9	86.71	PP-A18	75.70	5.34	37.69	39.5	71.28
PE-SA0	90.15	-0.05	1.94	7.2	3.56	PP-SA0	88.23	-0.78	4.68	4.8	8.36
PE-SA3	80.99	1.25	26.29	33.1	48.75	PP-SA3	85.74	-0.26	11.41	11.2	21.56
PE-SA10	91.40	-1.46	6.40	11.7	10.58	PP-SA10	86.97	-0.25	3.77	5.6	7.24
PE-SA18	51.54	17.3	35.12	59.2	103.08	PP-SA18	84.33	-2.58	24.24	23.5	40.50

**Fig. 15** Diagram of hue position of measured materials in  $L^*$ ,  $a^*$ , and  $b^*$  coordinate system. Drop in  $L^*$  axis means *darker hue*. Center of the  $a^*$   $b^*$  coordinates means “white” while deviations

from the center means *coloring from green (left, negative  $a^*$ ) to red (right, positive  $a^*$ ) and from blue (bottom, negative  $b^*$ ) to yellow (top, positive  $b^*$ ) color*. (Color figure online)

decreased; on the other hand, this may decrease also the luminosity of the “corrected white”.

## Conclusion

It was found that the surface-esterified cellulose is significantly less stable than the original material and that extent of instability grows with the increasing length of carboxylic acid chain. In addition, the unsaturated OA tends to create cross-links, which is then observable as second peak in derivation of TG curve, which makes model-free isoconversional

method inapplicable in this case. The time–temperature plots were, thus, calculated only for the original cellulose and material esterified with PA and DA. These plots can be further used in optimization of processing parameters or matrix selection.

When compounded with PE or PP matrix, the final composite got yellowish tint indicating its degradation. However, the evaluation or prediction of thermal degradation from TG of the composite is virtually unfeasible since no correlation is evident. Although many authors deal with the idea of cellulose esterification to improve its hydrophobicity and behavior in polymer matrix as a consequence, data in this paper



showed thermal instability of the ester bond. This narrows the time–temperature processing window and reduces feasible use with common machinery, even though the non-oxidative atmosphere is preserved.

**Acknowledgments** Authors gratefully acknowledge Mr. Radek Holubar for preparation of composites, Mr. Pavol Suly for his help with TG, Dr. Alena Kalendova for her assistance with initial FT-IR measurements, and Dr. Tomas Sedlacek for his help with supply of Arbocel<sup>®</sup>. All mentioned are from Tomas Bata University in Zlin. The work was supported by the Operational Programme Research and Development for Innovations cofounded by the European Regional Development Fund (ERDF) and national budget of Czech Republic within the framework of the Centre of Polymer Systems project (reg. no.: CZ.1.05/2.1.00/03.0111). Authors gratefully acknowledge also the financial support of this work by the internal grant of Tomas Bata University in Zlin, No. IGA/FT/2012/040 and No. IGA/FT/2013/012, funded from the resources of specific university research.

## References

- Abdelmouleh M, Boufi S, Belgacem MN, Dufresne A (2007) Short natural-fibre reinforced polyethylene and natural rubber composites: effect of silane coupling agents and fibres loading. *Compos Sci Technol* 67:1627–1639. doi:10.1016/j.compscitech.2006.07.003
- Bhuiyan MTR, Hirai N, Sobue N (2000) Changes of crystallinity in wood cellulose by heating treatment under dried and moist conditions. *J Wood Sci* 46:431–436. doi:10.1007/BF00765800
- Devallencourt C, Saiter JM, Capitaine D (1996) Characterization of recycled celluloses: thermogravimetry/Fourier transform infra-red coupling and thermogravimetry investigations. *Polym Degrad Stab* 52:327–334. doi:10.1016/0141-3910(95)00239-1
- George J, Sreekala MS, Thomas S (2001) A review on interface modification and characterization of natural fiber reinforced plastic composites. *Polym Eng Sci* 41:1471–1485. doi:10.1002/pen.10846
- Heinze T, Liebert T (2001) Unconventional methods in cellulose functionalization. *Prog Polym Sci* 26:1689–1762. doi:10.1016/S0079-6700(01)00022-3
- Huang MR, Li XG (1998) Thermal degradation of cellulose and cellulose esters. *J Appl Polym Sci* 68:293–304. doi:10.1002/(SICI)1097-4628(19980411)68:2<293:AID-APP11>3.0.CO;2-Z
- Jandura P, Kokta BV, Riedl B (2000a) Fibrous long-chain organic acid cellulose esters and their characterization by diffuse reflectance FTIR spectroscopy, solid-state CP/MAS 13C-NMR, and X-ray diffraction. *J Appl Polym Sci* 78:1354–1365. doi:10.1002/1097-4628(20001114)78:7<1354:AID-APP60>3.0.CO;2-V
- Jandura P, Riedl B, Kokta B (2000b) Thermal degradation behavior of cellulose fibers partially esterified with some long chain organic acids. *Polym Degrad Stab* 70:387–394. doi:10.1016/S0141-3910(00)00132-4
- Jawaid M, Abdul Khalil HPS (2011) Cellulosic/synthetic fibre reinforced polymer hybrid composites: a review. *Carbohydr Polym* 86:1–18. doi:10.1016/j.carbpol.2011.04.043
- John MJ, Thomas S (2008) Biofibres and biocomposites. *Carbohydr Polym* 71:343–364. doi:10.1016/j.carbpol.2007.05.040
- Klemm D, Heublein B, Fink HP, Bohn A (2005) Cellulose: fascinating biopolymer and sustainable raw material. *Angew Chem Int Ed* 44:3358–3393. doi:10.1002/anie.200460587
- Lee MY, Park WH (1999) Epoxidation of bacterial polyesters with unsaturated side chains V. Effect of crosslinking on thermal degradation of epoxidized polymers. *Polym Degrad Stab* 65:137–142. doi:10.1016/S0141-3910(98)00229-8
- Li XG (1999) High-resolution thermogravimetry of cellulose esters. *J Appl Polym Sci* 71:573–578. doi:10.1002/(SICI)1097-4628(19990124)71:4<573:AID-APP8>3.0.CO;2-R
- Li XG, Huang MR, Bai H (1999) Thermal decomposition of cellulose ethers. *J Appl Polym Sci* 73:2927–2936. doi:10.1002/(SICI)1097-4628(19990929)73:14<2927:AID-APP17>3.0.CO;2-K
- Park WH, Lenz RW, Goodwin S (1999) Epoxidation of bacterial polyesters with unsaturated side chains: IV. Thermal degradation of initial and epoxidized polymers. *Polym Degrad Stab* 63:287–291. doi:10.1016/S0141-3910(98)00107-4
- Polaskova M, Cermak R, Verney V et al (2013) Preparation of microfibrils from wood/ionic liquid solutions. *Carbohydr Polym* 92:214–217. doi:10.1016/j.carbpol.2012.08.089
- Spoljaric S, Genovese A, Shanks RA (2009) Polypropylene-microcrystalline cellulose composites with enhanced compatibility and properties. *Compos Part A Appl Sci* 40:791–799. doi:10.1016/j.compositesa.2009.03.011
- Tome LC, Freire MG, Rebelo LPN et al (2011) Surface hydrophobization of bacterial and vegetable cellulose fibers using ionic liquids as solvent media and catalysts. *Green Chem* 13:2464–2470. doi:10.1039/c1gc15432j
- Uschanov P, Johansson LS, Maunu SL, Laine J (2010) Heterogeneous modification of various celluloses with fatty acids. *Cellulose* 18:393–404. doi:10.1007/s10570-010-9478-7
- Vyazovkin S (1996) A unified approach to kinetic processing of nonisothermal data. *Int J Chem Kinet* 28:95–101. doi:10.1002/(SICI)1097-4601(1996)28:2<95:AID-KIN4>3.0.CO;2-G
- Vyazovkin S (1997) Advanced isoconversional method. *J Therm Anal* 49:1493–1499. doi:10.1007/BF01983708
- Vyazovkin S, Sbirrazuoli N (2006) Isoconversional kinetic analysis of thermally stimulated processes in polymers. *Macromol Rapid Comm* 27:1515–1532. doi:10.1002/marc.200600404
- Vyazovkin S, Wight C (1999) Model-free and model-fitting approaches to kinetic analysis of isothermal and nonisothermal data. *Thermochim Acta* 341:53–68
- Vyazovkin S, Burnham AK, Criado JM et al (2011) ICTAC Kinetics Committee recommendations for performing kinetic computations on thermal analysis data. *Thermochim Acta* 520:1–19. doi:10.1016/j.tca.2011.03.034



## **ARTICLE III**



# Surface-esterified cellulose fiber in a polypropylene matrix: impact of esterification on crystallization kinetics and dispersion

Miroslav Janicek · Martina Polaskova ·  
Radek Holubar · Roman Cermak

Received: 4 April 2014 / Accepted: 11 August 2014 / Published online: 23 August 2014  
© Springer Science+Business Media Dordrecht 2014

**Abstract** Cellulose powders hydrophobized by surface esterification with carboxylic acids with different chain lengths (3, 10 and 18 carbons) were dispersed in a polypropylene matrix. Quality of the dispersion and nucleation activity of the filler were investigated by means of differential scanning calorimetry and optical microscopy. The results showed that the esterification decreases the crystallization rate in case of cellulose esterified with propionic or decanoic acid. On the other hand, the oleic acid ester demonstrated slightly higher crystallization rates than the unmodified cellulose, which was ascribed primarily to the newly arisen non-esterified surface after disintegration of the filler. Optical microscopy with hot stage showed the high nucleation ability of the natural cellulose fiber and its suppression in case of esterified surfaces. A complete inability to nucleate polypropylene crystallization was observed in case of decanoyl ester, while the other two retained some activity, but lower than that of the natural fiber. Finally, analysis of the filler dispersion and distribution revealed that the decanoyl and octadecanoyl esters disintegrate during melt mixing, while both dispersion and distribution of the fibers modified with propionic acid are poor.

**Keywords** Cellulose · Esterification · Hydrophobization · Crystallization kinetics · Dispersion · Composite

## Introduction

Cellulose and cellulose-based materials have been studied for decades. It is primarily its renewable resources, plants, which have stimulated the utilization of this material (John and Thomas 2008; Jawaid and Abdul Khalil 2011). Composites made from cellulose and synthetic polymers then not only preserve non-renewable resources, but also reduce the so-called “carbon footprint” (Jawaid and Abdul Khalil 2011). The combination of hydrophobic polyolefins with organic and thus hydrophilic material is often challenging, since the filler should be evenly distributed and well dispersed to obtain a composite with good quality. Several techniques were therefore developed to increase the hydrophobicity of the cellulose (George et al. 2001; Heinze and Liebert 2001; Uschanov et al. 2010). A hydrophobic surface then may not only improve the filler distribution and dispersion, but it can also influence the process of crystallization of the matrix.

It is well known that the natural cellulose nucleates polypropylene (Borysiak and Doczekalska 2009). Considering fibers, the high density of nuclei on its surface is reflected in the specific morphology of the

M. Janicek (✉) · M. Polaskova · R. Holubar ·  
R. Cermak

Department of Polymer Engineering, Faculty  
of Technology, Tomas Bata University in Zlin,  
Nam. T.G. Masaryka 275, 762 72 Zlin, Czech Republic  
e-mail: mjjanicek@ft.utb.cz  
URL: <http://www.ft.utb.cz>

so-called transcrystalline layer (Wang and Liu 1999). The influence of this layer on the mechanical behavior of the composite is still questionable (Wang and Liu 1999; Son et al. 2000; Gray 2007). However, the nucleation activity is often advantageous in industrial practice since it shortens the production time and may induce a specific morphology, which affects the overall quality of the product.

Physical and chemical modifications definitely have an impact on nucleation (Heinze and Liebert 2001; John and Thomas 2008). In some cases, the esterification may primarily influence the content of the  $\beta$ -phase polypropylene polymorph (Borysiak 2009); in others, the impact of surface modification is mainly negative, since the epitaxiality is usually disturbed, as shown, for example, by Borysiak (2012) with wood esterified with propionic or succinic anhydrides. The question then arises concerning whether the hydrophobization done with long carboxylic acids (Uschanov et al. 2010; Janicek et al. 2013) enables some nucleation activity or the epitaxial surface is modified to such an extent that no nucleation can occur. Uschanov et al. (2010) also showed the different degrees of substitution achievable with various acids and noted the phenomenon connected with a lower degree of substitution when long or unsaturated acids are used. This is indeed connected with both different hydrophobicities and expectable distortion of the epitaxial surface. Possible destruction of the nucleation activity of the cellulose filler caused by either a high degree of substitution or sterical hindrances of long side chains then should be redeemed by improvement in other qualities, such as good distribution and dispersion of the filler.

To answer these questions, a complex analysis by means of differential scanning calorimetry is carried out in this article together with optical microscopy and particle analysis.

## Experimental

### Materials

Fibrous cellulose of cotton linter origin was purchased from Sigma-Aldrich. The fibers were high-purity cellulose (99.8 %) with a relative density of 0.6, 50–350  $\mu\text{m}$  in length; their diameter was in the range of 12–15  $\mu\text{m}$  and the crystallinity of 65 % (data

provided by the supplier). To increase the hydrophobicity of the cellulose, the material was surface-esterified with oleic acid (OA), decanoic acid (DA) and propionic acid (PA) as described elsewhere (Uschanov et al. 2010; Janicek et al. 2013). The used method then gave cellulose with a degree of substitution (DS, calculated from XPS data) of about 1.49 and 1.25 in case of DA and OA, respectively (Uschanov et al. 2010).

An isotactic polypropylene (iPP) HD601CF produced by Borealis AG, Austria, was used as a matrix for the composite. The material was characterized by a melt flow rate of 8 g/10 min (ISO 1133, 230 °C/2.16 kg), weight-average molecular weight of 570,000 and polydispersity index of 3.5 (Chvatalova et al. 2009).

Prior to the mixing, the cellulose and its esters were dried in a vacuum oven at 0.1 bar and 80 °C for 2 h. A Brabender PL 2000 laboratory kneader heated to 180 °C was subsequently used to mix the natural fibers and products of the esterification into the matrix at a weight ratio of 10:90. Loading the kneader chamber and polymer melting took approximately 5 min, after which the speed of the rotors was increased from an initial 15 to 45 rpm. The molten composite was removed from the chamber after an additional 5 min of kneading. The prepared composites were named after the matrix “iPP” followed with “C” for “cellulose” and denotation of the acid used in the esterification reaction or the suffix “natural” for the original non-esterified material.

### Characterization

Differential scanning calorimetry (DSC) was performed with a Mettler Toledo DSC 1 connected to an external cooler. Both isothermal and nonisothermal crystallization measurements were performed with approximately 3 mg of the sample closed in a 20- $\mu\text{l}$  aluminum pan and measured with an empty pan as a reference. The furnace was purged with nitrogen (20 ml/min) during the experiments to assure an inert atmosphere.

### *Isothermal crystallization*

The isothermal crystallization program was initiated by rapid heating (100 K/min) from 20 to 190 °C. The sample was held for 3 min isothermally at this

temperature to erase the previous thermal history. Subsequently, a jump to a specific temperature of isothermal crystallization was performed with a cooling rate of 300 K/min. The isothermal crystallization temperatures ( $T_{c,iso}$ ) were 133, 130, 128 and 125 °C, and at these temperatures the sample was held until the heat flow reached baseline. A second jump (300 K/min) down to 20 °C followed. At this temperature, the sample was held for another 3 min to settle the heat flow and subsequently heated up to 190 °C with a rate of 20 K/min to check the melting behavior.

#### Nonisothermal crystallization

The nonisothermal crystallization was measured with the same instrument and cycles with boundary temperatures of 20 and 190 °C at which the sample was held isothermally for 3 min. The rates of cooling ( $\beta$ ) were 40, 30, 20 and 10 K/min each followed by heating of 20 K/min. Obtained data were analyzed according to the isoconversional method.

#### Microscopy and image analysis

An Olympus BX-41 optical microscope equipped with polarizers and a Linkam hot stage was used to observe the process of crystallization and morphology of the PP/cellulose composites. The PP film was slightly sputtered with the cellulose and sandwiched between two cover slips, which were placed on the hot stage. The prepared sample was heated up to 190 °C and held isothermally for about 3 min to erase the previous thermal history. Isothermal crystallization was initiated by a temperature jump (90 K/min) down to the  $T_{c,iso}$ , which was 130 °C. The obtained video records were subsequently analyzed with the software provided by the microscope manufacturer.

Furthermore, the prepared composites were cut with a rotary microtome to assess the filler distribution, dispersion and possible disintegration. About ten cuts were prepared from each sample at different positions so that the total covered area was about 9.8 mm<sup>2</sup>. These cuts were then observed in the microscope in a bright field setup, and the obtained pictures were subject to analysis with ImageJ (Schneider et al. 2012). The procedure was initiated by a contrast adjustment followed by binarization. In the binary image, the particles smaller than 2 px were

removed since they were considered noise. The rest of the particles or more precisely agglomerates were then substituted with ellipses in which distributions of the area were assessed.

## Results and discussion

### Isothermal crystallization

Figure 1 shows exotherms of the neat iPP and its composites in which the shift of the crystallization peak toward a shorter crystallization time ( $t$ ) can be seen as the  $T_{c,iso}$  decreases. A crystallization half-time ( $t_{1/2}$ ) can be easily extracted from the records as the respective peak position. Although it is a technical parameter rather than precisely analytical, its dependence on the  $T_{c,iso}$  gives a good comparison of the impact of different celluloses. The dependence is here presented in Fig. 2 in which it is clear that both the neat cellulose and the OA-esterified cellulose accelerate the crystallization process with virtually the same efficiency particularly at the  $T_{c,iso}$  below 130 °C. On the other hand, the PA- and the DA-esterified celluloses slow down the crystallization. In case of the iPP/C-PA, the  $t_{1/2}$  are similar to those of neat iPP if the  $T_{c,iso}$  is, again, below 130 °C. In connection with previous study of the thermal stability of the esterified materials (Janicek et al. 2013), one can presume, the material tends to degrade at the higher temperatures, which may influence the speed of crystallization. The vicinity of  $t_{1/2}$  in case of neat iPP and iPP/C-PA at low temperatures could be explained after revealing the filler distribution and dispersion with the microscopy as described below.

Regarding the values of crystallization enthalpy ( $\Delta H_c$ ) arranged in Table 1, the evolved heat is virtually the same in neat PP and composites, taking into account that 10 % of the sample mass is filler, which does not contribute to the overall heat evolution. Yet the lowest enthalpies are found in case of iPP/C-DA. When the melting temperatures ( $T_m$ ) are compared (Table 1), one can see that, as expected, the  $T_m$  grows with the increasing  $T_{c,iso}$  and the  $T_m$  is virtually the same as the preceding  $T_{c,iso}$  for all the materials. This indicates the created structure should be comparable, although the material crystallizes with a decreased or increased rate compared to the neat matrix.

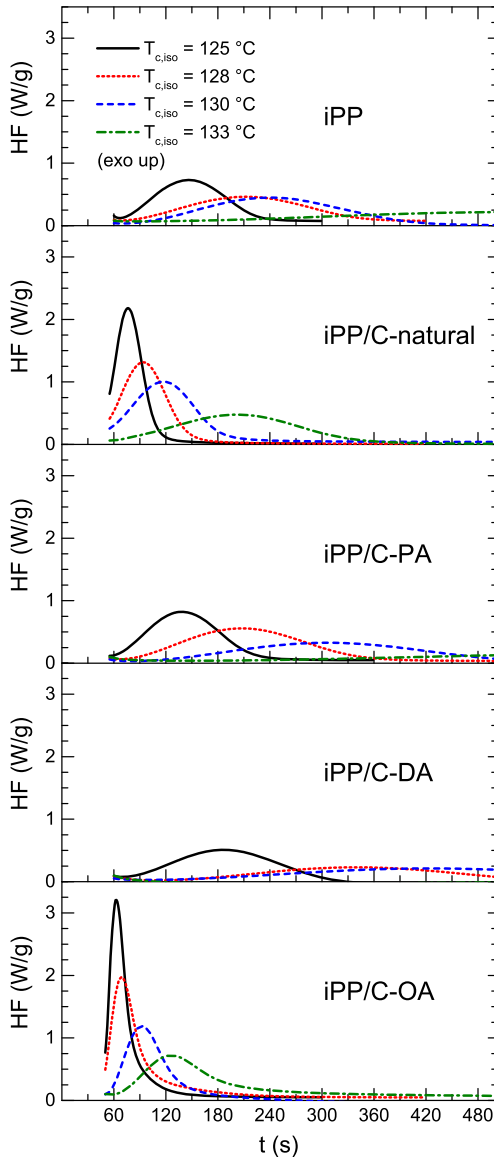


**Fig. 1** Thermograms showing isothermal segments of the crystallization process at various temperatures. In all the records, the first 40 s is omitted since the heat flow is not at the baseline because of the temperature lag that occurs at high  $\beta$

Nonisothermal crystallization

As mentioned in the work of Vyazovkin and other authors (Pijpers et al. 2002; Vyazovkin et al. 2011),

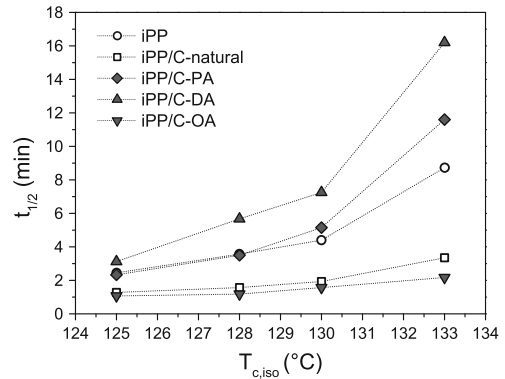


**Fig. 2** Crystallization half-time as a function of the temperature of isothermal crystallization

**Table 1** Data obtained by isothermal analysis

	$T_{c,iso}$ (°C)	$\Delta H_c$ (J/g)	$T_m$ (°C)
iPP	125	82.3	162.4
	128	82.7	163.7
	130	83.7	164.4
	133	80.0	166.4
iPP/C-natural	125	72.6	162.7
	128	69.4	163.7
	130	73.4	164.4
	133	70.2	164.4
iPP/C-PA	125	77.4	162.7
	128	77.0	163.7
	130	80.9	165.0
	133	79.3	166.4
iPP/C-DA	125	65.6	162.7
	128	67.2	163.7
	130	70.4	164.7
	133	70.7	165.1
iPP/C-OA	125	78.8	162.3
	128	77.2	163.7
	130	79.2	164.3
	133	75.8	165.4

achieving real isothermal conditions particularly in the initial stage of the isothermal analysis is difficult. Namely, those materials with relatively high rates of nucleation and crystal growth start to transform during the initial nonisothermal step. This drawback complicates the analysis and in some cases brings the credibility of the obtained results into question.



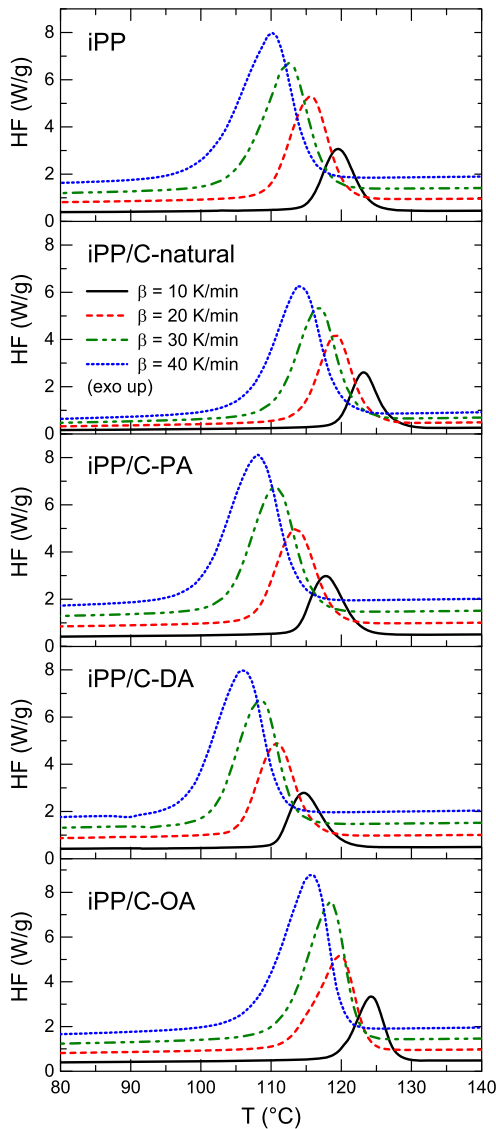


**Fig. 3** Exothermal peaks of cooling showing the crystallization process at various cooling rates

Therefore, series of nonisothermal linear cooling programs were carried out in this study to describe the crystallization process from the perspective of the kinetics with the activation energy.

Figure 3 shows exotherms of iPP and composites obtained at four different  $\beta$ . The shift of both the onset

**Table 2** Data obtained by nonisothermal analysis

	$\beta$ (K/min)	$T_p$ (°C)	$\Delta H_c$ (J/g)
iPP	10	119.5	97.7
	20	115.7	96.3
	30	112.3	92.8
	40	110.2	92.5
iPP/C-natural	10	123.1	76.4
	20	119.1	75.5
	30	116.9	74.4
	40	113.7	74.0
iPP/C-PA	10	117.7	92.1
	20	113.3	90.7
	30	110.7	89.4
	40	108.2	90.2
iPP/C-DA	10	114.7	83.5
	20	110.9	83.1
	30	108.7	79.4
	40	106.0	77.7
iPP/C-OA	10	124.3	94.3
	20	119.9	92.6
	30	118.3	92.0
	40	115.5	91.7

and peak toward lower temperatures as the  $\beta$  increases is seen in these records. Table 2 then summarizes the obtained values of both the peak position ( $T_p$ ) and calculated enthalpy ( $\Delta H_c$ ). Regarding the  $T_p$ , the assumption stated in the isothermal analysis is confirmed here—both the unmodified cellulose and the OA-esterified cellulose are nucleating the PP matrix, which is indicated by the increase of the  $T_p$ . The enthalpy has a tendency to drop with an increase in  $\beta$ , which is in agreement with other works ascribing this phenomenon to a decrease of the thermodynamically stable alpha phase content in favor of a mesomorphic structure (Lamberti 2011).

Considering the influence of the various  $\beta$  in the nonisothermal process, the activation energy ( $\Delta E$ ) can be calculated according to Kissinger, who proposed the  $\Delta E$  is determined by the variation of  $T_p$  with  $\beta$  (Vyazovkin and Sbirrazzuoli 2003):

$$\ln\left(\frac{\beta}{T_p^2}\right) = \ln Z - \Delta E/T_p R \quad (1)$$

$R$  is the molar gas constant, and  $Z$  is the temperature-independent preexponential factor.

**Table 3** Activation energies of the neat matrix and composites as calculated according to Kissinger

	iPP	iPP/C-natural	iPP/C-PA	iPP/C-DA	iPP/C-OA
$\Delta E$ (kJ/mol)	-191.4	-198.7	-188.6	-205.2	-215.7
$R^2$ (-)	0.989	0.979	0.995	0.988	0.984

From the slope of linear fit of a plot according to Eq. 1 in which the  $T_p$  is assumed to be an independent variable, the  $\Delta E$  was calculated and is presented in Table 3. In the listed values, a discrepancy is evident between the observed rates of crystallization, even though the coefficient of determination ( $R^2$ ) reaches high values for all the linearizations. Despite the wide use of this method, the obtained  $\Delta E$  is rather the mean value of the activation energy at a particular extent (usually at 50 %) and assumes that the  $\Delta E$  stays virtually constant over the whole process, which may not be true in this case.

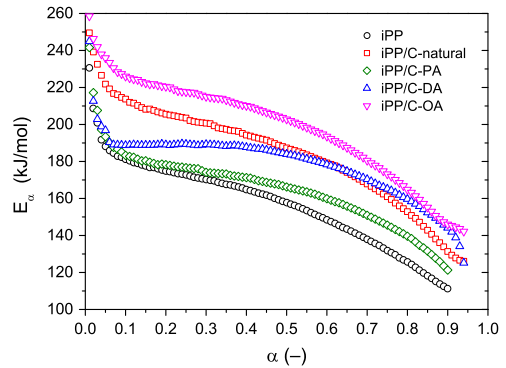
An isoconversional method using an integral equation was thus applied to determine the  $\Delta E$  as a function of conversion ( $\alpha$ ), i.e., the relative crystallinity, expressed as:

$$\alpha = \int_{T_0}^T (dH/dT)dT / Q \quad (2)$$

In Eq. 2, the  $T_0$  denotes the temperature at which the heat flow rises above baseline, and  $Q$  is the total evolved heat of crystallization. An Ozawa-Flynn-Wall (OFW) method with Doyle's approximation provides an equation in which the isoconversional activation energy ( $E_z$ ) can be calculated for each value of  $\alpha$  from the slope of linear fit of the respective plot (Sbirrazzulli et al. 2009).

$$\ln \beta_i \cong \ln(A_z E_z / R) - \ln g(\alpha) - 5.3305 - 1.052 \times (E_z / RT_{z,i}) \quad (3)$$

In Eq. 3, subscript  $i$  indicates every individual cooling rate;  $A_z$  stands for the temperature-independent pre-exponential factor of the Avrami equation;  $g(\alpha)$  is a function describing the crystallization process, which does not have to be known in this case, since it is hidden with the other constants in the intercept of the linear fit. The  $T_{z,i}$  then represents the thermodynamic temperature of the  $i$ -th  $\beta$  at which the respective  $\alpha$  was achieved. Since the DSC instrument was able to record the data only with a frequency of 1 Hz, the missing

**Fig. 4** Absolute isoconversional activation energy calculated by the OFW method as a dependence of conversion

values of  $T_{z,i}$  were extrapolated on a connecting line between the two recorded points by using the trapezoid rule.

Figure 4 shows the dependencies of the absolute value of  $E_z$  for all the materials. It is clear that none of the dependencies are constant as the conversion changes, indicating this is not a single-step reaction. Moreover, the value declines in a way typical for diffusion-complicated processes. The behavior in case of iPP/C-DA is, however, different until the conversion of 50 % has been reached. In the first part, the energy stays virtually constant at  $\sim 190$  kJ/mol, and then after reaching 50 % it starts to fall. This indicates the latter part of the crystallization of this composite is driven by the diffusion process, while the initial part is a rather reversible and complex process (Vyazovkin and Linert 1995; Vyazovkin and Wight 1997).

#### Optical microscopy

Optical microscopy was applied to gain a better insight into the different behaviors of iPP/C-DA. Figure 5 shows the structure of the composites in which one can find two phenomena connected with the cellulose

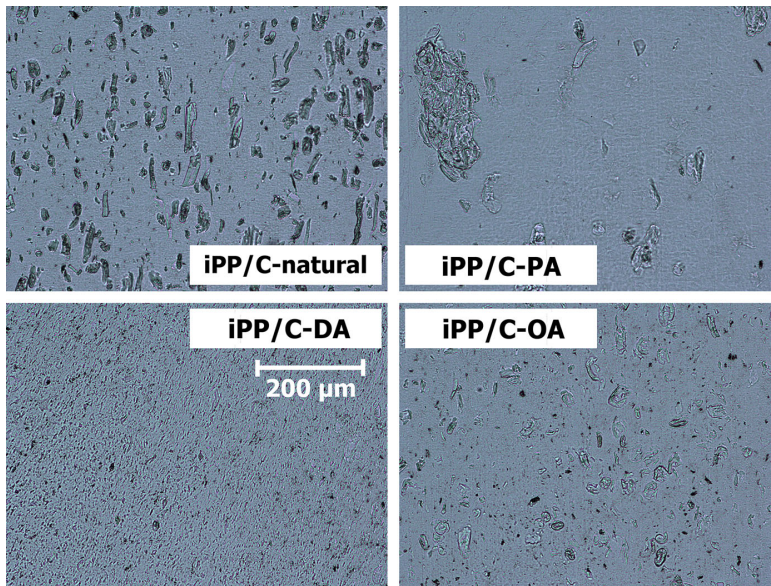


**Fig. 5** Images of the fillers in the PP matrix as observed with the optical microscope

modification. The first one is the distribution and dispersion, which seems to be good in all the materials except for iPP/C-PA, which contains large agglomerates of undispersed cellulose fibers. As mentioned above, the equality of the  $t_{1/2}$  in case of the iPP/C-PA and neat iPP (Fig. 2) arose from the poor dispersion. The composite then tends to behave rather like a neat matrix, since there is a small specific surface in contact with it.

Regarding the particle size, it is very small in case of DA- and OA-modified materials, particularly in the case of iPP/C-DA. This indicates that the modification procedure is possibly inducing structural changes in the cellulose, so its coherence is disrupted, or the adhesion of the polymer melt to the esterified surface is high enough to shear and break the cellulose in the process of mixing. As a result, a fine structure is obtained that possesses a large surface.

A previous article (Janicek et al. 2013) showed that the modification reduces the hydrophilicity among the tested materials particularly in the decanoyl ester. On the other hand, the cellulose modified with OA showed similar water adsorption (hydrophilicity) as the PA-modified one (Janicek et al. 2013). The slightly hydrophilic character of the C-OA may thus result in

**Table 4** Statistical data obtained from the image analysis

	$N$ (-)	$Q1$ ( $\mu\text{m}^2$ )	Median ( $\mu\text{m}^2$ )	$Q3$ ( $\mu\text{m}^2$ )	Mean ( $\mu\text{m}^2$ )
iPP	–	–	–	–	–
iPP/C-natural	6,841	5.0	17.4	99.2	$158 \pm 5$
iPP/C-PA	1,889	2.5	6.2	26.0	$190 \pm 60$
iPP/C-DA	35,314	3.7	9.9	29.8	$32.1 \pm 0.4$
iPP/C-OA	14,583	2.5	9.9	29.8	$40.7 \pm 0.9$

poor surface interaction with the matrix and inappropriate dispersion in comparison with the iPP/C-DA.

Concerning the disintegration of the fiber, only a small part of the surface of newly created particles is esterified. The newly arisen surface of the DA and OA esters then should nucleate in a similar way as the natural fibers, but the DA ester suppressed the crystallization process as observed in the isothermal and nonisothermal analyses. Degradation of the filler should be taken into consideration even though it was shown (Janicek et al. 2013) that the materials are relatively stable during the conditions chosen in this study. On the other hand, the effects caused by the

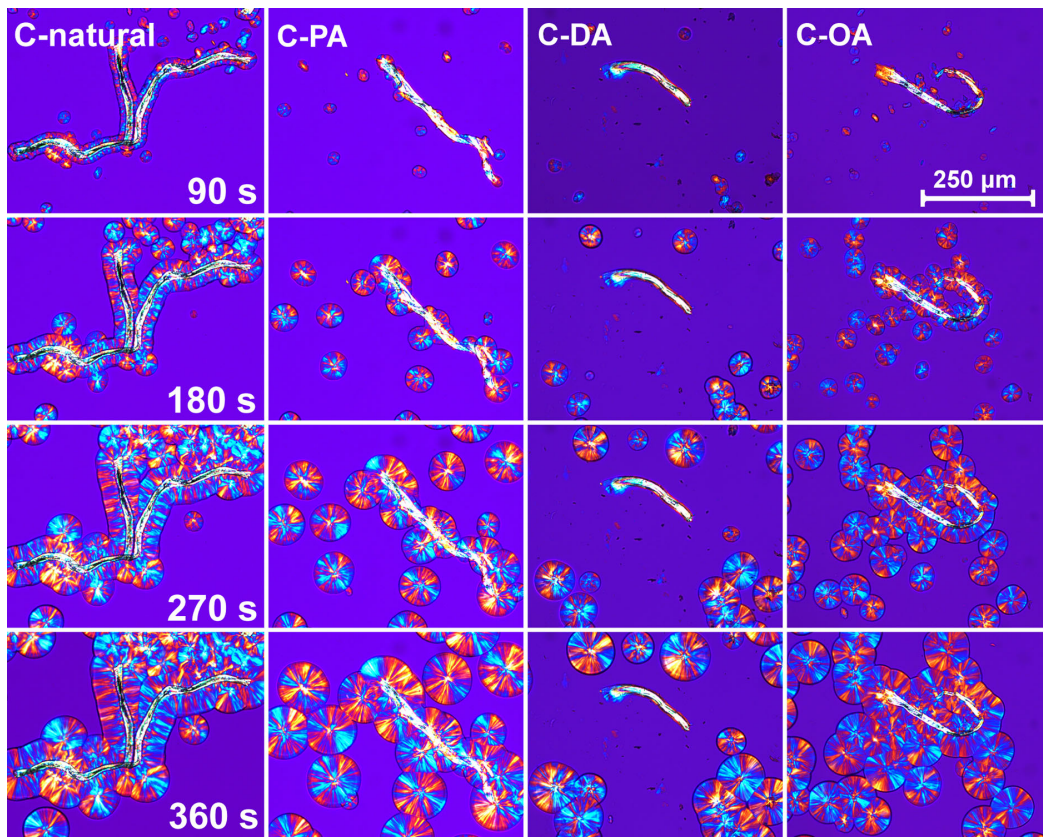


**Fig. 6** Nucleation efficiency and morphology as observed in a PLM equipped with a hot stage. The time increases from top to bottom; the fibers are natural (C-natural) cellulose and fibers esterified with the indicated acids

degradation products, no matter how low their concentration was, should not be ignored.

ImageJ was used to measure and count the particles. Statistical data are summarized in Table 4. Regarding the number of particles ( $N$ ) and the filling, which was always 10 wt%, a decrease is seen in the case of poorly dispersed PA-modified cellulose and a double or fivefold increase in case of iPP/C-OA and iPP/C-DA, respectively. The median and mean particle size decreased simultaneously.

The fine structure of the cellulose made direct observation of crystallization practically impossible; therefore, the process was observed on a thin iPP film sputtered with cellulose. Figure 6 gives a comparison of the spherulite growth in the form of snapshots taken every 90 s starting at the time when the Linkam device

reached the preset temperature of 130 °C (0 s, not included). Regarding the natural cellulose fiber, one can clearly see the nucleation ability resulting in transcrystalline growth all over the fiber surface, while crystallization in the bulk is rare. A different situation is observed in case of PA-esterified fiber in which the nucleation in the bulk and on the fiber is virtually equal. OA-esterified fiber then shows slightly improved interaction with the iPP as the crystallization starts in both the bulk and surface, yet the fiber is covered with a larger amount of nuclei than in the case of PA-modified cellulose. A completely different situation occurs with the DA-modified fibers. This material shows no interaction with the surrounding polymer, and the only nucleation and crystal growth were observed in the bulk. When the crystallization

had finished, the fiber was situated between the spherulite boundaries, which is unsuitable with respect to the stress transfer in the final composite. Moreover, such material may rather act as a defect, which impairs the final mechanical properties.

The root cause of this phenomenon should be the disruption of the epitaxial surface on the esterified fibers, particularly in case of C-DA. In connection with the previously discussed hydrophobicity (Janicek et al. 2013), this material exhibited the lowest water absorption and thus the highest hydrophobicity among the tested samples. In the process, its nucleation ability completely vanished. One can thus say that the more hydrophobic the material, the better it is dispersed in the matrix; the nucleation is, however, minimal. It is also worth noting that the C-PA and C-OA exhibited virtually the same water adsorption (Janicek et al. 2013), and within the current study, they are again similar concerning their nucleation properties. Thus, the distortion of the nucleation ability may not be solely related to the length of the acid. Furthermore, OA is unsaturated and thus inhomogeneous to some extent in its physicochemical nature compared to the polypropylene melt. In contrast, the DA chain grafted on the fiber surface is a saturated hydrocarbon, which could be considered a quasiliquid layer penetrating into the melt and creating no surface on which to crystallize.

## Conclusion

Analysis by means of DSC showed a decreasing crystallization rate in case of composites with cellulose esterified with propionic and decanoic acids. On the other hand, the oleic acid ester showed as good a nucleation ability as the natural cellulose, which should be ascribed primarily to its disintegration and exposition of the unmodified surface. Moreover, optical microscopy showed the suppression of the nucleation ability of cellulose fibers after esterification with carboxylic acid of various lengths. The cellulose modified with decanoic acid showed no nucleation ability, while the materials esterified with propionic or oleic acid showed some nucleation, but it was still low in comparison with the unmodified surface. When mixed into the matrix, the cellulose esterified with decanoic or oleic acid disintegrates, which results in fine dispersion and good distribution. This phenomenon

may be positive if the original fibrous structure is not needed.

**Acknowledgments** Authors gratefully acknowledge a financial support of this work by internal grants of Tomas Bata University in Zlin, No. IGA/FT/2013/012 and No. IGA/FT/2014/014, funded from the resources of specific university research.

## References

- Borysiak S (2009) Supermolecular structure of wood/polypropylene composites: I. The influence of processing parameters and chemical treatment of the filler. *Polym Bull* 64:275–290. doi:10.1007/s00289-009-0202-4
- Borysiak S (2012) Fundamental studies on lignocellulose/polypropylene composites: effects of wood treatment on the transcrystalline morphology and mechanical properties. *J Appl Polym Sci* 127:1309–1322. doi:10.1002/app.37651
- Borysiak S, Doczekalska B (2009) The influence of chemical modification of wood on its nucleation ability in polypropylene composites. *Polimery* 54:820–827
- Chvatalova L, Navratilova J, Cermak R, Raab M, Obadal M (2009) Joint effects of molecular structure and processing history on specific nucleation of isotactic polypropylene. *Macromolecules* 42:7413–7417. doi:10.1021/ma9005878
- George J, Sreekala MS, Thomas S (2001) A review on interface modification and characterization of natural fiber reinforced plastic composites. *Polym Eng Sci* 41:1471–1485. doi:10.1002/pen.10846
- Gray DG (2007) Transcrystallization of polypropylene at cellulose nanocrystal surfaces. *Cellulose* 15:297–301. doi:10.1007/s10570-007-9176-2
- Heinze T, Liebert T (2001) Unconventional methods in cellulose functionalization. *Prog Polym Sci* 26:1689–1762. doi:10.1016/S0079-6700(01)00022-3
- Janicek M, Krejci O, Cermak R (2013) Thermal stability of surface-esterified cellulose and its composite with polyolefinic matrix. *Cellulose* 20:2745–2755. doi:10.1007/s10570-013-0070-9
- Jawaid M, Abdul Khalil HPS (2011) Cellulosic/synthetic fibre reinforced polymer hybrid composites: a review. *Carbohydr Polym* 86:1–18. doi:10.1016/j.carbpol.2011.04.043
- John MJ, Thomas S (2008) Biofibres and biocomposites. *Carbohydr Polym* 71:343–364. doi:10.1016/j.carbpol.2007.05.040
- Lamberti G (2011) Isotactic polypropylene crystallization: analysis and modeling. *Eur Polym J* 47:1097–1112. doi:10.1016/j.eurpolymj.2011.02.005
- Pijpers TFJ, Mathot VBF, Goderis B, Scherrenberg RL, van der Vegte EW (2002) High-speed calorimetry for the study of the kinetics of (de)vitrification, crystallization, and melting of macromolecules. *Macromolecules* 35:3601–3613. doi:10.1021/ma011122u
- Sbirrazzuoli N, Vincent L, Mija A, Guigo N (2009) Integral, differential and advanced isoconversional methods. *Chemom Intell Lab Syst* 96:219–226. doi:10.1016/j.chemolab.2009.02.002

- Schneider CA, Rasband WS, Eliceiri KW (2012) NIH Image to ImageJ: 25 years of image analysis. *Nat Methods* 9:671–675. doi:[10.1038/nmeth.2089](https://doi.org/10.1038/nmeth.2089)
- Son SJ, Lee YM, Im SS (2000) Transcrystalline morphology and mechanical properties in polypropylene composites containing cellulose treated with sodium hydroxide and cellulase. *J Mater Sci* 5:5767–5778. doi:[10.1023/A:1004827128747](https://doi.org/10.1023/A:1004827128747)
- Uschanov P, Johansson LS, Maunu SL, Laine J (2010) Heterogeneous modification of various celluloses with fatty acids. *Cellulose* 18:393–404. doi:[10.1007/s10570-010-9478-7](https://doi.org/10.1007/s10570-010-9478-7)
- Vyazovkin S, Linert W (1995) Kinetic analysis of reversible thermal decomposition of solids. *Int J Chem Kinet* 27:73–84. doi:[10.1002/kin.550270109](https://doi.org/10.1002/kin.550270109)
- Vyazovkin S, Sbirrazzuoli N (2003) Isoconversional analysis of calorimetric data on nonisothermal crystallization of a polymer melt. *J Phys Chem B* 107:882–888. doi:[10.1021/jp026592k](https://doi.org/10.1021/jp026592k)
- Vyazovkin S, Wight CA (1997) Kinetics in solids. *Annu Rev Phys Chem* 48:125–149. doi:[10.1146/annurev.physchem.48.1.125](https://doi.org/10.1146/annurev.physchem.48.1.125)
- Vyazovkin S, Burnham AK, Criado JM, Perez-Maqueda LA, Popescu C, Sbirrazzuoli N (2011) ICTAC kinetics committee recommendations for performing kinetic computations on thermal analysis data. *Thermochim Acta* 520: 1–19. doi:[10.1016/j.tca.2011.03.034](https://doi.org/10.1016/j.tca.2011.03.034)
- Wang C, Liu CR (1999) Transcrystallization of polypropylene composites: nucleating ability of fibres. *Polymer* 40: 289–298. doi:[10.1016/S0032-3861\(98\)00240-7](https://doi.org/10.1016/S0032-3861(98)00240-7)

## **ARTICLE IV**





# Crystallization of Nucleated Isotactic Polypropylene Studied by Means of Conventional and Flash Differential Scanning Calorimetry

Miroslav JANICEK<sup>1</sup>, Radek HOLUBAR<sup>1</sup>, Martina POLASKOVA<sup>1</sup> and Roman CERMAK<sup>1</sup>

<sup>1</sup> Department of Polymer Engineering, Faculty of Technology, Tomas Bata University in Zlin, Nam. T. G. Masaryka 275, 762 72 Zlin, Czech Republic.

Corresponding author e-mail: mjanicek@ft.utb.cz; m.janicek@greiner-gpi.com

Corresponding author telephone: +420727875410

*Abstract:* Thermal behavior and structure of the neat and nucleated iPP is studied in this paper. The nucleation agents were common colorants which possess either  $\alpha$ -nucleating (phthalocyanine and indolone), or non-specific (quinacridone) nucleating activity. Besides the colorants, a non-coloring commercially available NJ Star NU-100 is used in the study. Nucleation ability and efficiency of the individual substances in concentration of 0.1 wt. % and under extreme cooling rates provided by flash differential scanning calorimetry (DSC) are assessed within this paper. The records obtained from flash DSC showed no evidence of the  $\beta$  phase presence, even though the melting of  $\beta$  phase is observed by the conventional DSC for the corresponding material. Concerning the high cooling rates, the absence of the  $\beta$  phase was probably caused by higher crystallization rate of the  $\alpha$  phase at the given temperatures of isothermal crystallization, or given cooling rates during the non-isothermal study. For the studied material, the measurements showed that neat polypropylene cease to crystallize at cooling rates of about 250 K/s, while the nucleated materials are still crystallizing up to the cooling rates of about 600 K/s at which the amount of amorphous material grows. There was no crystallization observed when cooled with rates above 1200 K/s.

*Keywords:* isotactic polypropylene, nucleating agent, isothermal, non-isothermal, crystallization, flash DSC

## Introduction

There are no doubts about the significant impact of the polymeric material structure on the end properties, quality and durability [1–5]. Concerning polymorphic material, such as isotactic polypropylene (iPP) is, the phase in which the material crystallizes during melt cooling influences virtually all of its final properties, which has been broadly studied in recent decades [4–6]. Some of these studies focused on one of the first non-coloring and commercially available nucleating agent (NA) NJ Star NU-100, which gained attention also due to its dual-selective nucleating ability [7,8]. This non-specific nucleation can be then used to some extent to tailor the phase composition of the iPP by both, the concentration of the NA and the cooling process [8].

A common technique for these studies is differential scanning calorimetry (DSC). Until the recent years, this technique was limited by the efficiency of heat transfer concerning the needed thermal quasi-equilibrium between the sample mass and sensor. Especially polymeric materials, which are poor heat conductors, were difficult to measure under real isothermal conditions or high cooling rates [1,9–11]. Recent technology, which use chip sensors in calorimetry, enabled not only to simulate and measure cooling processes at speeds as they commonly occur in real processes, but also enabled study of the processes

41 under real isothermal conditions, since the temperature jumps can be performed with such  
42 rates, the material cannot transform during the non-isothermal jump [1,11].

43 Aim of presented study is thus to assess the nucleation ability and efficiency of four  
44 nucleating agents by means of flash DSC and both isothermal and non-isothermal cooling  
45 regimes and compare the crystallization behavior of neat iPP.

## 46 **Experimental**

### 47 **Materials**

48 An isotactic polypropylene Borealis HB205TF was used as a base material for the study.  
49 This material is characterized with melt-flow index of 1.0 g/10 min, weight-averaged  
50 molecular weight of 830 000, and polydispersity index of 2.8 [1]. The material was  
51 nucleated by four substances already known for their nucleation ability [7,8,12,13]. The  
52 substances were common colorants – Phthalocyanine (CAS No. 147-14-8), Indolone (CAS  
53 No. 5590-18-1) and Quinacridone (CAS No. 1047-16-1), hereinafter abbreviated as Phth,  
54 Ind, and Qui, respectively. The only non-coloring agent was a broadly studied NJ Star NU-  
55 100, hereinafter abbreviated as NJStar, which is a sorbitol-based nonspecific nucleating  
56 agent (CAS No. 153250-52-3). Since the NA are commonly used in very low  
57 concentrations [1] – in our case 0.1 wt. %, the dispersion was made by four consecutive  
58 melt-mixing. The first step was preparation of masterbatch with the NA concentration of  
59 30 wt. % by using Thermo-Haake counter-rotating laboratory mixer (1 min at 200 °C and  
60 50 rpm). The second step was dilution of this masterbatch to obtain iPP with NA  
61 concentration of 1 wt. % by using counter-rotating twin-screw extruder attached to  
62 Branbender PL2000 driver. The extruded string was cut and finally mixed with additional  
63 neat iPP to obtain final concentration of NA 0.1 wt. %. In both steps the temperatures of  
64 the barrels were 180-200-220 °C (hopper to die). The speed of the screws was set to  
65 55 rpm. The fourth mixing was performed as a side effect of test specimen preparation by  
66 injection molding. The specimens were not used within this study; however, the sample  
67 material was taken from them and was used in DSC.

### 68 **Non-isothermal crystallization with conventional DSC**

69 Mettler-Toledo DSC 1 was used to measure transitions of the studied materials under non-  
70 isothermal conditions with low cooling and heating rates. This apparatus is hereinafter  
71 denoted as „conventional DSC“. In all the experiments with conventional DSC a 20 µL  
72 aluminum pan was loaded with ~3 mg of the studied material and measured together with  
73 an empty reference aluminum pan. The measuring cell was continuously purged with  
74 nitrogen (20 mL/min). All the measurements were initiated by heating up to 200 °C at  
75 which the material was held 2 min. Depending on the current run, the cooling rate was 5,  
76 10, 15, 20, 30, 50, 75, 100, 150, 200, or 300 K/min, and the cooling was performed down  
77 to 0 °C. At this temperature, the sample was held isothermally for 2 min to settle the heat  
78 flow. The analysis of the structure, which evolved during the cooling, was done in all the  
79 cases with the same heating rate of 20 K/min and the record was subsequently evaluated by  
80 using the instrument software.

## 81 Isothermal and non-isothermal crystallization with flash DSC

82 Mettler-Toledo Flash DSC 1 (FDSC) was, on the other hand, used to study the material  
83 transitions under both isothermal and non-isothermal conditions. For the study, proper chip  
84 sensors were loaded with the individual materials and the used amounts of the iPP and  
85 nucleated iPPs were determined by the direct correlation of the heat of fusion ( $\Delta h_f$ )  
86 measured with the FDSC and specific heat of fusion ( $\Delta H_f$ ) given by conventional DSC  
87 technique. The amount of the material was ~80 ng.

88 The non-isothermal study was performed by repetitive cooling and melting of the  
89 materials. The cooling rates were selected in range starting at 5 K/s (300 K/min) and  
90 growing up to 2 500 K/s (150 000 K/min) at which the material does not crystallize even if  
91 it is nucleated. The cooling rates are distributed quasi-logarithmically with smaller steps in  
92 the transition area. The analysis of the sample structure was then performed with heating  
93 rate of 1 000 K/s (60 000 K/min). The range of measurement was -75 °C to 200 °C with  
94 short isotherms (about 0.2 s) inserted between cooling and heating runs.

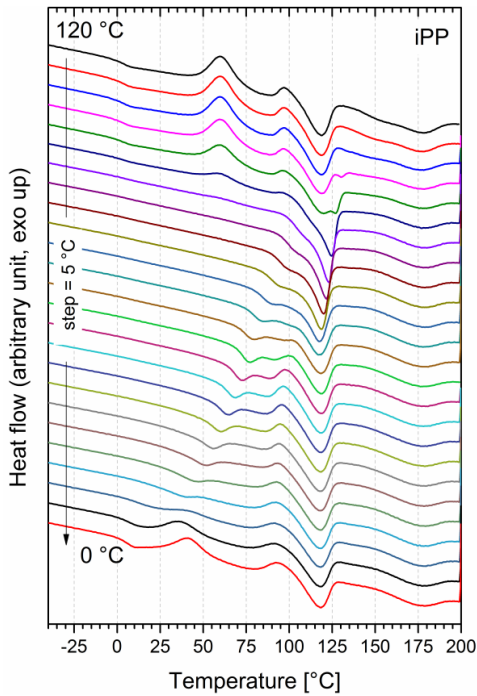
95 During the isothermal study, the samples were rapidly heated up to 200 °C and held at this  
96 temperature for 0.2 s. A jump cooling was performed with rate of 30 000 K/s down to the  
97 crystallization temperature ( $T_{c,iso}$ ) at which the material was held isothermally for 1 s. The  
98 sample was then cooled down to -75 °C with 30 000 K/s. After a short isothermal step of  
99 0.2 s a reading of the sample structure was performed similarly to the non-isothermal  
100 study.

101 It is worth to mention that both the lowest cooling rate during the non-isothermal study and  
102 the upper  $T_{c,iso}$  during the isothermal study are influenced by the thermophoresis. This  
103 phenomenon, which occurred during slow cooling rates or long isothermal steps at high  
104  $T_{c,iso}$ , moved the material eccentrically from the sensor “hot-spot” (area of about 150  $\mu\text{m}$   
105 by 150  $\mu\text{m}$ ). The material amount thus decreased continuously, when it was in molten stay.  
106 The lower cooling rate limit (5 K/s) and the upper  $T_{c,iso}$  (120 °C) with respect to the time of  
107 isothermal crystallization (1 s) were then subordinated to this phenomenon.

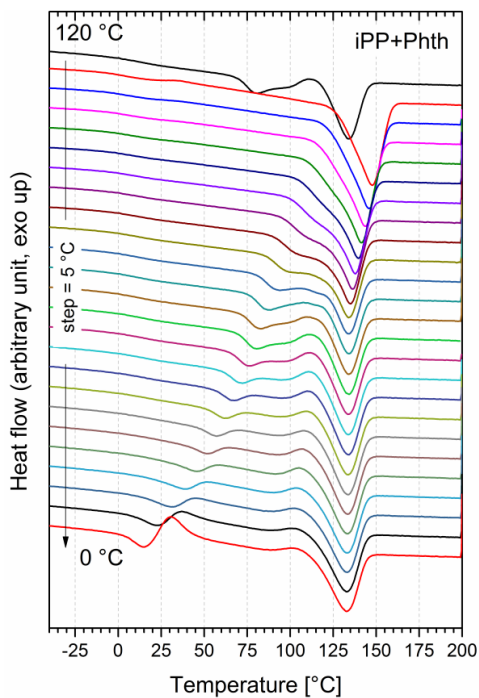
## 108 Results

109 **Figures 1–5** show records of the individual materials obtained during the heating of  
110 isothermally crystallized samples. One can clearly see cold crystallization peak appearing  
111 in at least the first line related to the melting of material previously isothermally  
112 crystallized at 120 °C for 1 s. Regarding the iPP (**Figure 1**), the cold crystallization  
113 appears even in the heating record following the isothermal crystallization at 95 °C, while  
114 the iPP+Phth does not possess cold crystallization. This indicates the low crystallization  
115 rate of iPP at elevated temperatures. Surely, the material would have crystallized  
116 completely, if the crystallization time had been long enough. Unfortunately, the  
117 thermophoretic forces then would have affected the measurement. The iPP+Phth, on the  
118 other hand, shows no cold crystallization but broad peak at about 80 °C which is melting of  
119 mesomorphic phase. The Phth thus performs as a very active NA with nucleation ability  
120 not observed within the other NAs (**Figures 3–5**). It is also worth to mention that the first  
121 melting at 80 °C in case of isothermally crystallized iPP+Phth at 120 °C is probably  
122 accompanied by crystallization, which superposes with the melting peak [14]. The cold

123 crystallization appears again in the records following the isothermal crystallization at  
124 temperatures close to 0 °C, which is close to the temperature of glass transition ( $T_g$ ) of iPP.  
125 This is in conformity with the theory, which says that the crystallization rates are low at  
126 both – high temperatures and  $T_g$  [15].

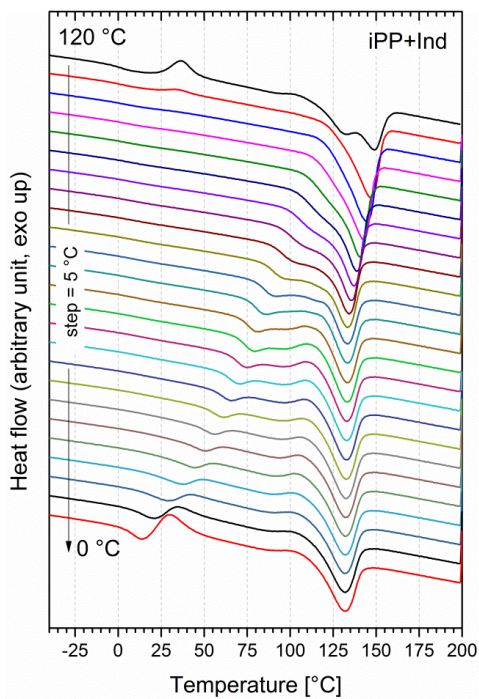


127  
128 **Figure 1.** Thermograms recorded during melting the neat iPP after cooling at individual  $T_{c,iso}$ . The curves are  
129 shifted vertically to better distinguish.



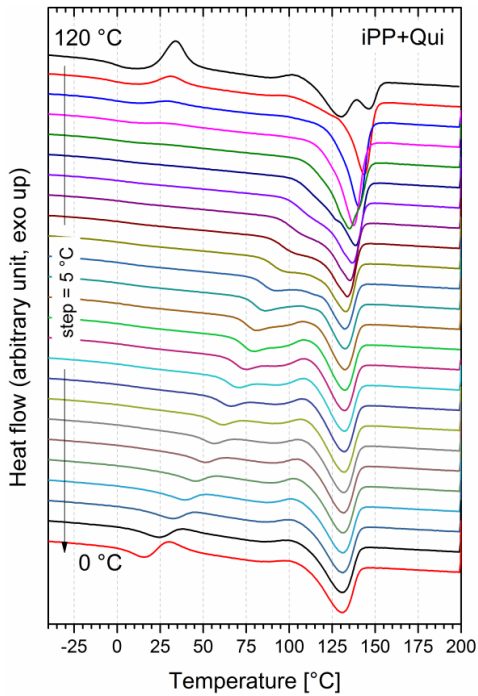
130  
131  
132

**Figure 2.** Thermograms recorded during melting the iPP nucleated with Phth after cooling at individual  $T_{c,iso}$ . The curves are shifted vertically to better distinguish.



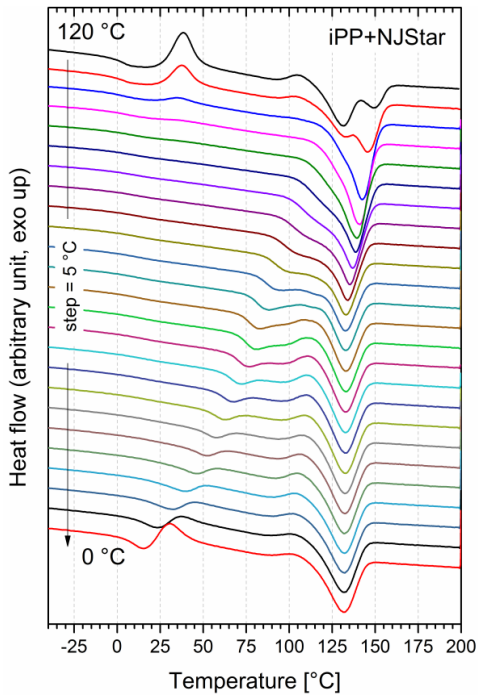
133  
134  
135

**Figure 3.** Thermograms recorded during melting the iPP nucleated with Ind after cooling at individual  $T_{c,iso}$ . The curves are shifted vertically to better distinguish.



136  
137  
138

**Figure 4.** Thermograms recorded during melting the iPP nucleated with Qui after cooling at individual  $T_{c,iso}$ . The curves are shifted vertically to better distinguish.

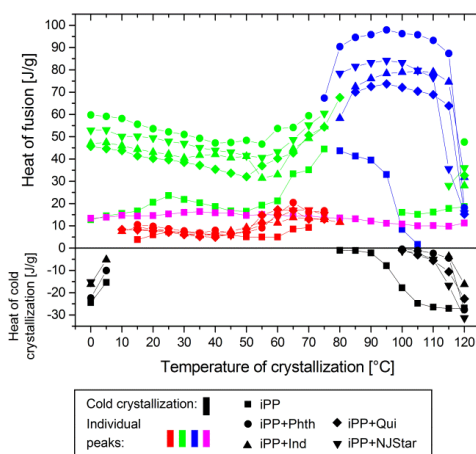


139  
140  
141

**Figure 5.** Thermograms recorded during melting the iPP nucleated with NJStar after cooling at individual  $T_{c,iso}$ . The curves are shifted vertically to better distinguish.

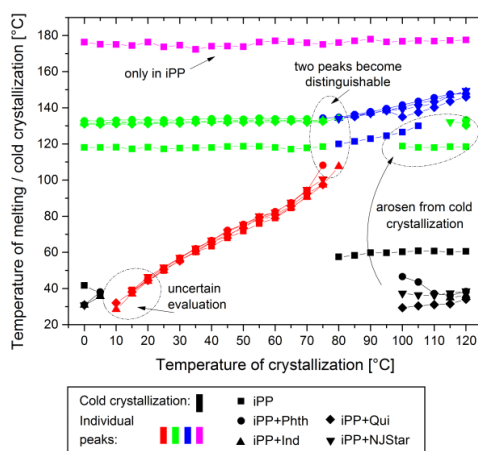
142 Concerning melting peaks, the behavior is complex. The neat iPP melting peak is located  
143 between 120 and 125 °C (**Figure 1**). The structure created during the cold crystallization

144 melts at even lower temperatures (about 115 °C). The melting peak of the isothermally  
 145 created crystalline structure appears in the fourth record in the **Figure 1**, which  
 146 corresponds to the melting after isothermal crystallization at 105 °C. This peak first grows  
 147 in intensity then drops down as the  $T_{c,iso}$  decreases and its intensity become virtually  
 148 constant with  $T_{c,iso}$  starting at 60 °C, which is shown in **Figure 6**. Concerning the neat iPP,  
 149 another melting appears at about 175 °C. This melting evolves virtually constant heat of  
 150 about 15 J/g. Regarding the fact that this peak was observed only in case of the neat iPP,  
 151 one can presume, the origins of this peaks are laid down during the cooling and  
 152 crystallization, which is done by the polymer itself and not due to the presence of the NA  
 153 surface. Although, this structure is early overgrown by the prevailing crystallites of poor  
 154 quality (low  $T_m$ , concerning Gibbs-Thomson effect [15]), the order and amount of this  
 155 material can possibly be improved and multiplied during the subsequent heating and  
 156 material reorganization after the  $T_g$  is reached. The improved orderliness then may allow  
 157 the material to melt at higher  $T_m$ .



158  
 159 **Figure 6.** Specific heat of fusion of the individual peaks as a dependence on  $T_{c,iso}$ . In the plot together with  
 160 the heat of cold crystallization (negative values).

161 **Figure 6** shows the comparison of  $\Delta H_f$  of the individual peaks. At the high temperatures  
 162 (above 80 °C) there are only two values for the nucleated materials, which correspond to  
 163 the single melting peak and initial cold crystallization. It is clear, from the highest  $\Delta H_f$  of  
 164 the iPP+Phth and absence of cold crystallization for this material, that Phth is the most  
 165 active NA followed by NJStar, Ind and Qui. Regarding the individual melting records  
 166 (**Figures 1–5**), one can see the asymmetry of the melting peak, which grows with decrease  
 167 of  $T_{c,iso}$ . This asymmetry is given by the presence of at least two crystalline qualities – the  
 168 predominant  $\alpha$  phase and the mesomorphic phase, which quality (crystallite size according  
 169 to Gibbs-Thomson equation [15,16]) decreases with decrease of  $T_{c,iso}$ . When the  $T_{c,iso}$  is  
 170  $\sim 80$  °C, the shoulder of the main peak transits into apparent peak, which was analyzed  
 171 separately and the  $\Delta H_f$  of it is plotted in the **Figure 6**, which shows relative invariability  
 172 with the mean value  $\sim 10$  J/g. On the other hand, **Figure 7**, which gives summary of the  $T_m$ ,  
 173 shows trend of this small peak, which is also evident within the melting records. The peak  
 174 shifts towards lower  $T_m$  as the  $T_{c,iso}$  decreases. At the temperatures  $\sim 15$  °C the glass  
 175 transition and cold crystallization interfere with this peak, which makes the evaluation of  
 176 this region ambiguous.



177  
178  
179

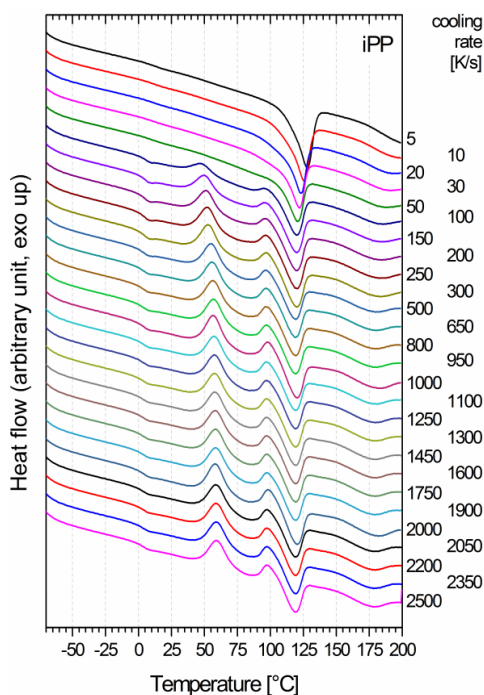
**Figure 7.** Melting temperatures as a dependence on  $T_{c,iso}$ . In the plot together with the temperature of cold crystallization.

180 In the **Figure 7**, the plotted  $T_m$  shows virtual invariability at  $T_{c,iso}$  below  $\sim 70$  °C, while the  
181 increase is evident with growing  $T_{c,iso}$ . This is in conformity with nucleation theory, which  
182 defines the critical nucleus size (i.e. thickness) at the  $T_c$  [15]. According to the **Figure 7** it  
183 may seem that the theory fails at low  $T_c$  since the decrease of the  $T_m$  stops at  $\sim 120$  °C in  
184 case of iPP and  $\sim 130$  °C in case of the nucleated materials. It is worth to mention, that  
185 according to the guidelines provided by Mettler-Toledo, the studied material was spread on  
186 the FDSC chip membrane to assure a good contact and heat transfer. Estimated thickness  
187 of this film was about 4  $\mu\text{m}$ . Concerning the large specific surface ( $\sim 10^4$   $\text{m}^2/\text{g}$ ), one can  
188 presume, the whole crystallization and melting processes shall be affected by the specific  
189 surface-related forces.

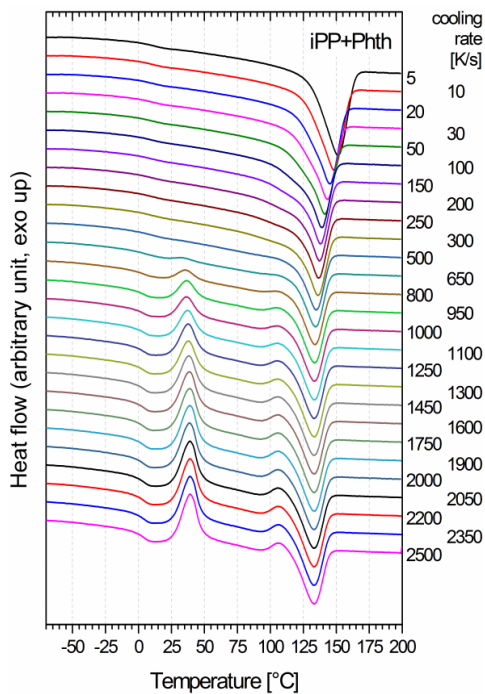
190 If one focuses on the analysis of the phase composition, there can be expectations, the  
191 iPP+Qui and iPP+NJStar should comprise primarily  $\beta$  phase since the Qui and NJStar are  
192  $\beta$ -nucleating, the rest then should comprise  $\alpha$  phase. Concerning the iPP and iPP+Phth, the  
193  $\alpha$  phase is evident, although, one would expect its  $T_m$  at about  $\sim 160$  °C. The relatively low  
194  $T_m$  measured within this study corresponds with lamellar thickness of 80–100 nm  
195 (according to Gibbs-Thomson equation considering equilibrium melting temperature of  
196 209 °C, fold-surface energy of 0.122  $\text{J}/\text{m}^2$  and volumetric heat of fusion of  $1.959 \times 10^8$   $\text{J}/\text{m}^3$   
197 [16–19]). **Figures 3–5** shows, in contrast with **Figures 1** and **2**, superposition of two peaks  
198 – one at  $\sim 130$  °C, the other at  $\sim 145$  °C. In case of iPP+Ind, this peak may be related to the  
199 cold crystallization of the supercooled polymer since the relevant intensities are relatively  
200 equal and the Ind is not expect to nucleate the  $\beta$ -crystallite growth. However, the Qui and  
201 NJStar nucleate the  $\beta$ -crystallites in many studies made with conventional DSC [7,8,20]  
202 and thus there should be present melting peak of  $\beta$  phase within the records shown in  
203 **Figures 4** and **5**. Focusing on the peak at  $\sim 130$  °C, its  $\Delta H_f$  is virtually equal to the heat  
204 evolved during the preceding cold crystallization. One can thus say that this peak does not  
205 represent the  $\beta$  phase but rather  $\alpha$  crystallites or mesomorphic phase. The absence of any  
206 evidence of  $\beta$  phase may be explained by the different growth rates of the  $\beta$  and  $\alpha$  phase at  
207 given temperatures [7]. Namely the NJStar is known for its nonspecific nucleation ability  
208 and probably nucleated  $\beta$  phase could have been overgrown by the  $\alpha$  phase exhibited in the  
209 records [7].



210 In the records of melting (**Figures 8–12**), which followed crystallization under non-  
 211 isothermal conditions, one can notice the neat iPP does not crystallize completely at the  
 212 cooling rates above 50 K/s. The amount of amorphous phase grows with further increase in  
 213 cooling rate, which then exhibits by cold crystallization with peak at about 50–60 °C. The  
 214 nucleated materials, on the other hand, reveals cold crystallization in melting of structures  
 215 created under non-isothermal cooling with rate of about 500 K/s, except the iPP+Phth  
 216 (**Figure 9**) which still crystallizes completely at the 500 K/s and starts to reveal cold  
 217 crystallization peak in the melting following the cooling at 650 K/s. It is worth to mention,  
 218 the iPP have all the cold crystallization  $T_c$  above 50 °C, while the nucleated materials  
 219 possess the  $T_c$  related to the cold crystallization in between 30–50 °C. Regarding the  $T_m$ ,  
 220 the situation is the inverse – all the melting peaks are below 130 °C in case of neat material  
 221 and above this temperature in cases of the nucleated materials. Similarly as in the  
 222 isothermal study (cf. **Figure 1**), the neat material possess another melting peak in its  
 223 melting records (**Figure 8**), which is at temperatures of about 175 °C. The origins of this  
 224 peak should be the same as in the isothermally crystallized material.

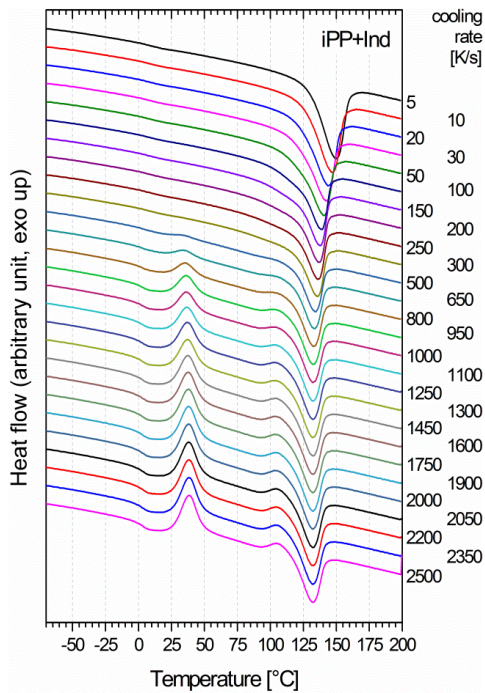


225  
 226 **Figure 8.** Thermograms recorded during melting the neat iPP after cooling at different cooling rates  
 227 (indicated at the right of each curve). The curves are shifted vertically to better distinguish.



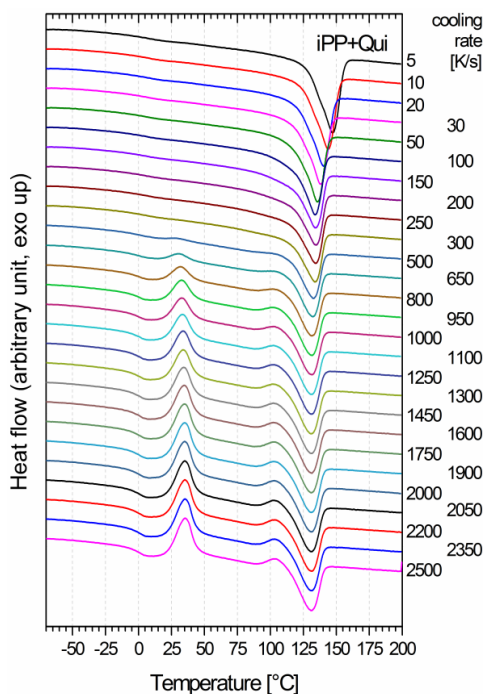
228  
229  
230

**Figure 9.** Thermograms recorded during melting the iPP nucleated with Phth after cooling at different cooling rates (indicated at the right of each curve). The curves are shifted vertically to better distinguish.



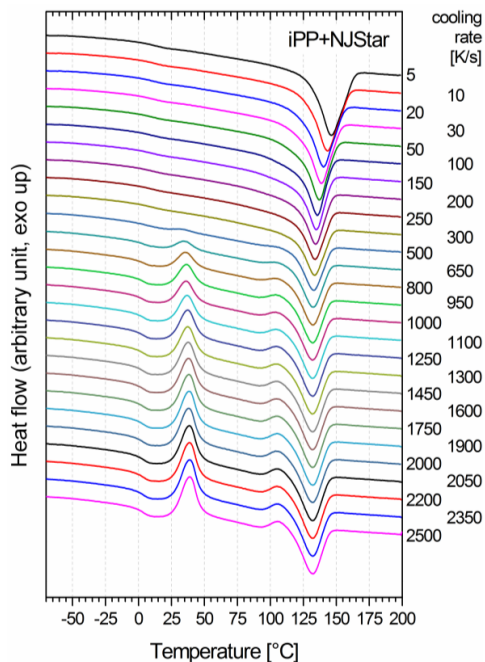
231  
232  
233

**Figure 10.** Thermograms recorded during melting the iPP nucleated with Ind after cooling at different cooling rates (indicated at the right of each curve). The curves are shifted vertically to better distinguish.



234  
235  
236

**Figure 11.** Thermograms recorded during melting the iPP nucleated with Qui after cooling at different cooling rates (indicated at the right of each curve). The curves are shifted vertically to better distinguish.

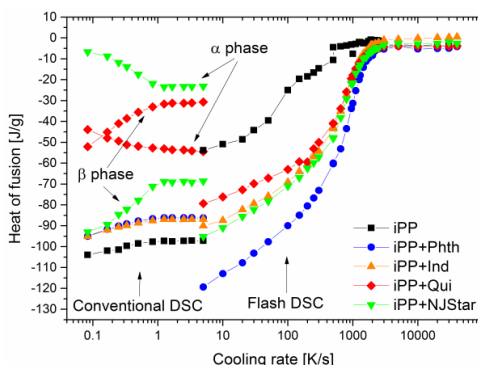


237  
238  
239

**Figure 12.** Thermograms recorded during melting the iPP nucleated with NJStar after cooling at different cooling rates (indicated at the right of each curve). The curves are shifted vertically to better distinguish.

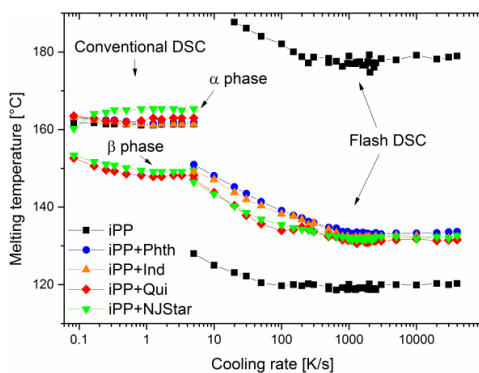
240 **Figure 13** gives the comparison of the  $\Delta H_f$  provided by the FDSC analysis with the  $\Delta H_f$   
241 evaluated in records of non-isothermal crystallization performed with conventional DSC.  
242 This comparison is worthwhile primarily in the non-isothermal study, since the isothermal

243 conditions are virtually unattainable (thus not here presented) with the conventional DSC.  
 244 Main reason of this is the apparatus construction and the sample size [1,9,21]. Regarding  
 245 the dependence of  $\Delta H_f$  on cooling rate presented in **Figure 13**, there are two dependencies  
 246 for the iPP+Qui and iPP+NJStar at the lower part of the cooling rate axis. These points are  
 247 related to the data measured by the conventional DSC in which the two melting peaks were  
 248 apparent. In both materials, the two peaks are present regardless the cooling rate, but their  
 249 intensity changes. The intensity (represented by the  $\Delta H_f$ ) of the peak related to melting of  $\beta$   
 250 phase decreases and settles at about -30 J/g and -70 J/g for the iPP+Qui and iPP+NJStar,  
 251 respectively. In contrary, the intensity of the peak related to the  $\alpha$  crystallites grows and  
 252 settles at about -55 J/g and -25 J/g for the iPP+Qui and iPP+NJStar, respectively, which  
 253 demonstrates the fact that increase in cooling rate favor the  $\alpha$  crystallites growth – namely  
 254 in case of the iPP+Qui in which the  $\beta$  phase amount drops of nearly 50 % in comparison  
 255 with approx. 35 % decrease in case of iPP+NJStar. Similar findings were published by  
 256 Kang et al. [22] who studied rare-earth based NA with so called dual-selectivity. In the  
 257 paper, Kang et al. showed the constant growth of  $\alpha$  phase accompanied with proportional  
 258 decrease in  $\beta$  phase amount with the increase of the cooling rate. From this perspective, the  
 259 NJStar is more effective  $\beta$ -nucleating agent, than the Qui is. One can expect, on the other  
 260 hand, the rapid cooling in present paper enabled the process to skip the  $\beta$  crystallization  
 261 considerably [7]. Thus the prevailing demonstrations of  $\alpha$  phase are seen in presented  
 262 records.



263  
 264 **Figure 13.** Specific heat of fusion as a dependence on previous cooling rate.

265 In the **Figure 13** a discontinuity is seen in the overlapping points of the conventional DSC  
 266 and FDSC data. Obviously, the sample size and shape play a significant role in both the  
 267 processes – crystallization and melting. Namely the data obtained by conventional DSC  
 268 can be affected as mentioned above and also in literature [1,9,21]. On the other hand, the  
 269 FDSC related data may be influenced by the surface related forces. Taking into account  
 270 both, it may seem to be impossible to directly correlate the data without any further  
 271 correction, when speaking about the  $\Delta H_f$  as well as the  $T_m$  (**Figure 14**). Both depend not  
 272 only on the cooling regime, but also on the heating rate and the heat transfer through the  
 273 mass, since the structure may evolve after the  $T_g$  is passed.

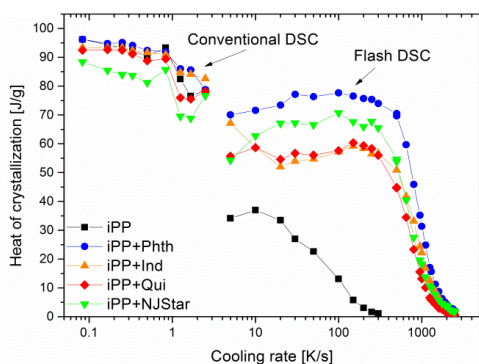


274  
275

**Figure 14.** Melting temperature as a dependence on previous cooling rate.

276 In the **Figure 14**, the decrease of the  $T_m$  is clearly seen as the cooling rate increases, which  
277 is due to the poor quality of the created crystalline phase – the size of crystallites decreases  
278 with the growing cooling rate. The only exception may be the arisen  $\alpha$  phase after melting  
279 of the  $\beta$  phase in the iPP+NJStar sample. The  $\alpha$  crystallites were able to use “molten”  
280 material of the former  $\beta$  phase to improve their structure, which is commonly observed  
281 during annealing treatment at temperatures above the  $T_m$  of  $\beta$  phase [23–25]. A similar  
282 effect may be the cause of the presence of another melting peak in case of neat iPP, which  
283 appears at about 175 °C.

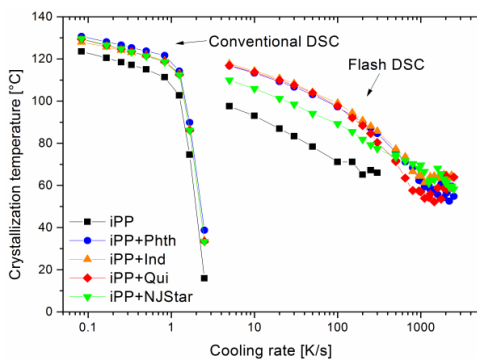
284 In contrast to the melting behavior, the data related to the crystallization shows quite good  
285 continuation. In the **Figure 15**, the evolved heat remains quite the same for all the  
286 materials, which may be due to the limitations in cooling performance and resolution of the  
287 conventional DSC in which it is difficult to achieve quasi-isothermal state of the specimen,  
288 which exchange the heat primarily by its bottom surface [9,21]. Nevertheless, the data  
289 shows an early drop of the heat evolved by the crystallizing iPP, which virtually stops its  
290 crystallization after achieving the cooling rate of ~200 K/s. The nucleated materials still  
291 crystallize at this rate, while their ability to crystallize drops rapidly when the cooling rate  
292 reaches ~1000 K/s and there is no crystallization under the cooling with rate of ~1100 K/s.  
293 These data are in accordance with the melting data shown in **Figure 13**, although the exact  
294 values are not equal, possibly due to the cold crystallization processes, still the trend is the  
295 same. Concerning the NA efficiency, the Phth seems to be the most active NA as the  
296 evolved heat of the iPP+Phth remains all the time above the other materials.



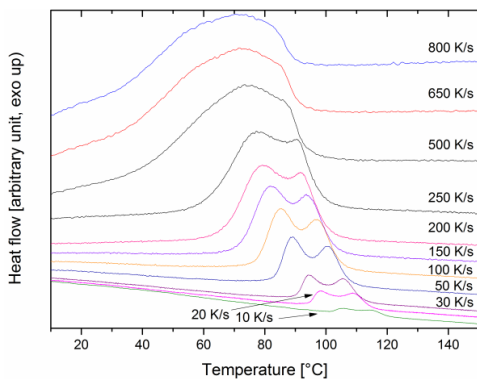
297  
298

**Figure 15.** Specific heat of crystallization as a dependence on cooling rate.

299 The  $T_c$  dependency shown in **Figure 16** demonstrates the abovementioned performance  
 300 and resolution limitations of the conventional DSC – a drop in the  $T_c$  at higher cooling  
 301 rates is evident. Omitting these values, one can get again a good trend of smooth decrease  
 302 in  $T_c$  with the increasing cooling rate. Expectably, the  $T_c$  of the iPP is the lowest regardless  
 303 the cooling rate followed by the  $\alpha$  phase crystallization of iPP+NJStar observed with  
 304 FDSC. The  $\alpha$  crystallization related peak seems to be the most intensive peak as shown in  
 305 **Figure 17**, which is the cooling record of the iPP+NJStar. Only these records shows two  
 306 peaks which should be related to crystallization of both the  $\alpha$  and  $\beta$  phase. It is worth to  
 307 mention, the other materials showed only one crystallization peak with no evidence of  
 308 separate crystallization processes. On the other hand, it is commonly known fact, the  
 309 NJStar nucleates both  $\alpha$  and  $\beta$  phase simultaneously. Thus the evidence of the separate  
 310 crystallization processes.



311  
 312 **Figure 16.** Temperature of crystallization as a dependence of cooling rate.



313  
 314 **Figure 17.** Cooling record of iPP+NJStar.

### 315 **Conclusions**

316 In the presented paper, we have studied the thermal behavior and structure of the neat and  
 317 nucleated iPP. The nucleation agents were namely  $\alpha$ -nucleating phthalocyanine and  
 318 indolone, and non-specific nucleating agents quinacridone and NJ Star NU-100. Both latter  
 319 mentioned are known for their dual-selectivity. The aim was to assess the nucleation ability  
 320 and efficiency of the individual substances under extreme cooling rates. The records  
 321 obtained from flash DSC showed no evidence of the  $\beta$  phase presence, even though the  
 322 melting of  $\beta$  phase is observed by the conventional DSC. Concerning the high cooling rates  
 323 and informations published by Varga et al. [7] and Kang et al. [22], the absence of the  $\beta$

324 phase is given by higher crystallization rate of the  $\alpha$  phase at the given temperatures of  
325 isothermal crystallization, or given cooling rates during the non-isothermal study. It  
326 follows from the non-isothermal study that namely the skin layers of injection-molded  
327 products can crystallize in  $\alpha$  phase modification rather than  $\beta$  phase, when nucleated by the  
328 proper  $\beta$  nucleating agent. This is due to the extreme cooling rates especially when thin-  
329 walled products are taken into account. Indeed, other phenomena should be considered too,  
330 such as shear rate. For the studied material, the measurements showed, that neat iPP cease  
331 to crystallize at cooling rates of about 250 K/s, while the nucleated iPPs are still  
332 crystallizing up to the cooling rates of about 600 K/s at which the amount of amorphous  
333 material grows. There was no crystallization observed when cooled with rates above  
334 1200 K/s.

### 335 **Acknowledgement**

336 Authors acknowledge the assistance of Mss. Sarka Zatloukalova, Tomas Bata University in Zlin,  
337 who did the masterbatch preparation and subsequent dispersion of it into the polypropylene.  
338 Miroslav Janicek and Radek Holubar also gratefully acknowledge a financial support of this work  
339 by internal grants of Tomas Bata University in Zlin, No. IGA/FT/2014/014, funded from the  
340 resources of specific university research. The helpfulness of the reference laboratory of Synthesia  
341 a.s., Pardubice, Czech republic, is acknowledged for provision of samples of the used colorants.

### 342 **References**

- 343 [1] Mathot V, Pyda M, Pijpers T, Vanden Poel G, van de Kerkhof E, van Herwaarden S, et al. *Thermochim*  
344 *Acta* 2011;522:36–45. doi:10.1016/j.tca.2011.02.031.
- 345 [2] Schawe JEK. *J Therm Anal Calorim* 2013;116:1165–73. doi:10.1007/s10973-013-3563-8.
- 346 [3] Vychopnova J, Cermak R, Obadal M, Raab M, Verney V, Commereuc S. *Polym Degrad Stab*  
347 *2007*;92:1763–8. doi:10.1016/j.polymdegradstab.2007.07.010.
- 348 [4] Cermak R, Obadal M, Ponizil P, Polaskova M, Stoklasa K, Heckova J. *Eur Polym J* 2006;42:2185–91.  
349 doi:10.1016/j.eurpolymj.2006.03.014.
- 350 [5] Vychopnova J, Cermak R, Obadal M, Verney V, Commereuc S. *J Therm Anal Calorim* 2009;95:215–  
351 20.
- 352 [6] Cermak R, Obadal M, Ponizil P, Polaskova M, Stoklasa K, Lengalova A. *Eur Polym J* 2005;41:1838–  
353 45. doi:10.1016/j.eurpolymj.2005.02.020.
- 354 [7] Varga J, Menyhard A. *Macromolecules* 2007;40:2422–31. doi:10.1021/ma062815j.
- 355 [8] Chvatalova L, Navratilová J, Cermak R, Raab M, Obadal M. *Macromolecules* 2009;42:7413–7.  
356 doi:10.1021/ma9005878.
- 357 [9] Vyazovkin S, Burnham AK, Criado JM, Pérez-Maqueda L a., Popescu C, Sbirrazzuoli N. *Thermochim*  
358 *Acta* 2011;520:1–19. doi:10.1016/j.tca.2011.03.034.
- 359 [10] Vyazovkin S, Sbirrazzuoli N. *Macromol Rapid Commun* 2006;27:1515–32.  
360 doi:10.1002/marc.200600404.
- 361 [11] Poel G Vanden, Istrate D, Magon A, Mathot V. *J Therm Anal Calorim* 2012;110:1533–46.  
362 doi:10.1007/s10973-012-2722-7.
- 363 [12] Varga J, Mudra I, Ehrenstein GW. *J Appl Polym Sci* 1999;74:2357–68.
- 364 [13] Sterzynski T, Calo P, Lambla M, Thomas M, Oyonnm F. *Polym Eng Sci* 1997;37.
- 365 [14] Yamamoto Y, Inoue Y, Onai T, Doshu C, Takahashi H, Uehara H. *Macromolecules* 2007;40:2745–50.  
366 doi:10.1021/ma062784s.
- 367 [15] Wunderlich B. *Macromolecular Physics. Volume 2: Crystal Nucleation, Growth, Annealing*. New York:  
368 Academic Press, Inc.; 1976.
- 369 [16] Muthukumar M. *Adv Chem Phys* 2004;128:1–63.

- 370 [17] Juhász P, Varga J, Belina K, Marand H. *J Therm Anal* 2002;69:561–74. doi:10.1023/A:1019916007954.
- 371 [18] Galeski A. Crystallization. In: Karger-Kocsis J, editor. *Polypropyl. An A-Z Ref.*, Dordrecht: Kluwer  
372 Academic Publishers; 1999.
- 373 [19] Brandrup J, Immergut EH, Grulke EA. *Polymer Handbook*. New York: John Wiley & Sons, Inc.; 1999.
- 374 [20] Menyhard A. Crystallization and Melting Characteristics and Supermolecular Structure of the beta-  
375 Modification of Isotactic Polypropylene and its Multi-Component Systems. *Budapest University of*  
376 *Technology and Economics*, 2007.
- 377 [21] Van Herwaarden S, Iervolino E, van Herwaarden F, Wijffels T, Leenaers A, Mathot V. *Thermochim*  
378 *Acta* 2011;522:46–52. doi:10.1016/j.tca.2011.05.025.
- 379 [22] Kang J, Peng H, Wang B, Chen Z, Li J, Chen J, et al. *J Appl Polym Sci* 2014;131.  
380 doi:10.1002/app.40115.
- 381 [23] Bai H, Luo F, Zhou T, Deng H, Wang K, Fu Q. *Polymer* 2011;52:2351–60.  
382 doi:10.1016/j.polymer.2011.03.017.
- 383 [24] Kotek J, Kelnar I, Baldrian J, Raab M. *Eur Polym J* 2004;40:2731–8.  
384 doi:10.1016/j.eurpolymj.2004.07.017.
- 385 [25] Na B, Li Z, Lv R, Zou S. *Polym Eng Sci* 2012;52:893–900. doi:10.1002/pen.22156.



## CURRICULUM VITAE

Miroslav Janíček was born in Zlín, on the 21<sup>st</sup> of October 1983. He attended grammar school in Otrokovice and graduated in 2003. Subsequently, he started his studies at Tomas Bata University in Zlín – a study program which included chemistry and technology of materials with focus on plastics engineering. During his studies he was on a short-term study visit at the Ecole Nationale Supérieure de Chimie de Clermont-Ferrand, France, where he cooperated on a project of characterization of photo-oxidative aging of EPDM compounds. His studies were successfully completed with a Master Thesis on structure characterization of ethylene/ $\alpha$ -olefin copolymers with regular comonomer distribution. In 2009 he joined the application group in Nestlé production plant Sfinx in Holešov, where he was responsible for packaging technology as a project leader and packaging specialist. After a year in Nestlé, he decided to continue in study of polymeric materials in doctoral study programme at Tomas Bata University in Zlín with the thesis theme as presented in this essay. The main fields of interests are then in materials characterization by thermal techniques and X-ray diffraction. During his Ph.D. studies he was employed at the University Institute of Tomas Bata University as a team member in the project of Centre of Polymer Systems; at the Faculty of Technology he led and cooperated with two pre-graduate students, and irregularly contributed to *Plasty&Kaučuk* journal. Since the May of 2014 he works as a technical project manager at both the KAVO and K divisions of the Greiner Packaging Slušovice, which is the subsidiary of the Greiner Packaging International (GPI) company headquartered in Austrian city of Kremsmünster.



Ing. Miroslav Janíček

**Crystallization of Polymeric Materials: Study  
of Nucleation on Active Particles with  
Large Specific Surface**

Krystalizace polymerních materiálů: Studium nukleace na  
aktivních částicích s velkým specifickým povrchem

Doctoral Thesis

Published by Tomas Bata University in Zlín  
nám. T. G. Masaryka 5555, 760 01 Zlín

Typesetting: Ing. Miroslav Janíček

Typeset in L<sup>A</sup>T<sub>E</sub>X

This publication has not been neither edited nor linguistically corrected.

2015